NASA Contractor Report 181744

Development and Application of a Program To Calculate Transonic Flow Around an Oscillating Three-Dimensional Wing Using Finite Difference Procedures

Warren H. Weatherill
F. Edward Ehlers

Boeing Commercial Airplanes
Seattle, Washington

Prepared for
Langley Research Center
Under Contract NAS1-17977

NASA
National Aeronautics and
Space Administration

February 1989

1. Report No.	2. Government Accession No.	3. Recipient's Catalog No.
NASA CR-181744		

4. Title and Subtitle	5. Report Date
Development and Application of a Program To Calculate Transonic Flow Around an Oscillating Three-Dimensional Wing Using Finite Difference Procedures	January 1989
	6. Performing Organization Code
7. Author(s)	8. Performing Organization Report No.
Warren H. Weatherill and F. Edward Ehlers	D6-54693
9. Performing Organization Name and Address	10. Work Unit No.
Boeing Commercial Airplanes P.O. Box 3707 Seattle, WA 98124-2207	505-63-21-01
	11. Contract or Grant No.
	NAS1-17977
	13. Type of Report and Period Covered
12. Sponsoring Agency Name and Address	
National Aeronautics and Space Administration Langley Research Center Hampton, VA 23665-5225	14. Sponsoring Agency Code

15. Supplementary Notes

Contract monitor: Robert M. Bennett
Final Report

16. Abstract

A finite difference method for solving the unsteady transonic flow about harmonically oscillating wings is investigated. The procedure is based on separating the velocity potential into steady and unsteady parts and linearizing the resulting unsteady differential equation for small disturbances. The differential equation for the unsteady potential is linear with spatially varying coefficients and with the time variable eliminated by assuming harmonic motion.

Difference equations are derived for harmonic transonic flow to include a coordinate transformation for swept and tapered planforms.

A pilot program is developed for three-dimensional planar lifting surface configurations (including thickness) for the CRAY-XMP at Boeing Commercial Airplanes and for the CYBER VPS-32 at the NASA Langley Research Center.

An investigation is made of the effect of the location of the outer boundaries on accuracy for very small reduced frequencies.

Finally, the pilot program is applied to the flutter analysis of a rectangular wing.

17. Key Words (Suggested by Author(s))	18. Distribution Statement
Unsteady flow Transonic flow Oscillating wings Flutter	Unclassified—unlimited Subject category 02

19. Security Classif. (of this report)	20. Security Classif. (of this page)	21. No. of Pages	22. Price
Unclassified	Unclassified	91	

FORM 0005

For sale by the National Technical Information Service, Springfield, Virginia 22151

NASA Contractor Report 181744

Development and Application of a Program To Calculate Transonic Flow Around an Oscillating Three-Dimensional Wing Using Finite Difference Procedures

Warren H. Weatherill
F. Edward Ehlers

Boeing Commercial Airplanes
Seattle, Washington

Prepared for
Langley Research Center
Under Contract NAS1-17977

National Aeronautics and
Space Administration

February 1989

CONTENTS

LIST OF FIGURES

1.0 SUMMARY

A finite difference method for solving the unsteady transonic flow about harmonically oscillating wings is investigated. The procedure is based on separating the velocity potential into steady and unsteady parts and linearizing the resulting unsteady differential equation for small disturbances. The differential equation for the unsteady potential is linear with spatially varying coefficients and with the time variable eliminated by assuming harmonic motion.

The work of this report is a direct extension of earlier studies and includes extension of a program using a direct solution procedure to include coordinate transformations for swept and tapered planforms and modification of the program to work on the new generation of vector computers with very large memory capabilities.

The main results of the study are–

1. Rederivation of the difference equations for harmonic transonic flow to include a coordinate transformation for swept and tapered planforms.

2. Development of programs for three-dimensional planar configurations (including thickness) for the CRAY-XMP at Boeing and the CYBER VPS-32 system at the NASA Langley Research Center at Hampton, Virginia.

3. An investigation of the effect of the location of the outer boundaries on accuracy for very small reduced frequencies.

4. Application of the developed program to the flutter analysis of a rectangular wing of aspect ratio 3.0.

2.0 INTRODUCTION

The development of an efficient and practical procedure for calculating unsteady transonic air forces for use in flutter analyses continues to be of interest to the aircraft industry. The work of this report extends a series of studies into a finite difference solution procedure applied to the small disturbance velocity potential equation, which has been linearized by assuming simple harmonic motion. These studies, which have been documented in References 1 through 8, have resulted in a pilot program that has been used successfully for the two-dimensional, typical section problem. Extension of the two-dimensional program to three dimensions, with the corresponding increase in the number of problem unknowns, resulted in a program that was very expensive to run.

The studies described in this report include the derivation of a coordinate transformation for swept and tapered wings, the rewriting of a CRAY-1 program for use on the CRAY-XMP and the NASA Langley VPS-32 computer system in order to reduce running cost, correlation studies for the new pilot program for small values of reduced frequency, and application of the new program to a flutter example.

The development and characteristics of the new pilot program are discussed in Section 5.0.

The coordinate transformation, discussed in Section 6.0 and derived in the Appendix, aligns the mesh points with the leading and trailing edges of a planform. It is essentially a shearing transformation in the plane of the planform, but with additional terms in the expressions for the streamwise variable so that continuity of second derivatives is maintained across the planform edges.

Several correlation studies are presented in Section 7.0. Generally good agreement is shown between pressure distributions from OPTRAN3 and a kernel function program for planforms of vanishing thickness. An example is presented for a wing of finite thickness. Also, it is shown that the boundaries of the finite difference solution region must be moved away from the wing as the reduced frequency is decreased in order to maintain accuracy.

The application of the program to the flutter analysis of a wing with finite thickness is presented in Section 8.0.

Finally, the authors would like to acknowledge the valuable contributions of Dr. Elizabeth L. Yip in the development of the solution routines, of Dr. Michael B. Bieterman in converting the OPTRAN3 code for the CRAY-XMP to code for the VPS-32 system, and of Dr. Robert M. Bennett to the calculations for the flutter example.

3.0 ABBREVIATIONS AND SYMBOLS

a	Amplitude of wing oscillations
b	Root semichord
C_p	Pressure coefficient, $(p-p_0)/(1/2\rho_0 U_0^2)$ where p is the local pressure, p_0 the freestream static pressure, and ρ_0 the freestream air density
f	Frequency in hertz
f_0	Undisturbed wing or airfoil shape
f_1	Unsteady contribution to wing or airfoil shape
i,j,k I,J,K	x,y,z subscripts and indices for points in the mesh
i	$\sqrt{-1}$
k	Reduced frequency based on semichord, $2\pi fb/U$; same as ω
K	Transonic parameter, $(1 - M^2)/M^2\epsilon)$
KFB	Kernel function program for two-dimensional flow by Bland (ref. 18)
le, LE	Leading edge
M	Freestream Mach number
M_0	Mass of wing excluding support shaft
q	$\omega^2/\epsilon - i\omega(\gamma - 1)\varphi_{0_{xx}}$
Q_{mn}	Generalized force due to pressure from the nth mode weighted with the deflection of the mth mode
RHO4	Kernel function program for three-dimensional flow by Rowe, Redman, and Winther (refs. 14 and 15)
s	Wing semispan
t	Time in units of b/U
te, TE	Trailing edge

u	$K - (\gamma + 1)\varphi_{0_x}$
U, U_0	Freestream velocity
x,z x,y,z	Scaled and nondimensional coordinates for two- and three-dimensional problems ($x = x_0/b$, $y = \mu y_0/b$, $z = \mu z_0/b$)
x_0,z_0 x_0,y_0,z_0	Nondimensional and unscaled coordinates for two- and three-dimensional problems
γ	Ratio of specific heats for air
$\Delta\tilde{C}_p$	Jump in pressure coefficient across airfoil or wake per unit amplitude of oscillation
$\Delta\varphi_1$	Jump in φ_1 at plane of wing or vortex wake
$\Delta\varphi_{1_{te}}$	Jump in φ_1 at wing trailing edge
δ	Thickness ratio
ϵ	$(\delta/M)^{2/3}$
λ_1	$\omega M/(1-M^2)$
μ	Scale factor of y_0 and z_0, $\mu = \delta^{1/3} M^{2/3}$; also mass ratio, $M_0/(\pi b^2 s\rho)$
$\bar{\eta}$	Fraction of semispan
ξ,η,ζ	Sweptwing coordinates
ρ	Air density
ρ_0	Freestream air density
φ	Complete, scaled perturbation velocity potential; also used for the unsteady potential in finite difference equations with subscripts
φ_0	Steady scaled perturbation velocity potential
φ_1	Unsteady scaled perturbation velocity potential
ω	Frequency in radians; also reduced frequency, same as k
ω_0	Reference frequency in radians. For the example in Figures 20 and 21, ω_0 is the second natural frequency of the model

SUBSCRIPTS

F	Flutter value
0	Freestream value
r	Root or reference value

4.0 FORMULATION AND SOLUTION

Since the mathematical derivation of the method for the solution of the unsteady velocity potential for the flow about a harmonically oscillating wing is presented in Reference 1, the discussion here will be limited to a brief outline of the procedure for two dimensions. The complete nonlinear differential equation was simplified by assuming the flow to be a small perturbation from a uniform stream near the speed of sound. The resulting equation for unsteady flow is

$$\left[K-(\gamma-1)\varphi_t-(\gamma+1)-\varphi_x\right]\varphi_{xx}+\varphi_{yy}-\left(2\varphi_{xt}+\varphi_{tt}\right)/\epsilon=0 \tag{1}$$

where $K = (1\text{-}M^2)/(M^2\epsilon)$, M is the freestream Mach number of velocity U_0 in the x-direction, x and y are made dimensionless to the semichord b of the airfoil and the time t to the ratio b/U_0. With the airfoil shape as a function of time defined by the relation

$$y_0=\delta f(x,t)$$

the linearized boundary condition becomes

$$\varphi_y=f_x(x,t)+f_t(x,t) \tag{2}$$

The quantity δ is associated with properties of the airfoil (such as maximum thickness ratio, camber, or maximum angle of attack) and is assumed to be small. The coordinate y is scaled to the dimensionless physical coordinate y_0 according to

$$y=\delta^{1/3}M^{2/3}y_0$$

and ϵ is given in terms of δ by

$$\epsilon=(\delta/M)^{2/3}$$

The pressure coefficient is found from the relation

$$C_p=-2\epsilon\left(\varphi_x+\varphi_t\right)$$

The preceding differential equation is simplified by assuming the velocity potential to be separable into a steady-state potential and a potential representing the unsteady effects. We write for the perturbation velocity potential

$$\varphi=-\varphi_0(x,y)+\varphi_1(x,y)e^{i\omega t} \tag{3}$$

and for the body shape

$$y_0=\delta f(x,t)=\delta\left[f_0(x)+f_1(x)e^{i\omega t}\right].$$

Since the steady-state terms must satisfy the boundary conditions and the differential equation in the absence of oscillations, we obtain

$$\left[K - (\gamma + 1)\,\varphi_{0_x}\right]\varphi_{0_{xx}} + \varphi_{0_{yy}} = 0 \tag{4}$$

with

$$\varphi_{0_y} = f_0(x), \qquad y = 0, \quad -1 \le x \le 1 \tag{5}$$

On the assumption that the oscillations are small and products of φ_1 may be neglected, equations (4.1) and (4.2) with the aid of equations (4.4) and (4.5) yield

$$\left\{\left[K - (\gamma + 1)\varphi_{0_x}\right]\varphi_{1_x}\right\}_x + \varphi_{1_{yy}} - (2i\omega/\epsilon)\,\varphi_{1_x} + q\varphi_1 = 0 \tag{6}$$

where

$$q = \omega^2/\epsilon - i\omega(\gamma - 1)\varphi_{0_{xx}}$$

subject to the wing boundary conditions

$$\varphi_{1_y} = f_{1_x} + i\omega f_1(x), \quad y = 0, \quad -1 \le x \le 1 \tag{7}$$

The boundary condition that the pressure be continuous across the wake from the trailing edge was found in terms of the jump in potential $\Delta\varphi_1$ to be

$$\Delta\varphi_1 = \Delta\varphi_{1_{te}} e^{-i\omega\,(x - x_{te})} \tag{8}$$

where $\Delta\varphi_{1_{te}}$ is the jump in the potential at $x = x_{te}$ just downstream of the trailing edge and is determined to satisfy the Kutta condition that the jump in pressure vanish at the trailing edge. The quantity $\Delta\varphi_1$ is also used in the difference formulation for the derivative $\varphi_{1_{yy}}$ to satisfy continuity of normal flow across the trailing edge wake.

For the set of difference equations to be determinate, the boundary conditions on the outer edges of the mesh must be specified. In the original unsteady formulation, these boundary conditions were derived from asymptotic integral relations in a manner parallel to that used by Klunker (ref. 9) for steady flow. A later formulation (ref. 3) applies an outgoing plane wave boundary condition to the outer edges of the mesh. This boundary condition is numerically simpler to apply and is equivalent to the first-order nonreflecting boundary conditions derived by Engquist and Majda (ref. 10).

A computer program for solving the steady-state transonic flow about lifting airfoils based on equations (4.4) and (4.6) was developed by Cole, Murman, and Krupp (refs. 11 and 12).

The similarity of the unsteady differential equation to the steady-state equation suggests that the method of Cole, Murman, and Krupp should be an effective way to solve equation (4.6) for the unsteady potential φ_1. Note that equation (4.6) is of mixed type, being elliptic or hyperbolic whenever equation (4.4) is elliptic or hyperbolic. Central differencing was used at all points for the y derivative and all subsonic or elliptic points for the x derivatives. Backward (or upstream) differences were used for the x derivatives at all hyperbolic points. The preferred numerical approach to solving the resulting large-order set of difference equations is a relaxation procedure, which permits the calculation to be made as a sequence of relatively small problems. However, as discussed in preceding NASA reports by the authors (refs. 3 and 4), a significant problem of solution convergence with the relaxation procedure was encountered that severely limits the range of Mach number and reduced frequency for which solutions may be obtained. Accordingly, an out-of-core solver (ref. 8) was developed to solve the complete set of difference equations simultaneously, which for two-dimensional flow is relatively efficient.

The size of practical three-dimensional problems is such that the program of Reference 8 was too expensive for practical application. In Reference 8, the authors explored alternatives to the direct solution procedure and ways of making the direct solution more efficient. The conclusions from this work provided the motivation for work discussed in the following sections.

5.0 THE PILOT PROGRAM FOR LIFTING SURFACES

The initial block of work was to develop a pilot program for three-dimensional lifting surfaces utilizing the harmonic procedures for unsteady transonic flow developed in References 1 through 8. This program was to be designed for use on the CRAY-XMP and was to be a refinement of a pilot program developed for the the CRAY-1. This initial program was developed and tested for a machine with 1 million words of core storage and was written during the installation at Boeing of both the CRAY hardware and software. The Boeing CRAY-XMP has 4 million words of core storage, which permits working with larger blocks of data in memory. Larger blocks mean a smaller number of longer do-loops; vectorizing the longer do-loops reduces execution time. Another key element of the XMP is its solid-state disk (SSD) with some 128 million words of storage and a data transfer rate 100 times that of a conventional disk. These were significant elements in the motivation to refine a program for which I/O requirements accounted for 75% of the run cost.

After completion, the CRAY-XMP version of the pilot program was modified for use on the VPS-32 system at NASA Langley. The CRAY-XMP version, for example, included calls to a number of subroutines in VectorPak and BCSLIB. VectorPak is a subroutine library of carefully optimized mathematical subprograms for the CRAY-XMP and some of the other vector computers. BCSLIB is a comprehensive, general-purpose library of mathematical, statistical, and utility subprograms. Since BCSLIB and VectorPak are not available on the NASA Langley VPS-32 system, OPTRAN3 was augmented with FORTRAN equivalents of the required subroutines. Conversion was accomplished in a relatively direct fashion, and the resulting program is not as efficient on the VPS-32 system as it is on the CRAY-XMP. Relative run times are discussed below in Section 5.2.

5.1 PROGRAM CHARACTERISTICS

The program is set up for a single, noninterfering surface with straight leading and trailing edges. It includes a coordinate transformation to align the computational mesh with the leading and trailing edges of swept and tapered planforms. It includes capabilities for calculating the downwash for vertical translation, pitch, flapping, or full span control surface modes. However, with relatively simple changes in the subroutine that calculates the downwash distribution (subroutine AIRFOIL), the program can be adapted to run user-supplied modal deflections and slopes (as was done for the flutter calculation in sec. 8.0). The modal information is supplied to the program only at the mesh point locations. No specific information is provided for discontinuities in slopes in the deflection pattern such as occur in (for example) a control surface mode. However, if mesh points are concentrated about the hingeline, the proper gradients in the pressure pattern will be observed. The program has no means for calculating slopes from input deflections.

Program output includes pressure distributions and sectional and generalized forces. Relatively simple changes to the subroutine CPR would permit obtaining the pressure or force data in nearly any form desired.

Care must be taken in calculating sectional generalized forces from pressure distributions defined with a limited number of finite difference points. For configurations with subsonic leading edges and thus pressure distributions that are singular at the leading edge, use of trapezoidal integration may significantly underestimate the total sectional force. In OPTRAN3, an assumed pressure distribution with a square root singularity is used in the vicinity of the leading edge. The

second mesh point aft of the leading edge, $x(I0 + 1)$, is used as a critical point. The force due to the pressure ahead of this point is obtained analytically using the formula

$$\Delta\tilde{C}_p = \Delta\tilde{C}_p\left(x(I0 + 1)\right) * \frac{\sqrt{x(I0 + 1) + 1}}{\sqrt{x + 1}}$$

The force due to the pressure aft of $x(I0 + 1)$ is obtained using trapezoidal integration. Using this procedure, results from OPTRAN3 correlated well with results from RHO4 (see sec. 8). Pressure and sectional force data were not available for correlation with a finite thickness case. Care should be taken in applying this procedure to thick wings with blunt leading edges for which the usual rapid rise in pressure at the leading edge may be attenuated.

For purposes of this report, the number of points in a mesh is given in terms of a full mesh about the right-hand side of the planform. Thus, an IMAX × JMAX × KMAX mesh has IMAX points in the x-direction (streamwise) with x(1) on the upstream boundary and x(IMAX) on the downstream boundary, JMAX points in the y-direction (spanwise) with y(2) on the planform centerline, $y(3) = -y(1)$, and y(JMAX) on the outboard boundary, and KMAX points in the z-direction (vertical) with $z(1)$ on the lower boundary and z(KMAX) on the upper boundary. A full-mesh solution for problems without symmetry about the $x-y$ plane has $(IMAX-2)\times(JMAX-2)\times(KMAX-2)$ unknowns. A half-mesh solution, for problems with symmetry about the $x-y$ plane and for which only points below the planform need be included, has $(IMAX-2)\times(JMAX-2)\times(KMAX/2-1)$ unknowns.

In similar fashion, for two-dimensional problems, an IMAX × KMAX mesh would have $(IMAX-2)\times(KMAX-2)$ unknowns for a full solution and $(IMAX-2)\times(KMAX/2-1)$ unknowns for a half-mesh or symmetric solution.

All the examples in this report are problems with symmetry about the $x-y$ plane and thus are half-mesh solutions.

5.2 PROGRAM RUNNING TIME

The new program, when run on the CRAY-XMP, is significantly more efficient than the CRAY-1 version. The cost of a typical run for the new program in CPU seconds is one-tenth that of the original program. Also, due to the use of the SSD, the I/O cost for the refined program is 25% of the total run cost according to the Boeing cost algorithm rather than the 75% for the CRAY-1 program.

The running time for the new program on the CRAY-XMP for a half-mesh solution using $48\times17\times32$ mesh (10,350 unknowns) is about 120 CPU seconds. The number of right-hand sides (the number of mode shapes) has a small effect on the running time. The running time increases roughly as a cubic of the increase in the number of spanwise and/or vertical points. The running time variation is roughly linear with increasing points in the streamwise direction. A plot of running time versus the number of points spanwise is shown in Figure 1, which generally confirms these variations in running times. The cubic curve is based on JMAX − 2, where JMAX is defined as the number of spanwise points in the mesh including one point on the wing centerline and one point to the left of the centerline.

The VPS-32 version of the program requires about ten times more CPU seconds than the version on the CRAY-XMP.

6.0 A TRANSFORMATION FOR SWEPT AND TAPERED PLANFORMS

A very desirable characteristic of finite difference programs for three-dimensional lifting surfaces is the matching of the calculation mesh to the planform geometry of swept and tapered wings. This is particularly important in the vicinity of surface leading edges, where there are large gradients in the pressure distributions, and for highly tapered wings, where, with rectangular grids, it is difficult to obtain a practical number of points along both the root and tip chords.

The coordinate transformation derived in the Appendix and included in the pilot program generally aligns mesh points with the leading and trailing edges of a swept and tapered planform using a stretching and shearing algorithm. The calculation volume is divided into three regions by vertical planes through the leading and trailing edges of the planform. These extend from the centerline to the side boundary. The upstream and downstream boundaries are perpendicular to the root plane.

The transformation is set up for wings with straight leading and trailing edges. For wings with swept edges, the apex at the centerline is rounded to remove singularities in the distributions. The rounding is accomplished so that the new edges have continuous second-order derivatives with respect to the spanwise variable.

The swept edges are also extended to meet the outside boundary at right angles. Here again the functions are made continuous in the second derivative with respect to the spanwise variable.

Generally, this transformation conforms to the suggestion of Goorjian and Guruswamy in Reference 13 and used in the XTRAN3 programs. The transformations used here for the upstream and downstream regions employ additional nonlinear terms in the expressions for the streamwise variable.

A complete derivation of the transformation and its incorporation into the finite difference equations is presented in the Appendix. Section A.1 presents the basic transformation equations. Implementation requires definition of the planform leading and trailing edges from the wingtip to the outer (side) mesh boundary. This may be accomplished in an automated fashion using the equations presented in A.2, which are included in OPTRAN3. However, this procedure will work well only if the planform has a moderate taper ratio. The problem is that the location of the outer boundary is determined by intersection of extensions of the edges. Thus if the taper ratio is large, the outer boundary will be too close to the wingtip; conversely, if the taper ratio is small, the outer boundary will be too far from the wingtip. Also, the procedure of A.2 assumes the planform edges are straight and without breaks. As an alternative, the leading and trailing edge extensions may be worked out by hand and entered as data input. For OPTRAN3, this means modifying subroutine PLNFORM to read the edge extension data rather than calculating it. The transformation of A.1 is applied to the equation for harmonic transonic flow in A.3.1, and the resulting finite difference equations are derived in A.3.2 and A.3.3.

7.0 CORRELATION OF PRESSURE DISTRIBUTIONS

Validation of the new pilot program was accomplished by matching results from the new pilot program for OPTRAN3 with distributions from a reliable kernel function program, RHO4 (refs. 14 and 15). Discussions in this section will center mainly on correlation with RHO4. For planforms of vanishing thickness and thus linear flow, results from OPTRAN3 and RHO4 should match exactly.

Section 7.1 presents an example for a swept and tapered planform. Section 7.2 discusses the effects of the location of the outer boundaries for small values of reduced frequency.

7.1 A SWEPT AND TAPERED WING EXAMPLE

Pressure distributions are presented in this section for a swept and tapered wing of vanishing thickness. A sketch of the planform is shown in Figure 2. The surface studied has a 30-deg swept leading edge and a taper ratio of 0.5, with a semispan equal to 1.25 semichords. The calculations were made for a Mach number of 0.8 and with the wing oscillating in pitch about the root midchord at a reduced frequency of 0.06 based on the root semichord. The results should match pressure distributions from a linear solution. For this study, results are correlated with distributions from the RHO4 program described in references 14 and 15.

Results from OPTRAN3 correlate well with corresponding results from RHO4. Examples of this correlation for the root and tip ($\eta = 0.8$) chords are shown in Figures 3a through 4b. Distributions are shown from RHO4, and from OPTRAN3 for half-mesh solutions using a $30 \times 12 \times 20$ mesh and a $44 \times 14 \times 32$ mesh. For the root chord, all three calculations include rounding of the leading and trailing edge. For the real part, there is little difference between the two OPTRAN3 calculations and RHO4. Both meshes do a good job of predicting the leading edge singularity. For the imaginary part, the finer mesh does a noticeably better job of matching the RHO4 results over the the forward part of the wing. For the 80% spanwise chord, the finer mesh again does a better job of matching RHO4. Although the difference is marginal for the real part, it is significant over the leading edge region for the imaginary part.

For both meshes, the upstream and downstream boundaries were at $x = -2.0$ and 3.0 and the side boundary was at $y = 4.5$. The upper and lower boundaries were at $z = +4.5$ for the fine mesh and $z = +3.0$ for the coarse mesh.* In view of the subsequent difficulties with the location of the mesh boundaries at low reduced frequencies, results might well be improved by moving the boundaries further out. This point will be discussed in the next section.

7.2 A FINITE THICKNESS EXAMPLE

Pressure distributions are presented in this section for a rectangular wing with a 10% thick parabolic arc airfoil section. The semispan is 1.5 times the semichord, and results are presented for

* The x, y, and z values are given here in units of root semichord. Thus the upstream boundary is 1/2 root chord length in front of the upstream boundary at the root; the downstream boundary is one root chord length aft of the trailing edge; and the spanwise boundary is four semispans from the root.

M = 0.9 and k = 0.06. The mesh used is $44 \times 12 \times 32$ with the boundaries relatively close to the wing: $-2.0 \leq x \leq 3.0$, $y \leq 4.5$, $-4.5 \leq z \leq 4.5$. The flow condition is symmetric ($\alpha = 0$) and the wing is oscillating in pitch about the leading edge. The steady velocity potential distribution was calculated with XTRAN3S (ref. 16). Computer resources required are essentially the same as required for the flat plate case. Results are presented in Figures 4a and 4b for the root section and for the 80% spanwise station. We do not have matching results from another source, and thus the most that we can say is that the results appear reasonable. We have run the OPTRAN3-ADI program (OPTRAN3 with an alternating direction solution package, ref. 8) with essentially the same results. It should be noted that other three-dimensional correlation studies are presented in References 4 through 8. It is surprising to find a blip in the curves of Figures 4a and 4b at the sonic line, where the flow is changing from subsonic to supersonic flow on the forward half of the section. Changing the Mach number and the point distributions (slightly in both cases) made no difference in this blip. On looking back at the calculations in Reference 8, hints of a blip appear in the two-dimensional results for the NACA-64A010 airfoil (see figs. 8 and 9 of ref. 8) but not in the three-dimensional results for the circular arc airfoil.

7.3 SENSITIVITIES TO BOUNDARY LOCATIONS

Initial results for the flutter analysis indicated a problem with the generalized forces for small values of reduced frequency, in this particular case for a reduced frequency of 0.01 based on the root semichord. It is possible that this is really a problem of Mach number as well as reduced frequency since the solution procedure was found to be sensitive to the parameter

$$\lambda = \omega M/(1 - M^2)$$

In this study, only sensitivities to reduced frequency have been examined. The concern was that the imaginary parts of the generalized forces were not going to zero as the reduced frequency went to zero. Indeed, correlation of the imaginary part of the pressure between OPTRAN3 and RHO4 was very poor at low values of k.

The problem appeared during the flutter analysis of the wing in Section 8.0 and may most easily be illustrated by plotting the imaginary part of the Q_{22} term (the generalized force due to the pressure from the second mode weighted with itself) versus reduced frequency. The second elastic mode of this wing, a rectangular wing with an aspect ratio of 3.0, is essentially a pitch mode. The imaginary part of the Q_{22} term should go to zero as k goes to zero. Results for the rectangular wing of aspect ratio 3.0 and of vanishing thickness are presented in Figure 5 for both OPTRAN3 and a reliable three-dimensional kernel function program, RHO4. It is seen that the results from RHO4 do tend to zero as k goes to zero, while those from OPTRAN3 as calculated with a relatively small finite difference volume do not. However, even at k = 0.1 the two imaginary parts of Q_{22} are relatively close together and, although not shown in Figure 5, become even closer at higher values of reduced frequency.

For reference purposes, the pressure distributions for the second mode for M = 0.8 and k = 0.3 from OPTRAN3 and RHO4 are shown in Figures 6a through 6d. OPTRAN3 results are shown for two different meshes, both with a $44 \times 14 \times 32$ mesh and both with the side boundary at y = 4.5: a "small" mesh with the upstream boundary at $x = -2.0$, the downstream boundary at x = 3.0, and the upper/lower boundaries at $z = +4.5$, and a "large" mesh with the upstream/downstream boundaries at $x = +8.0$ and the upper/lower boundaries at $z = +8.0$. Results are presented for two

chords, the root chord and a chord near the tip. First, for this particular case, the correlation between OPTRAN3 and RHO4 is good for both the "small" and the "large" meshes and for both chords. Moreover, the two OPTRAN3 results are noticeably more like each other than either of them is like the RHO4 result. Thus, in this case, the larger solution area does not affect the result.

The phenomenon of deteriorating accuracy as the reduced frequency went to zero had been noted in the two-dimensional problem by Siedel, Bennett, and Whitlow (ref. 17) and was resolved by moving the upstream boundary further upstream. This was immediately tried on the three-dimensional problem but with only limited success. It ultimately proved that all the mesh boundaries had to be moved out to obtain the desired correlation between OPTRAN3 and RHO4.

The next part of the discussion centers on results for a two-dimensional airfoil section of vanishing thickness oscillating in pitch about the leading edge. The results will be presented in terms of the pressure distributions. It is recognized that, for small k values, the amplitudes of the imaginary parts of the generalized force are small relative to the real part. Indeed, the difference in imaginary parts would not be noticeable if they were plotted on the same scale as the real parts. However, in light of the importance of the imaginary part of Q_{22} having the proper behavior as k goes to zero, it is of interest to investigate this problem in some detail. Due to the computer costs entailed in running the three-dimensional program, it was decided to begin by comparing results from OPTRAN2 and a well-tested two-dimensional kernel function program by Bland (ref. 18), hereafter called KFB.

Figures 7 through 10 present results for M = 0.8 and k values of 0.3 to 0.001 for a "reasonable-sized" two-dimensional mesh: a 72×60 point pattern (see sec. 5.1 for definition of mesh sizes) with $|x| < 10$ and $|y| < 10$. The intent is to show (1) the relative amplitudes of the real and imaginary parts and how they change with k value, and (2) how the correlation between OPTRAN2 and KFB degrades as the k-value is reduced while the solution area is held constant. The correlation at $k = 0.3$ (fig. 7) is excellent. The falloff in correlation at $k = 0.1$ (fig. 8) is barely discernible. At $k = 0.01$ (fig. 9), the real parts still coincide, but there is a noticeable difference in the imaginary parts. This is the expected behavior where, for a given finite difference mesh sized to provide good answers at nominal values of k, accuracy is lost at very small values of k. However, at $k = 0.001$ (fig. 10), the pressures from the two methods appear to again coincide. This latter result is considered fortuitous for reasons illustrated in Figure 11, which presents plots of the imaginary part of the pressure for several upper/lower boundary locations. In this case, the correlation between OPTRAN2 and the KFB method decreases as the boundary is moved out, although not in the expected sequence. Here, the correlation is best with the upper/lower boundaries at $y = +10$, significantly worse with the boundaries a $y = +50$, and then somewhat better with the boundaries at $y = +100$. This inconsistency is probably due to the need for more mesh points as the boundaries are moved out. Finally, it is noted that in this particular case ($k = 0.001$) the imaginary parts are very small and the differences discussed may not be very significant.

An example of the pressure distribution from OPTRAN2 moving across the results from the KFB method is shown in Figure 12 for $k = 0.01$. Here, the boundaries are moved from $y = +10$ (the OPTRAN2 result is below that from the KFB method) to $y = +30$ (the OPTRAN2 result is above that from the KFB method), to $y = +100$ (little change in the OPTRAN2 result). When the upstream/downstream boundaries are set at $x = +40$ and with the upper/lower boundaries at $y = +60$, the OPTRAN2 results correlate with the KFB results very well.

A three-dimensional example is presented in Figures 13a through 14b for a full-span, aspect ratio 3.0 rectangular wing of vanishing thickness and oscillating in pitch about the leading edge. Pressure distributions for OPTRAN3 for four different mesh areas and for RHO4 are presented for two chords, the root chord and for $\bar{\eta} = 0.885$. Figures 13a and 13b present both the real and imaginary parts of the pressure, showing the relative amplitudes of the two parts and with very good correlation between all five sets of results for the real part. The RHO4 results, represented by the solid line, are "buried" in the curves for the three large-area solutions for the real part, and are the uppermost curve for the imaginary part. This latter curve may be seen more clearly in Figures 14a and 14b, which show the imaginary part of the pressure to a larger scale. As the outboard boundary is moved out by adding mesh points (the original spanwise point distribution is left unchanged) the imaginary part of the pressure moves toward the RHO4 results.

The reasons for needing to move the boundaries out for very small values of reduced frequency is not completely clear. It would seem logical that the boundaries must be far enough out and enough mesh points must be used so that the wave pattern in the potential distribution would be well defined. Samples of the two-dimensional velocity potential for $k = 0.001$ along a constant x-line are shown in Figures 15a and 15b for a column of points just aft of the leading edge. The pressure is calculated by extrapolating the velocity potential to the wing surface ($z = 0$) along each column of points and then calculating the pressure coefficient as

$$C_p = 2\epsilon\,(\varphi_x + \varphi_t)$$

The pattern is shown out to $z = 16$ in Figure 15a and then an enlarged section $-2.0 < z < 0$ is shown for Figure 15b. Although the patterns do vary as the upper/lower boundaries are moved away from the airfoil, the differences over the first two points (which are the points used in the interpolation) are very subtle. One would not expect to see the differences in the pressure distributions of Figure 11, which are calculated from the potential distributions of Figure 15b.

Generally, these examples show that, for small values of reduced frequency, the outer boundaries of the solution mesh must be much further from the wing planform than for larger values of k. There will always be a dilemma of using enough mesh points to properly define the waves in the velocity potential field while keeping the number of points to a minimum to reduce computer costs. It is practical to vary the location of the outer boundaries with k value. However, it is recommended that the meshes be evaluated by correlating results from OPTRAN3 and a kernel function program such as RHO4.

In conclusion, compared to higher values, lower values of reduced frequency require more remote boundaries and larger numbers of mesh points, resulting in larger computer costs, in order to retain accuracy.

8.0 A FLUTTER EXAMPLE

OPTRAN3 was applied to the flutter analysis of the rectangular wing studied by Cole in Reference 19. This wing, with an aspect ratio of 1.5 and a 64A010 airfoil section, had been tested in the LaRC 0.3m Cryogenic Wind Tunnel (TCT). The model consisted of a rigid wing with an integral flexible support that was cantilevered from the wind tunnel wall. Experimental flutter points were obtained over the Mach number range of 0.5 to 0.9. There were no signs of transonic flow effects on the flutter results at the higher Mach numbers. Analytical results were obtained using the NASA-Langley Flutter-Analysis-System (ref. 20), FAST, which uses subsonic lifting surface theory analogous to RHO4 (ref. 21) to calculate the aerodynamic forces. The flutter analysis was performed using a combination of calculated and measured properties. A set of four natural modes was used as generalized coordinates. The FAST results ". . . predicted the experimental flutter dynamic pressures rather well, with analytical results ranging up to 5 percent nonconservative at the lowest Mach number tested and 5 percent conservative at the higher Mach numbers tested" (ref. 19).

To demonstrate its application of OPTRAN3 to the flutter problem, OPTRAN3 was used to calculate a flutter point at M = 0.8. The calculations were made on the NASA-Langley VPS-32 computer system using NASA-supplied modal and velocity potential data as input. The resulting generalized forces were used in FAST for a V-g type flutter solution.

The flutter analyses were made using the first four natural modes as generalized coordinates. The modal deflections and slopes were interpolated from the NASA structural grid to the aerodynamic control points used by OPTRAN3. A steady state velocity potential distribution, calculated with the NASA-Langley CAP-TSD program (refs. 22 and 23), was also interpolated for input. The effects of a thickness distribution are included in OPTRAN3 through this steady potential, which is used in calculating the spatially varying coefficients of the finite difference equations. For the current problem, a set of generalized forces for five k-values over the range of 0.01 to 0.2 with forces for intermediate k-values being found by interpolation. A separate OPTRAN3 run is required for each k-value. However, each run includes all the mode shapes, and additional modes do not significantly effect the cost of a run. Computer costs, then, are linear with respect to the number of reduced frequencies for which generalized forces must be calculated, but are nearly independent of the number of generalized coordinates used.

The steady pressure distribution calculated from the velocity potential used as input to OPTRAN3 is presented in Figures 16 and 17. The steady chordwise pressure distribution at the wing root shown in Figure 16 has a small supersonic region centered about a point 40% of the chord aft from the leading edge, and there is no discernible shock at the aft end of the supersonic region. Thus the flow is nearly subsonic at the root, and this pattern holds outboard as shown by the distribution for the complete planform in Figure 17.

Figures 18a through 18d present the generalized air forces for the first two modes. Here, the kernel function forces from FAST are compared with forces from OPTRAN3 both with and without thickness. Generally, the three curves lie very close together for all four generalized forces and for both the real and imaginary parts. Differences between the two flat plate cases (FAST and OPTRAN3 without thickness), and small inconsistencies between the flat plate and with-thickness results, such as Q_{12} (fig. 17) where FAST and OPTRAN3 with-thickness results match exactly and the forces from OPTRAN3 without thickness are slightly different, are probably caused by the

limited number of mesh points used as a result of practical restrictions on available computer resources. In this case a relatively coarse grid of 48x17x32 was used. In addition, due to the low k-values at which flutter was expected, it was important to have the boundaries of the finite difference mesh as far from the planform as possible. After consideration of the number of mesh points to be used, the grid boundaries were set at

$$-10.0 \leq x \leq +10.0 \qquad y \leq 12.75 \qquad -10.0 \leq z \leq +10.0$$

Improved correlation with the FAST results would be expected from using more mesh points for the existing solution volume. Even better correlation would be expected if, with the increased number of mesh points, the boundaries were moved out even further.

As would be expected from looking at the generalized forces, the flutter results for the three calculations also match each other very closely. A large variation in the flutter-reduced frequency-with-mass ratio $\left(\text{defined as } M_0/(\pi b^2 s\,\rho)\right)$ is shown in Figure 19, with the critical k-value for the problem being solved here of order 0.05. Figures 20 and 21 present the flutter speed index $\left(\text{defined as } U_F/(b\,\omega\,\sqrt{\mu})\right)$ and flutter frequency ratio (defined as ω_F/ω) versus mass ratio. Both the flutter speed index and the frequency ratio are relatively insensitive to the mass ratio. The exception is the flutter speed index for low values of reduced frequency, which shows the expected rapid increase in index at very small values of mass ratio.

The curves of flutter speed index versus mass ratio are smooth and essentially parallel to each other. Assuming the FAST results match the experimental results, OPTRAN3 without thickness provides a flutter speed index curve that is between 2% and 3% nonconservative, and OPTRAN3 with thickness provides a boundary that is between 1% and 2% nonconservative.

9.0 CONCLUSIONS

The work for this report includes a derivation of a coordinate transformation for swept and tapered wings, reprogramming a CRAY-1 program for the CRAY-XMP and the Langley VPS-32 computer system, an investigation of the effect on accuracy of the location of the outer mesh boundaries, and a sample flutter calculation of a low-aspect-ratio rectangular wing.

The coordinate transformation for swept and tapered wings is essentially a shearing transformation in the plane of the planform, but with additional terms in the expressions for the streamwise variable so that continuity of second derivatives is maintained across the planform edges. This transformation was included in a pilot program and checked out on a planform of vanishing thickness.

An existing CRAY-1 program was rewritten to include the transformation described above for the Boeing CRAY-XMP and the NASA Langley VPS-32 computer system. The CRAY-XMP version, which made full use of the solid-state disk and the larger available core storage, proved to be nearly ten times more efficient than the CRAY-1 program. The VPS-32 version of the program was not nearly as efficient as the CRAY-XMP program.

Even with these improvements in efficiencies, the CRAY-XMP program is marginally efficient for practical flutter evaluation problems. However, another version of the program developed by Rowe and Ehlers (ref. 21), in which improved boundary conditions permit a reduction in mesh size and (ultimately) in the number of unknowns, may provide a means for reducing computer costs to the point where these harmonic finite difference programs would be practical.

A study was made of the effect of mesh boundary location on accuracy for small values of reduced frequency. It was found that for smaller k-values, the boundaries had to be moved further out to retain accuracy. Relatively good correlation was obtained down to $k = 0.01$ at $M = 0.8$.

Finally, the application of OPTRAN3 to a flutter analysis was demonstrated with calculations for a rectangular wing.

REFERENCES

1. Ehlers, F. E.: "A Finite Difference Method for the Solution of the Transonic Flow Around Harmonically Oscillating Wings." NASA CR-2257, January 1974.

2. Weatherill, W. H.; Ehlers, F. E.; and Sebastian, J. D.: "Computation of the Transonic Perturbation Flow Fields Around Two- and Three-Dimensional Oscillating Wings." NASA CR-2599, December 1975.

3. Weatherill, W. H.; Sebastian, J. D.; and Ehlers, F. E.: "The Practical Application of a Finite Difference Method of Analyzing Transonic Flow Over Oscillating Airfoils and Wings." NASA CR-2933, 1978.

4. Ehlers, F. E.; Sebastian, J. D.; and Weatherill, W. H.: "An Investigation of Several Factors Involved in a Finite Difference Procedure for Analyzing the Transonic Flow About Oscillating Airfoils and Wings." NASA CR-159143, 1979.

5. Weatherill, W. H.; and Ehlers, F. E.: "A User's Guide for A344–A Program Using a Finite Difference Method to Analyze Transonic Flow Over Oscillating Airfoils." NASA CR-159141, 1979.

6. Weatherill, W. H.; Ehlers, F. E.; Yip, E.; and Sebastian, J. D.: "Further Investigation of a Finite Difference Procedure for Analyzing the Transonic Flow About Harmonically Oscillating Airfoils and Wings." NASA CR-3195, May 1980.

7. Ehlers, F. E.; and Weatherill, W. H.: "A Harmonic Analysis Method for Unsteady Transonic Flow and Its Application to the Flutter of Airfoils." NASA CR-3537, May 1982.

8. Ehlers, F.E.; Weatherill, W.H.; and Yip, E.L.: "Development and Application of Algorithms for Calculating the transonic Flow About Harmonically Oscillating Wings." NASA CR-172376, October 1984.

9. Klunker, E. B.: "Contribution to Methods of Calculating the Flow About Thin Lifting Wings at Transonic Speeds—Analytic Expressions for the Far Field." NASA TN D-6530, 1971.

10. Engquist, B.; and Majda, A.: "Radiation Boundary Conditions for Acoustic and Elastic Wave Calculations." *Communications on Pure and Applied Mathematics,* Vol. 32, May 1979, pp. 313-357.

11. Murman, E. M.; and Cole, J. D.: "Calculation of Plane Steady Transonic Flow." *AIAA Journal,* Vol. 9, January 1971, pp. 114-121.

12. Krupp, J. A.; and Murman, E. M.: "Computation of Transconic Flows Past Lifting Airfoils and Slender Bodies." *AIAA Journal,* Vol. 10, July 1972, pp. 880-887.

13. Goorjian, P.; and Guruswamy, P.: "An Efficient Coordinate Transformation Technique for Unsteady Transonic Aerodynamic Analysis of Low Aspect Ratio Wings." AIAA Paper 84-8072-CP, 25th AIAA SDM Conference, May 1984.

14. Rowe, W. S.; Winther, B. A.; and Redman, M. C.: "Prediction of Unsteady Aerodynamic Loadings Caused by Trailing Edge Control Surface Motions in Subsonic Compressible Flow–Analysis and Results," NASA CR-2003, March 1972.

15. Redman, M. C.; Rowe, W. S.; and Winther, B. A.: "Prediction of Unsteady Aerodynamic Loadings Caused by Trailing Edge Control Surface Motions in Subsonic Compressible Flow–Computer Program Description," NASA CR-112015, March 1972.

16. Borland C. J.; and Rizzetta, D. P.: "Transonic Unsteady Aerodynamics for Aeroelastic Applications–Vol. I: Technical Development Summary," AFWAL TR 80-3107, April 1982.

17. Seidel, D.A., Bennett, R. M., and Whitlow, W., Jr.: "An Exploratory Study of Finite Difference Grids for Transonic Unsteady Aerodynamics." AIAA Paper No. 83-0503, presented at the AIAA 21st Aerospace Sciences Meeting and Technical Display, Reno, Nevada, January 10-13, 1983, also NASA TM 84583, February 1972.

18. Bland, S. R.: "Development of Low Frequency Kernel Function Aerodynamics for Comparison with Time Dependent Finite Difference Methods," NASA Technical Memorandum 83283, May 1982.

19. Cole, Stanley R.: "Exploratory Flutter Test in a Cryogenic Wind Tunnel." AIAA Paper No. 85-0736, Presented at the 26th AIAA SDM Conference, April 1985.

20. Desmarais, R. N., and Bennett, R. M.: "User's Guide for a Modular Flutter Analysis System (FAST version 1.0)." NASA TM-78720, 1978.

21. Rowe, W. S., and Ehlers, F. E.: "Coupling Linearized Far-field Boundary Conditions with Non-linear Near-field Solutions in Transonic Flow." Final Report for AFOSR Contract F49620-83-c-0118, also Boeing document No. D6-52895, February 1988.

22. Batina, J. T., Seidel, D. A., Bland, S. R., and Bennett, R. M.: "Unsteady Transonic Flow Calculations for Realistic Aircraft Configurations." AIAA Paper No. 87-8050, April 6-8, 1987.

23. Batina, J. T.: "Unsteady Transonic Algorithm Improvements for Realistic Aircraft Applications." AIAA Paper No. 88-0105, January 11-14, 1988.

24. Yip, Elizabeth L.: "FORTRAN Subroutine for Out-of-Core Solutions of Large Complex Linear Systems." NASA CR-159142, November 1979.

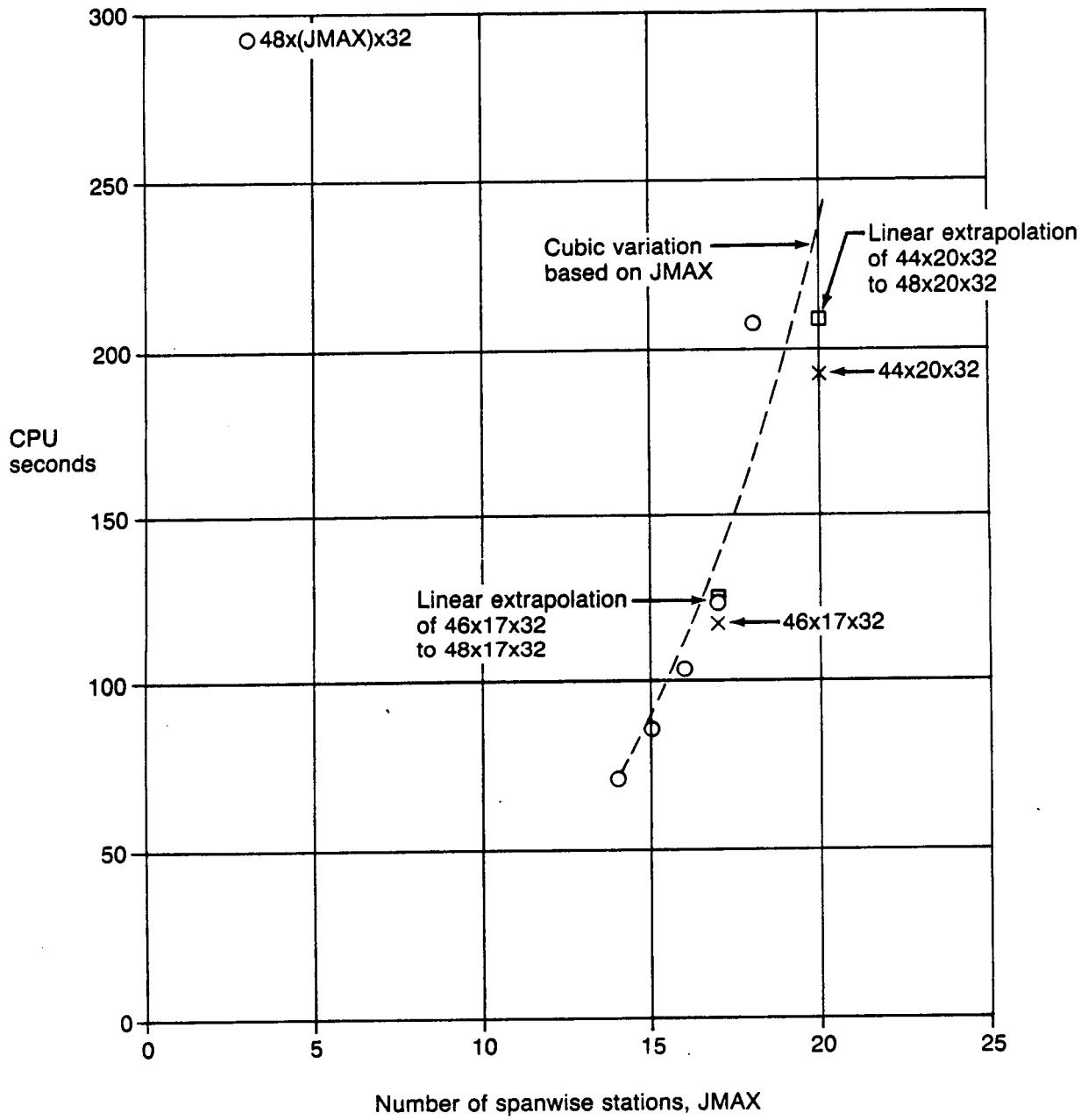

Figure 1. CPU Seconds Versus Number of Spanwise Stations; CRAY-XMP With SSD, Symmetric Problem

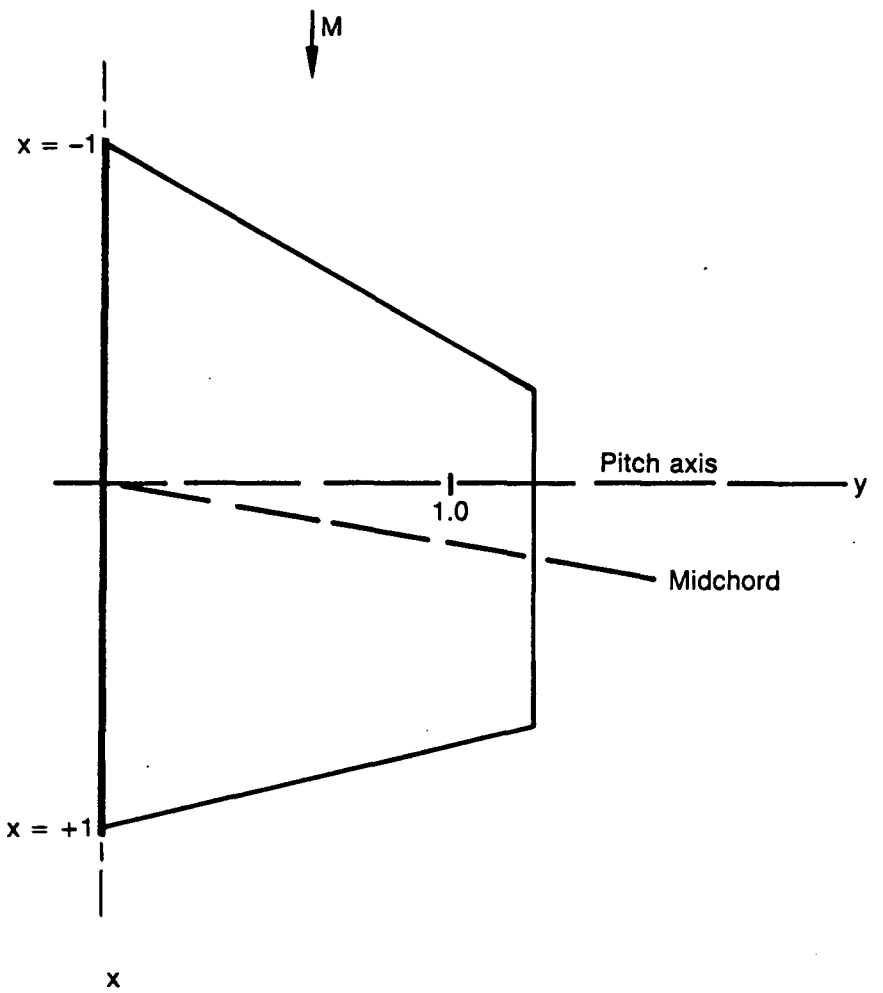

Figure 2. Planform for Swept and Tapered Wing Example

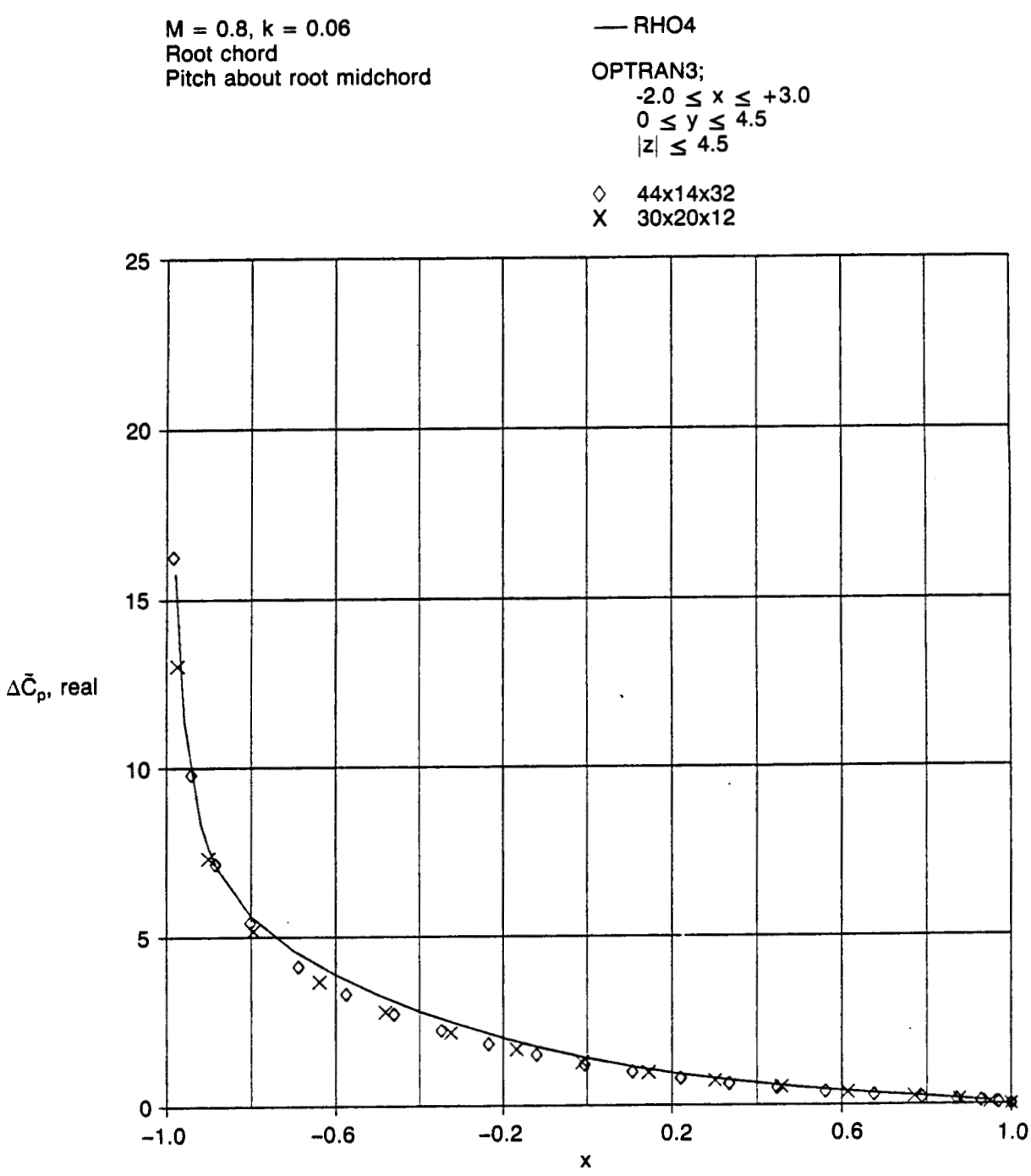

Figure 3a. Comparison of Pressure Distributions From OPTRAN3 and RHO4 for a Swept and Tapered Wing of Vanishing Thickness; M = 0.8, k = 0.06, Root Chord, Real Part

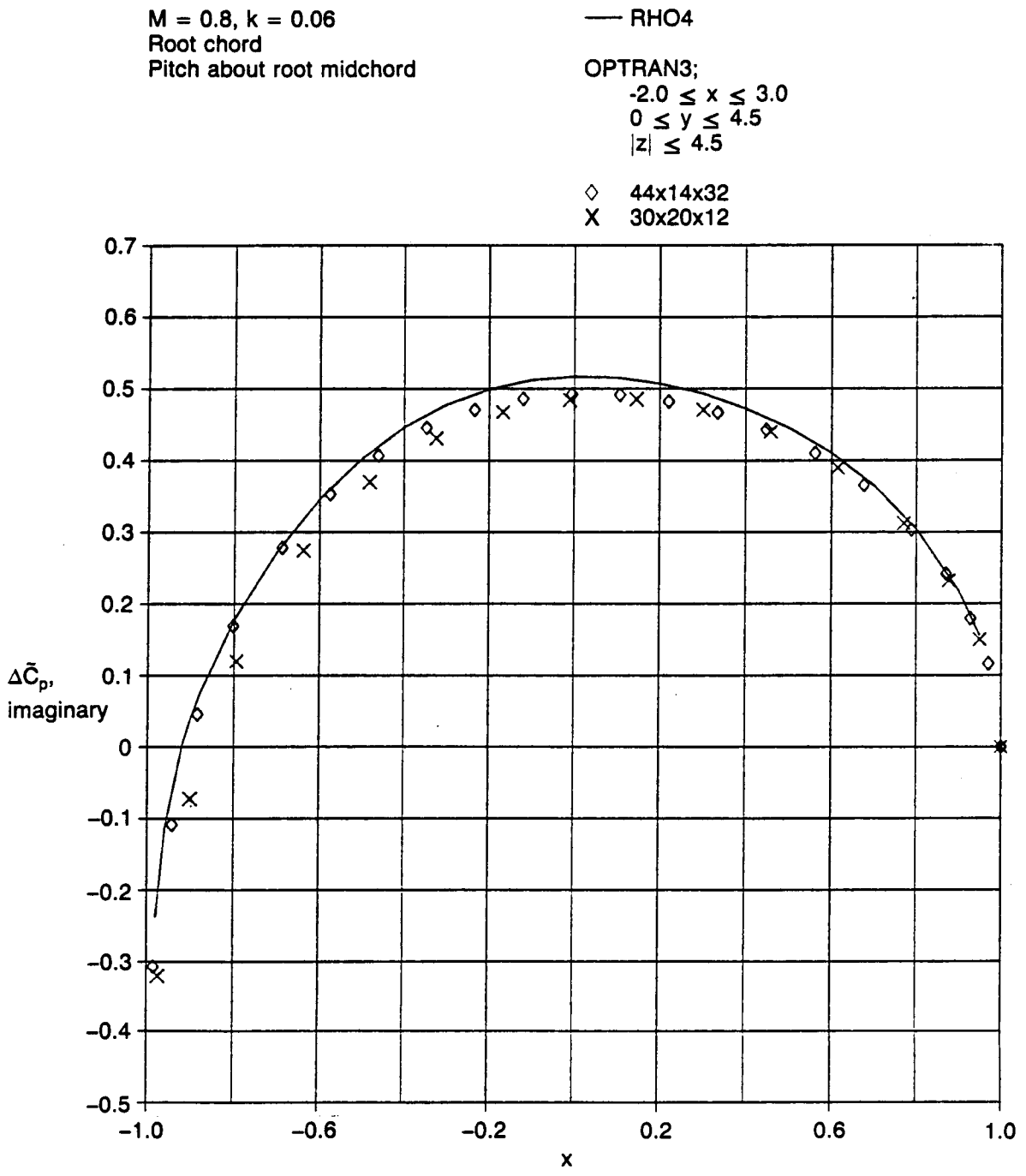

Figure 3b. Comparison of Pressure Distributions From OPTRAN3 and RHO4 for a Swept and Tapered Wing of Vanishing Thickness; M = 0.8, k = 0.06, Root Chord, Imaginary Part

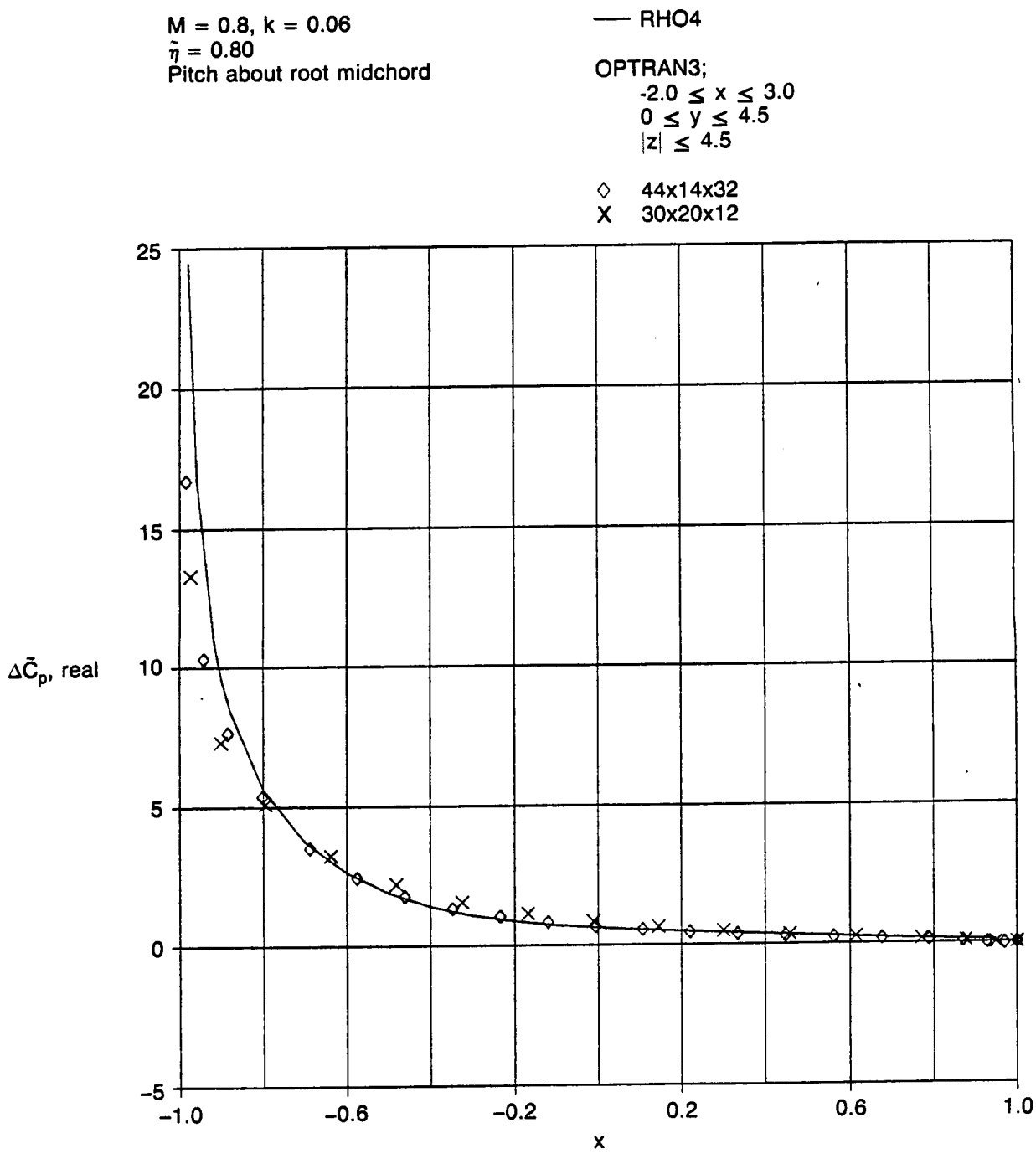

Figure 3c. Comparison of Pressure Distributions From OPTRAN3 and RHO4 for a Swept and Tapered Wing of Vanishing Thickness; M = 0.8, k = 0.06, $\tilde{\eta}$ = 0.8, Real Part

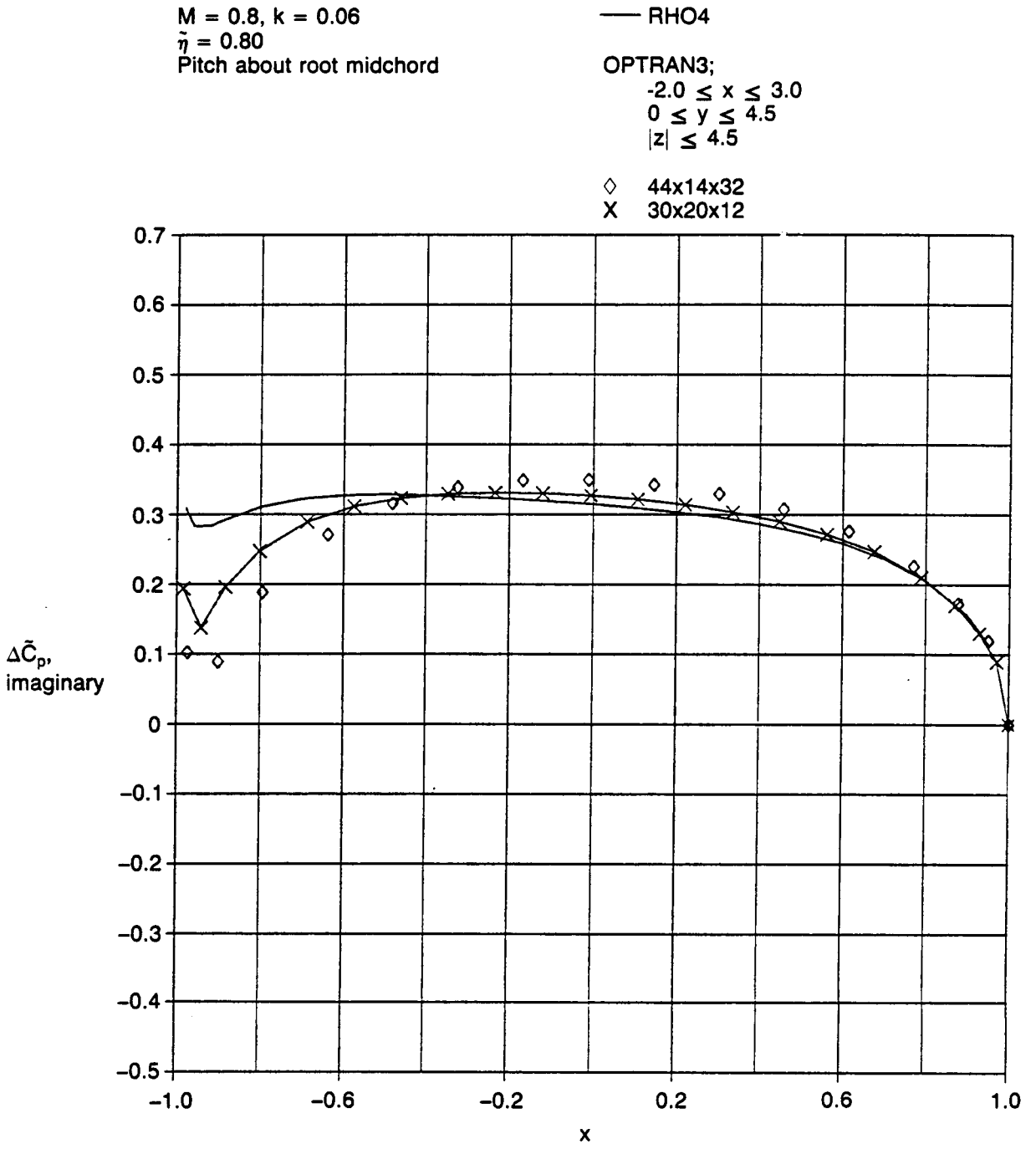

Figure 3d. Comparison of Pressure Distributions From OPTRAN3 and RHO4 for a Swept and Tapered Wing of Vanishing Thickness; M = 0.8, k = 0.06, $\tilde{\eta}$ = 0.8, Imaginary Part

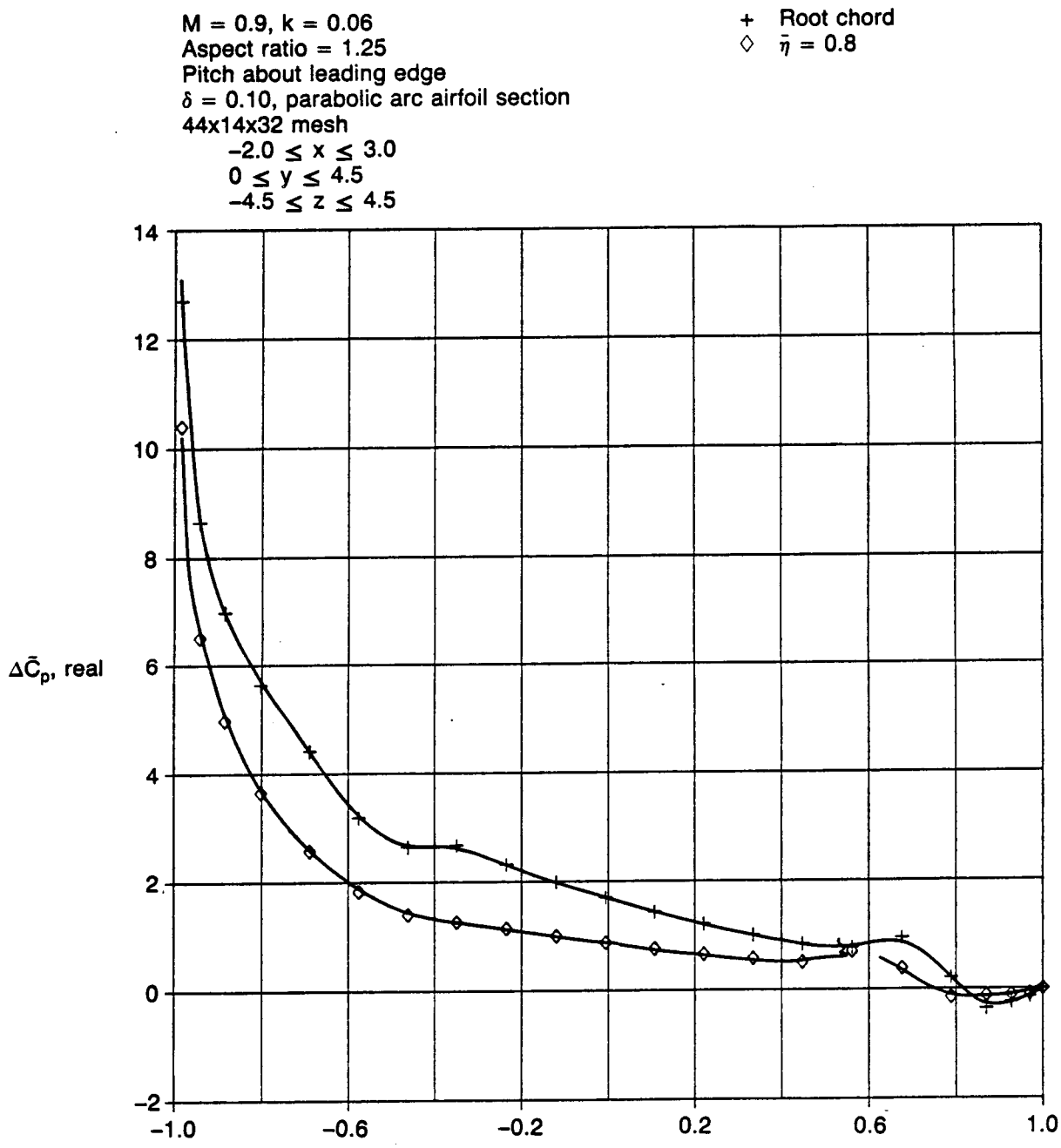

Figure 4a. Pressure Distributions for a Rectangular Wing With a Parabolic Arc Airfoil Section; M = 0.9, k = 0.06, Real Part

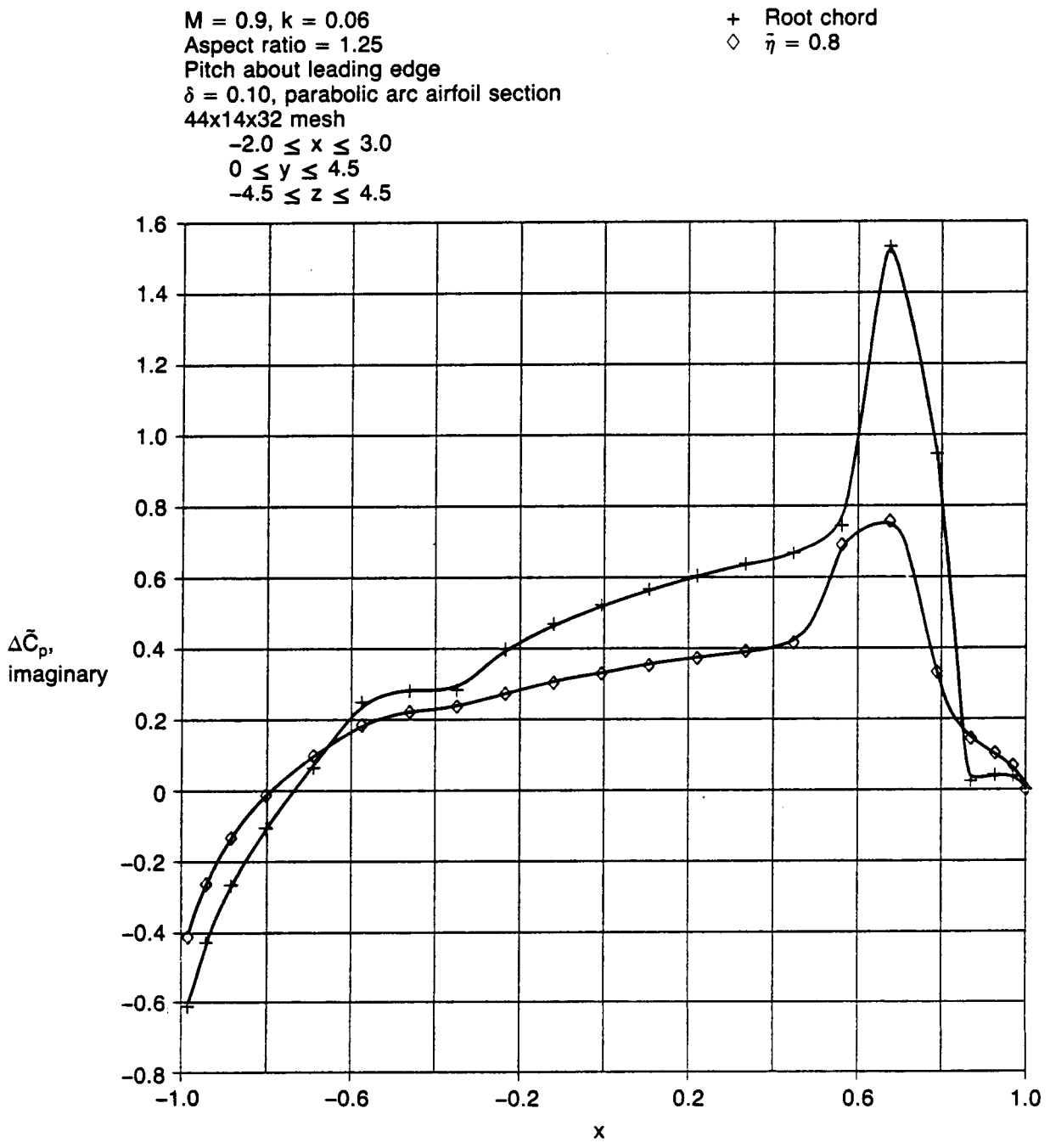

Figure 4b. Pressure Distributions for a Rectangular Wing With a Parabolic Arc Airfoil Section; M = 0.9, k = 0.06, Imaginary Part

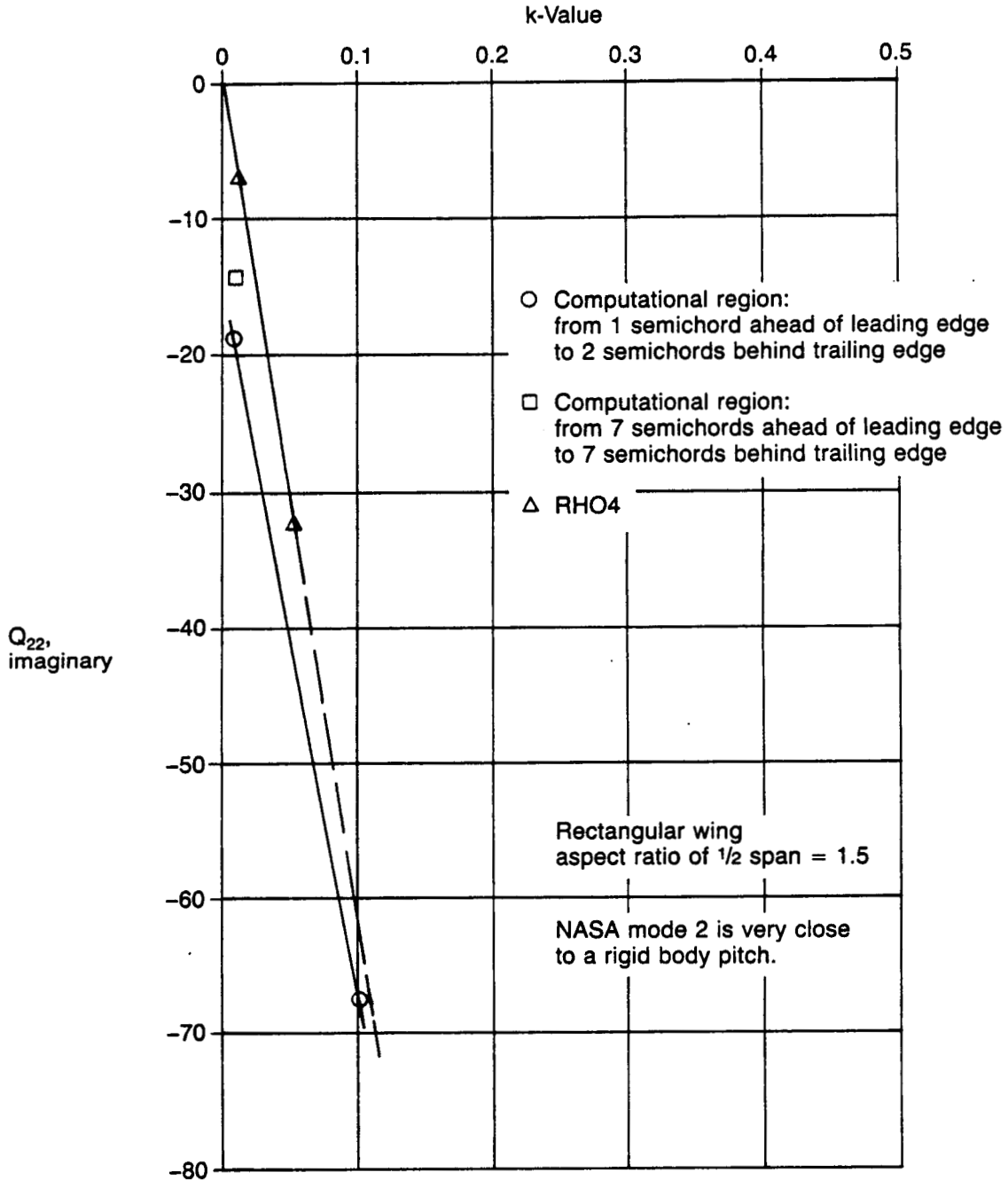

Figure 5. Imaginary Part of the Total Generalized Force Versus k-Value for NASA Mode 2 for M = 0.8

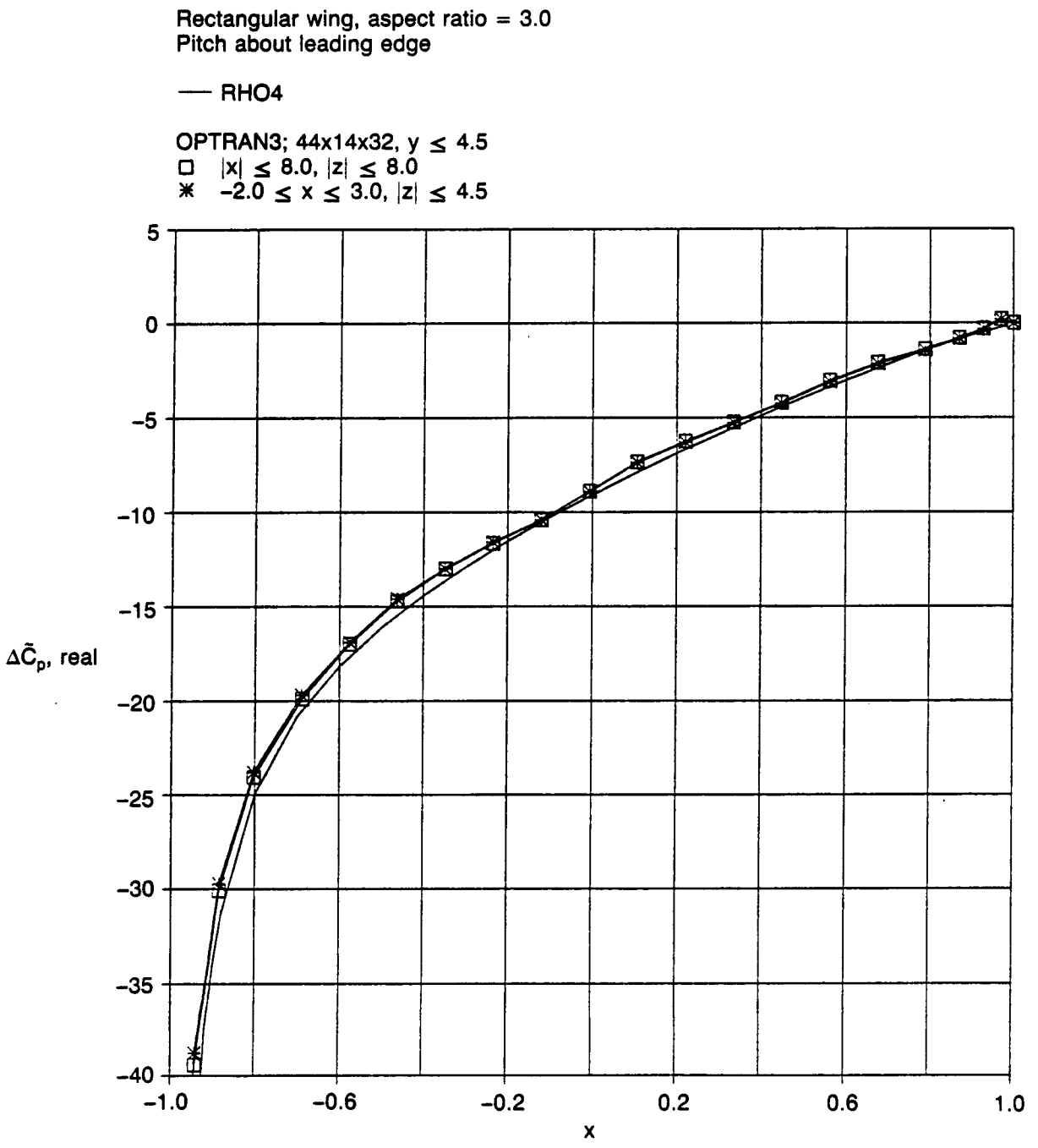

Figure 6a. Comparison of Pressure Distributions From OPTRAN3 for Two Outer Boundary Locations and for RHO4; Rectangular Wing, M = 0.8, k = 0.3, Root Chord, Real Part

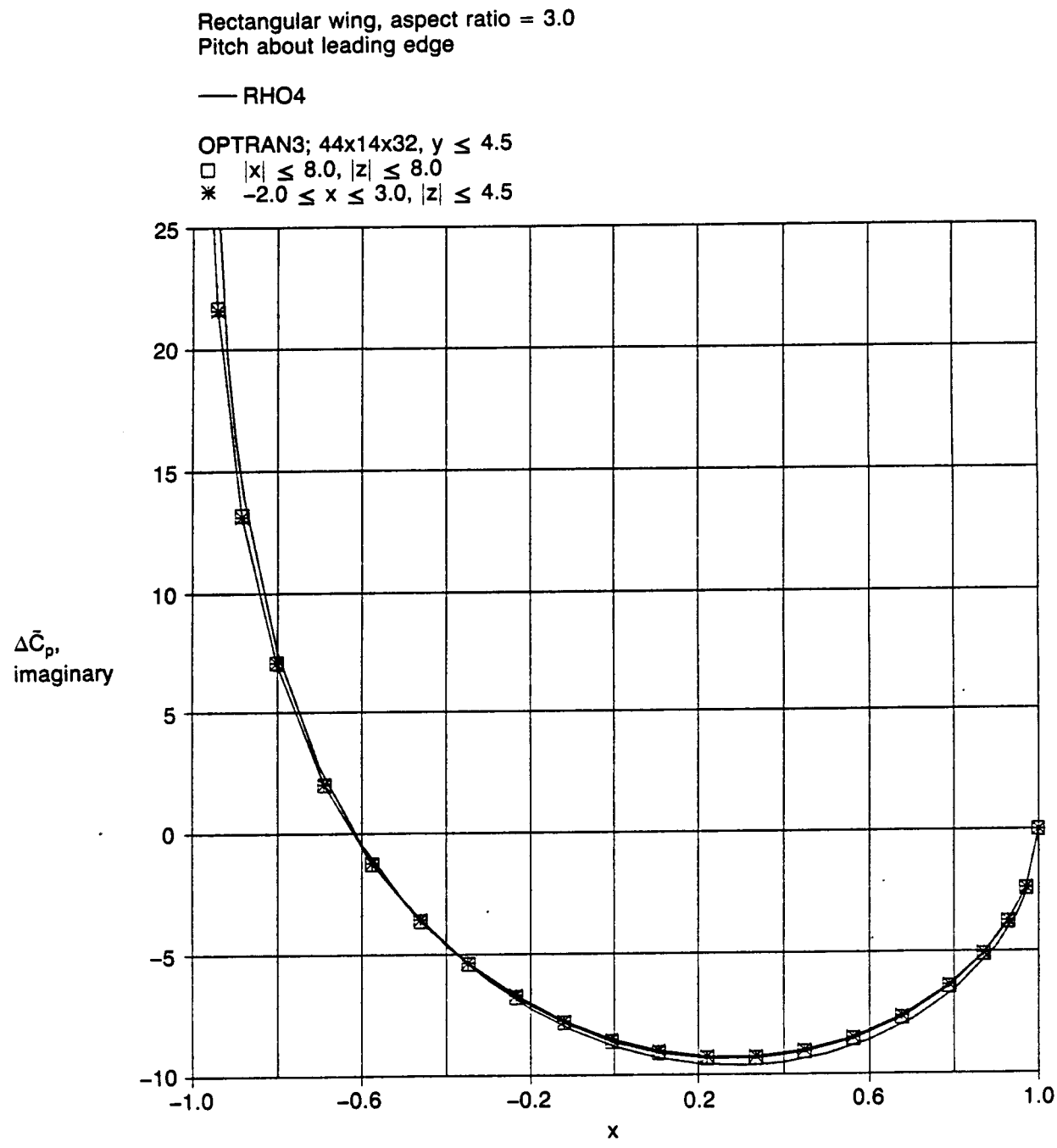

Figure 6b. Comparison of Pressure Distributions From OPTRAN3 for Two Outer Boundary Locations and for RHO4; Rectangular Wing, M = 0.8, k = 0.3, Root Chord, Imaginary Part

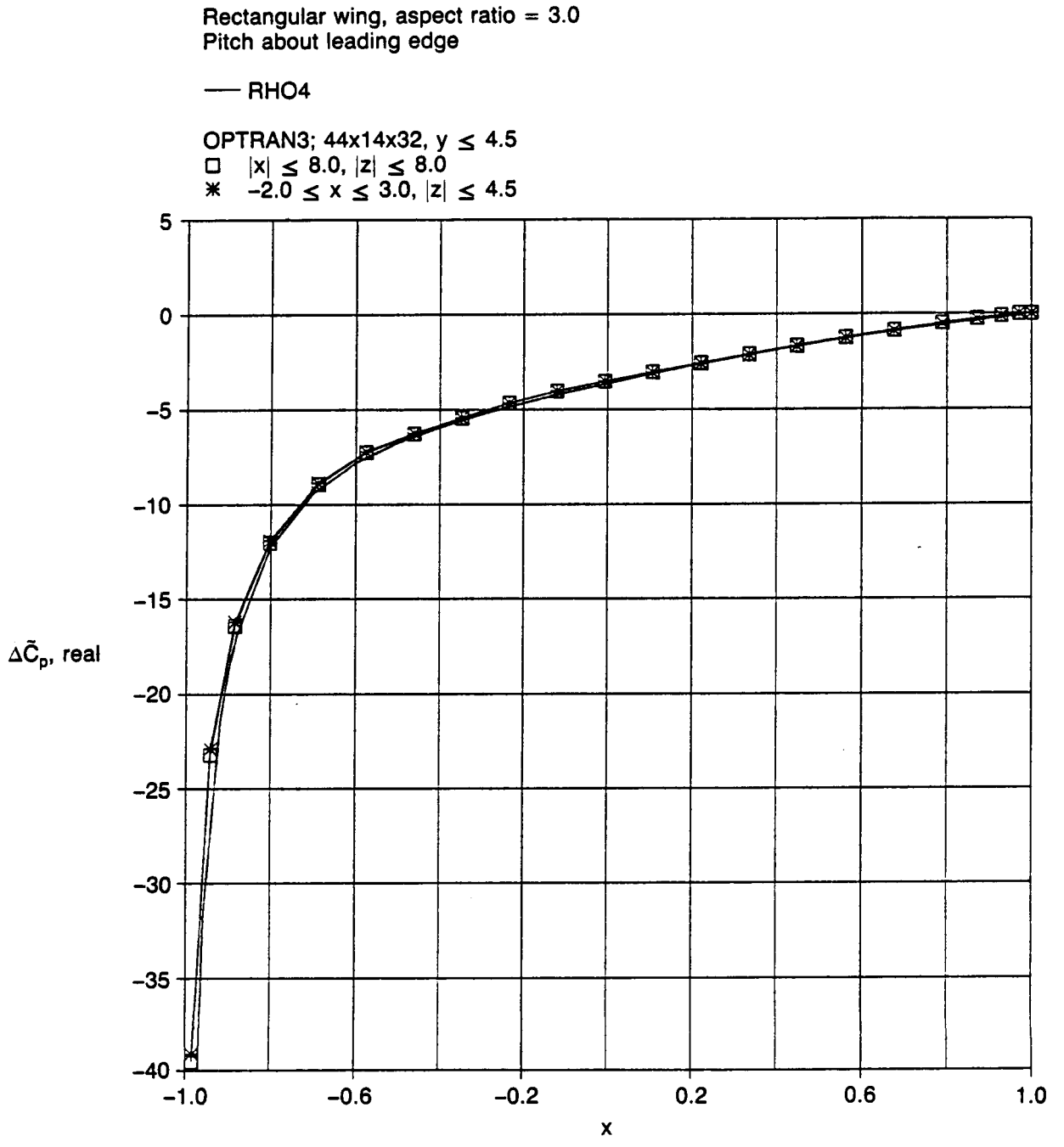

Figure 6c. Comparison of Pressure Distributions From OPTRAN3 for Two Outer Boundary Locations and for RHO4; Rectangular Wing, M = 0.8, k = 0.3, $\tilde{\eta}$ = 0.885, Real Part

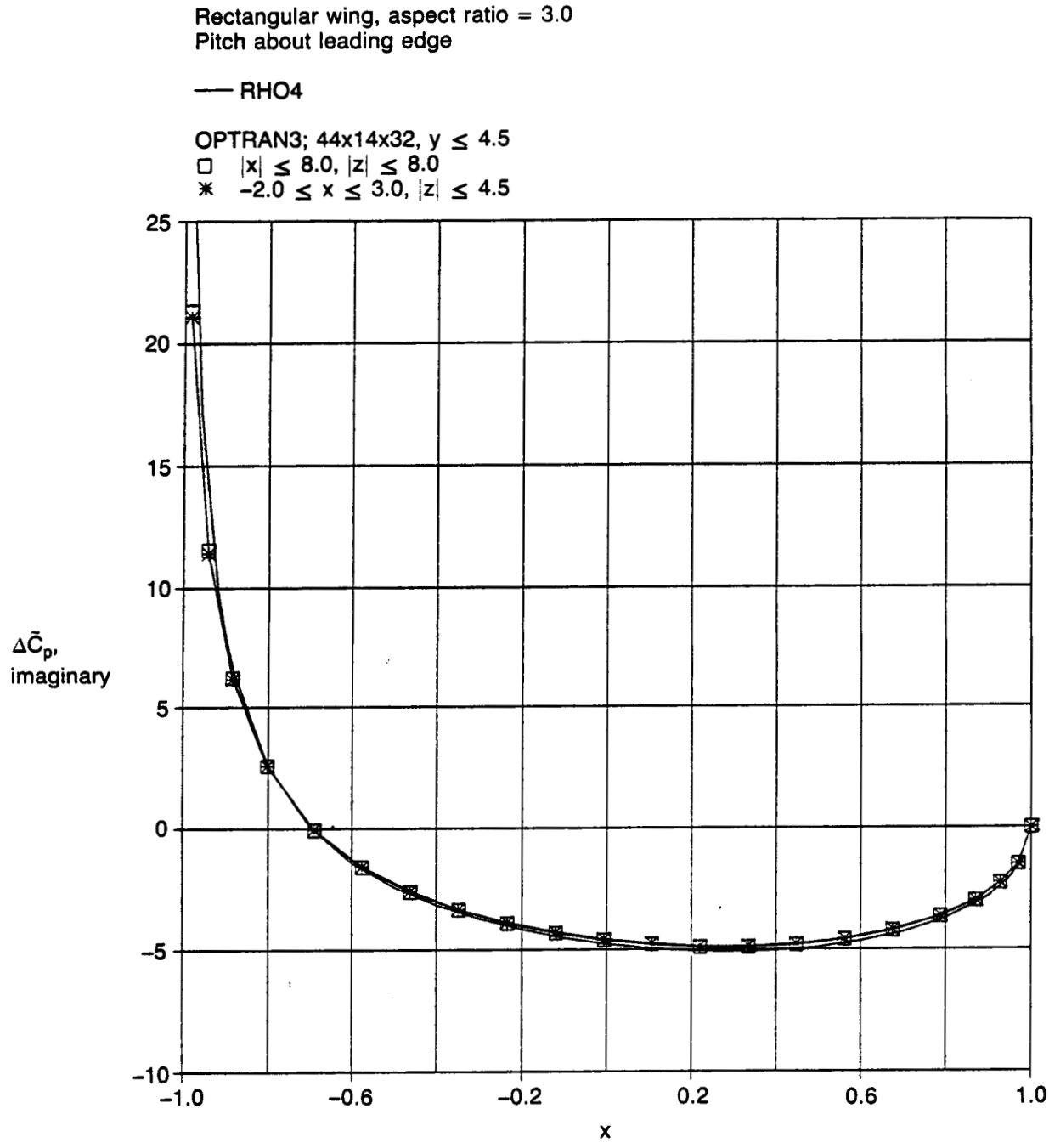

Figure 6d. Comparison of Pressure Distributions From OPTRAN3 for Two Outer Boundary Locations and for RHO4; Rectangular Wing, M = 0.8, k = 0.3, $\tilde{\eta}$ = 0.885, Imaginary Part

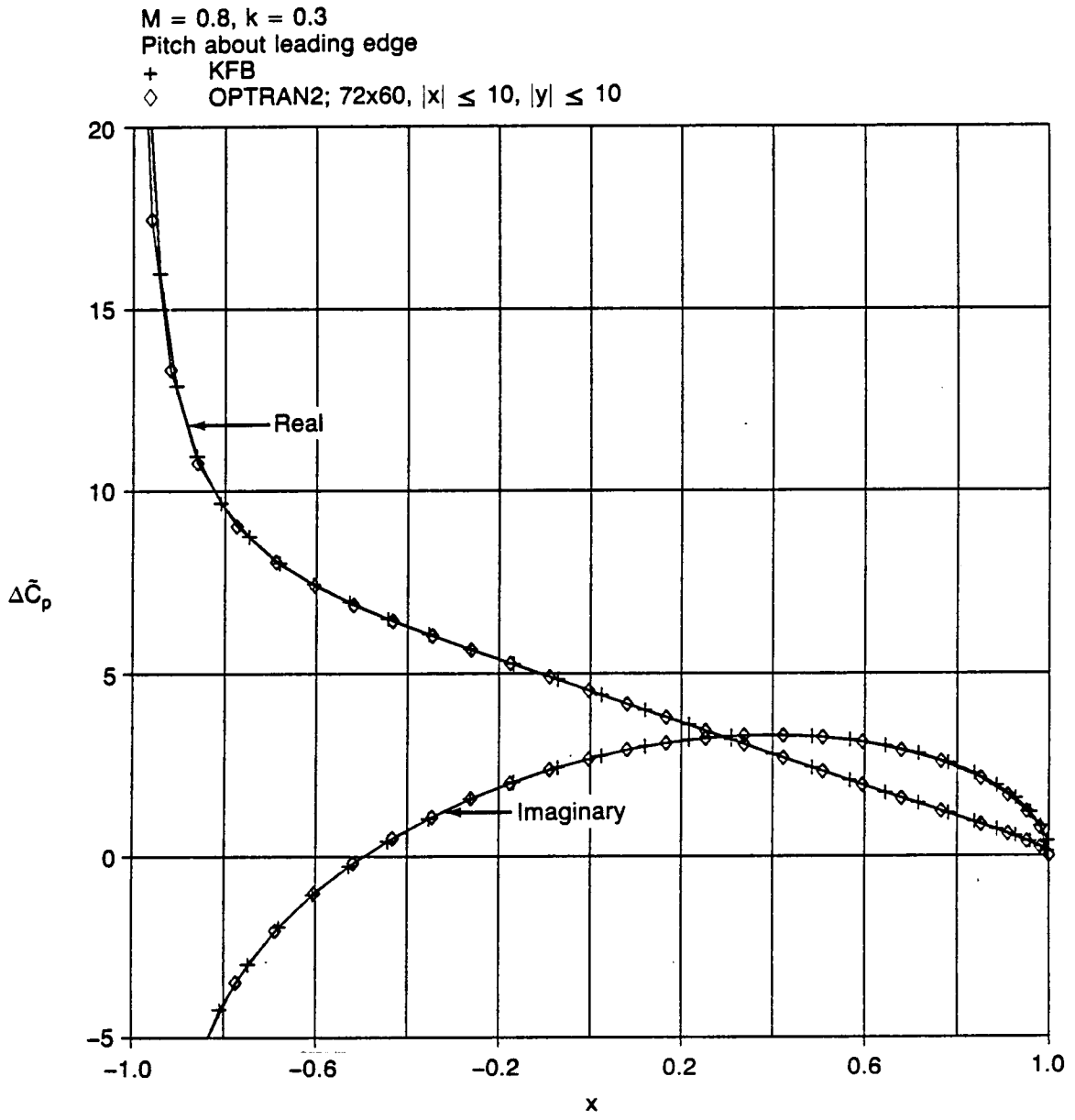

Figure 7. Comparison of Pressure Distributions From OPTRAN2 and KFB for a Typical Section; M = 0.8, k = 0.3

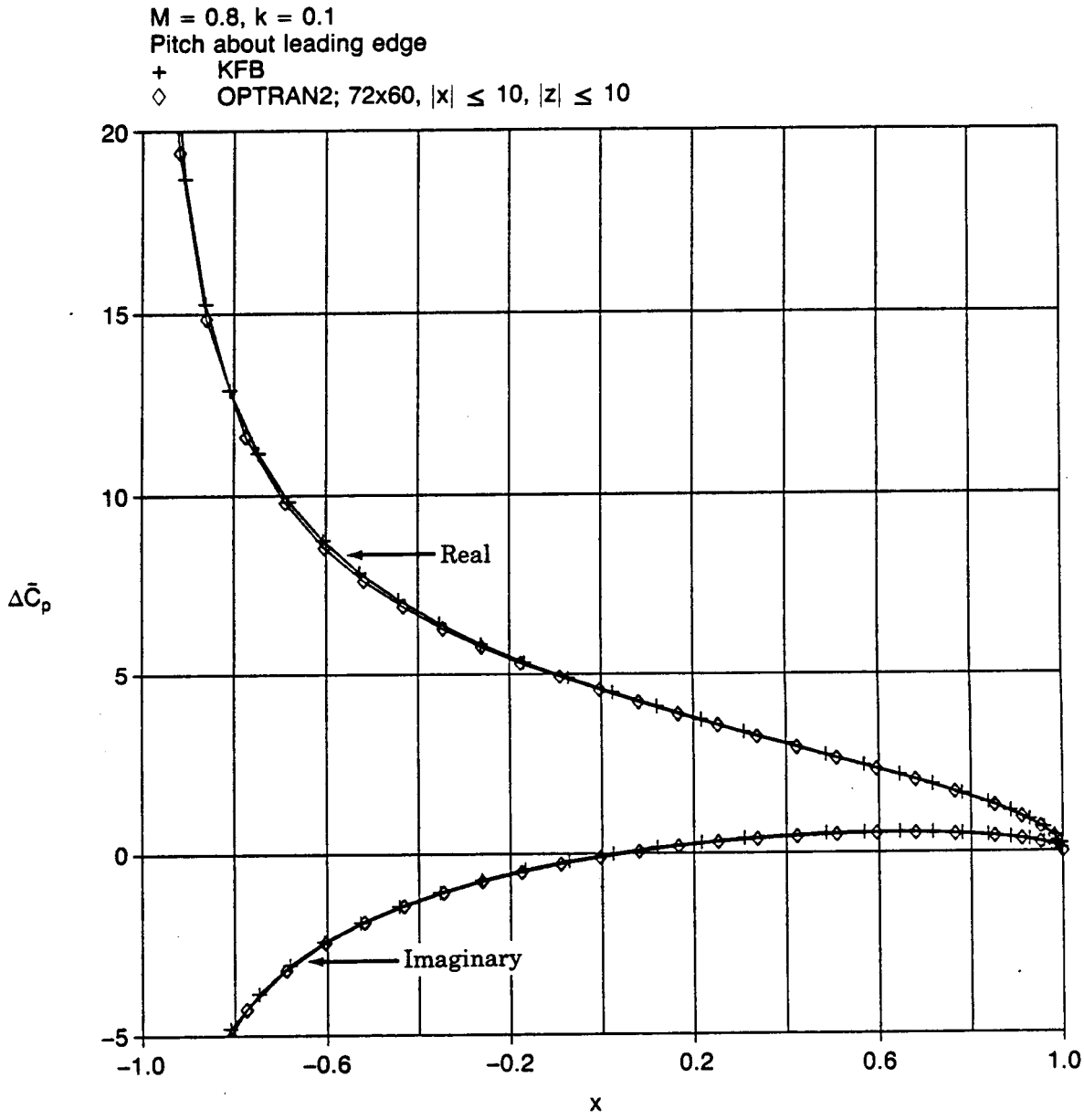

Figure 8. Comparison of Pressure Distributions From OPTRAN2 and KFB for a Typical Section; M = 0.8, k = 0.1

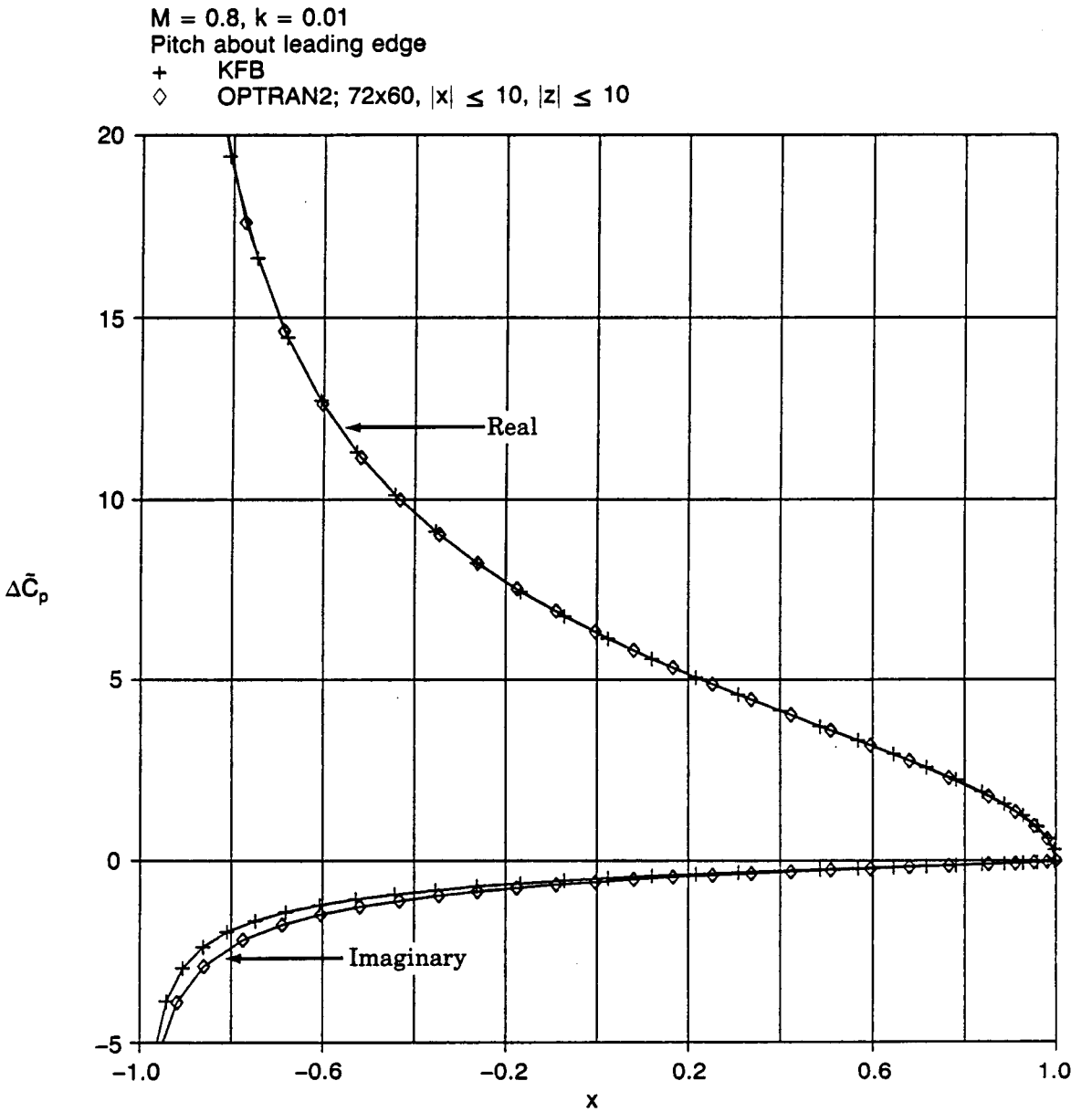

Figure 9. Comparison of Pressure Distributions From OPTRAN2 and KFB for a Typical Section; M = 0.8, k = 0.01

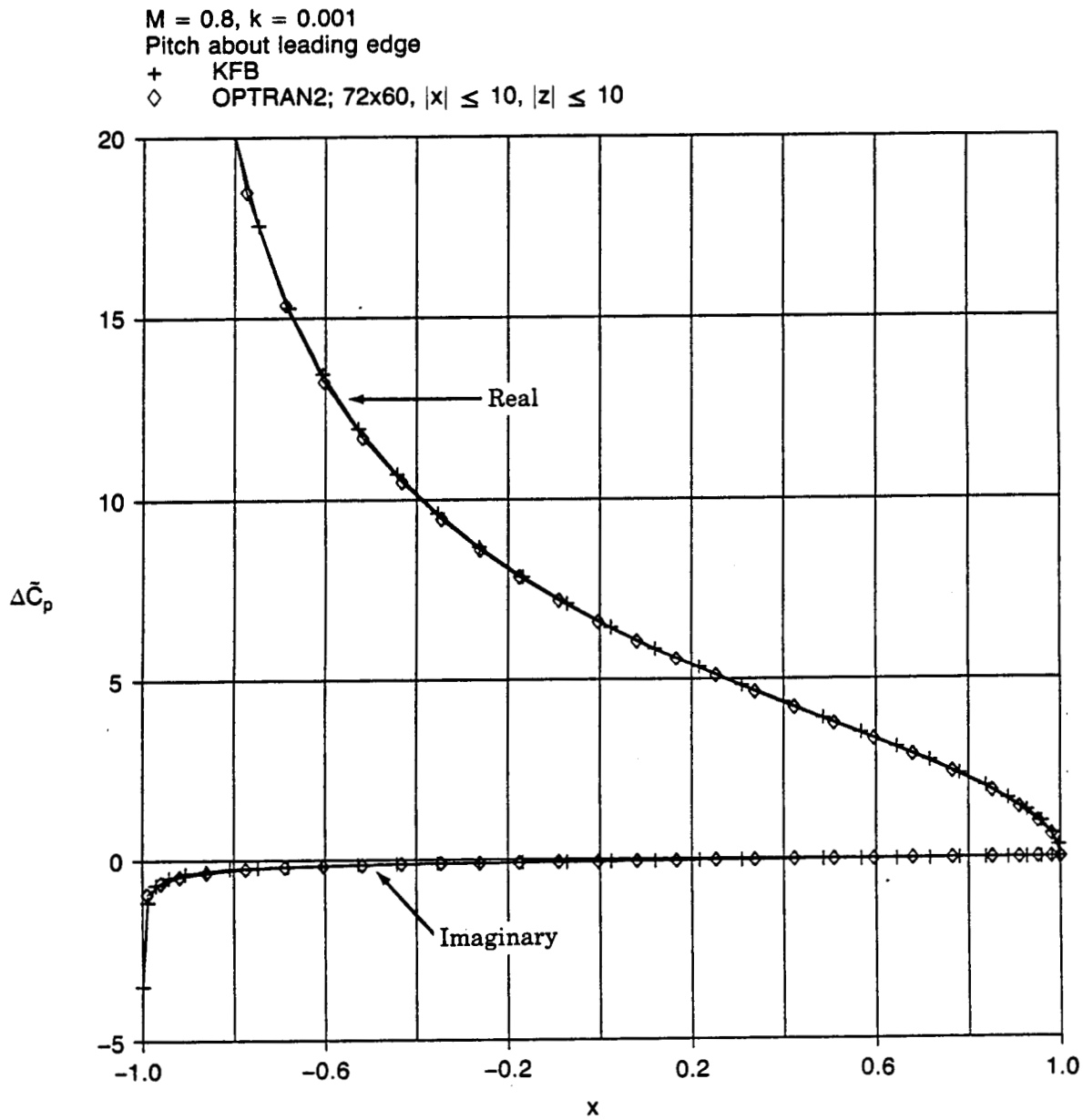

Figure 10. Comparison of Pressure Distributions From OPTRAN2 and KFB for a Typical Section; M = 0.8, k = 0.001

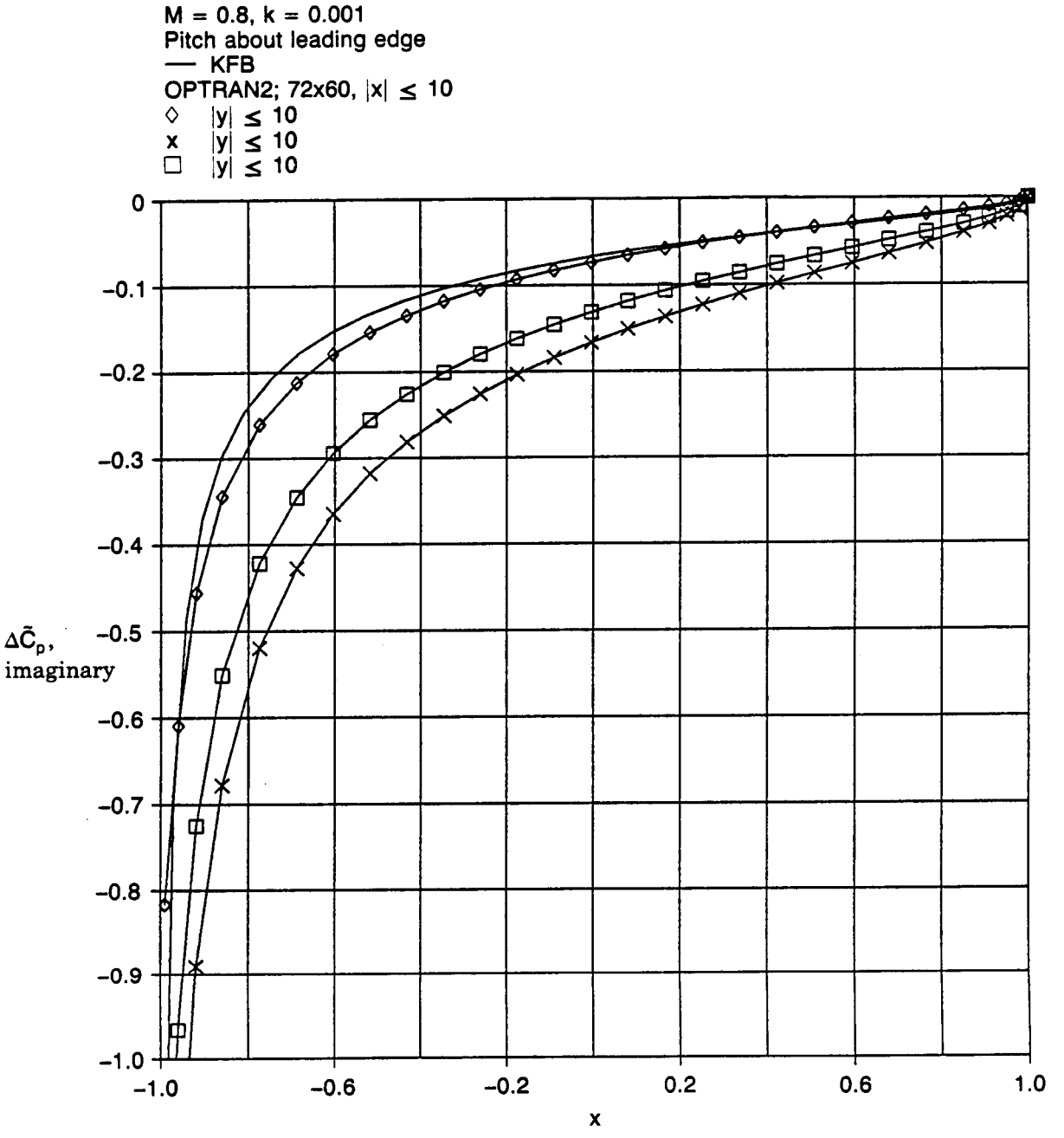

Figure 11. Comparison of Pressure Distributions From OPTRAN2 for Three Upper/Lower Boundary Locations and from KFB for a Typical Section; M = 0.8, k = 0.001, Imaginary Part

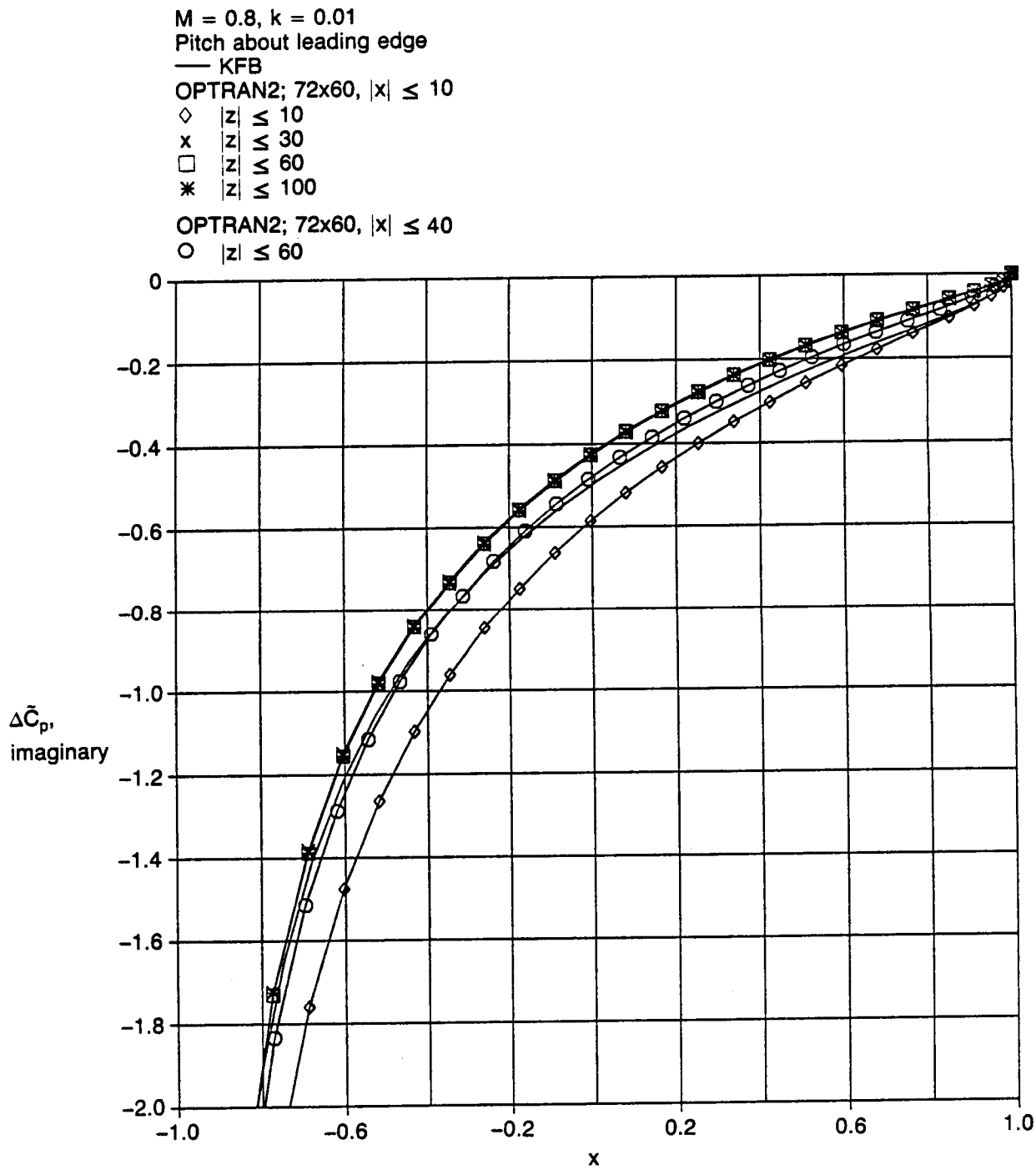

Figure 12. Comparison of Pressure Distributions From OPTRAN2 for Several Outer Boundary Locations and From KFB for a Typical Section; M = 0.8, k = 0.01, Imaginary Part

M = 0.8, k = 0.01
Rectangular wing, aspect ratio = 3.0
Pitch about leading edge
Root chord

— RHO4

OPTRAN3; 48 points in x, $|x| \leq 8.0$
32 points in z, $|z| \leq 8.0$
◇ 15 points in y, $y \leq 7.0$
x 16 points in y, $y \leq 11.75$
□ 17 points in y, $y \leq 16.75$

OPTRAN3:
✱ 48x14x32; $-8.0 \leq x \leq 3.0$, $|y| \leq 4.5$, $|z| \leq 4.5$

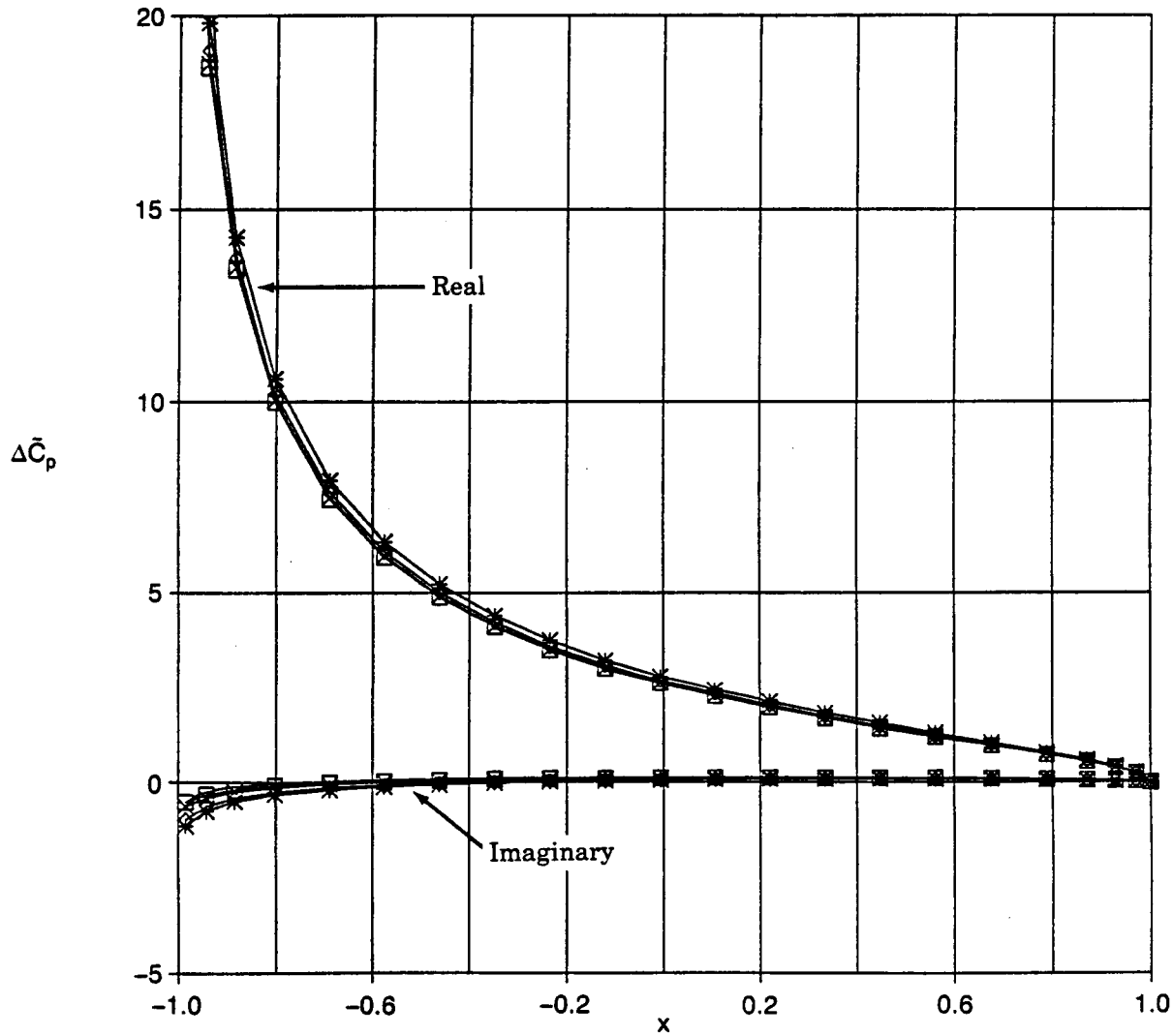

Figure 13a. Comparison of Pressure Distributions From OPTRAN3 for Four Outboard Boundary Locations and From RHO4 for a Rectangular Wing; M = 0.8, k = 0.01, Root Chord

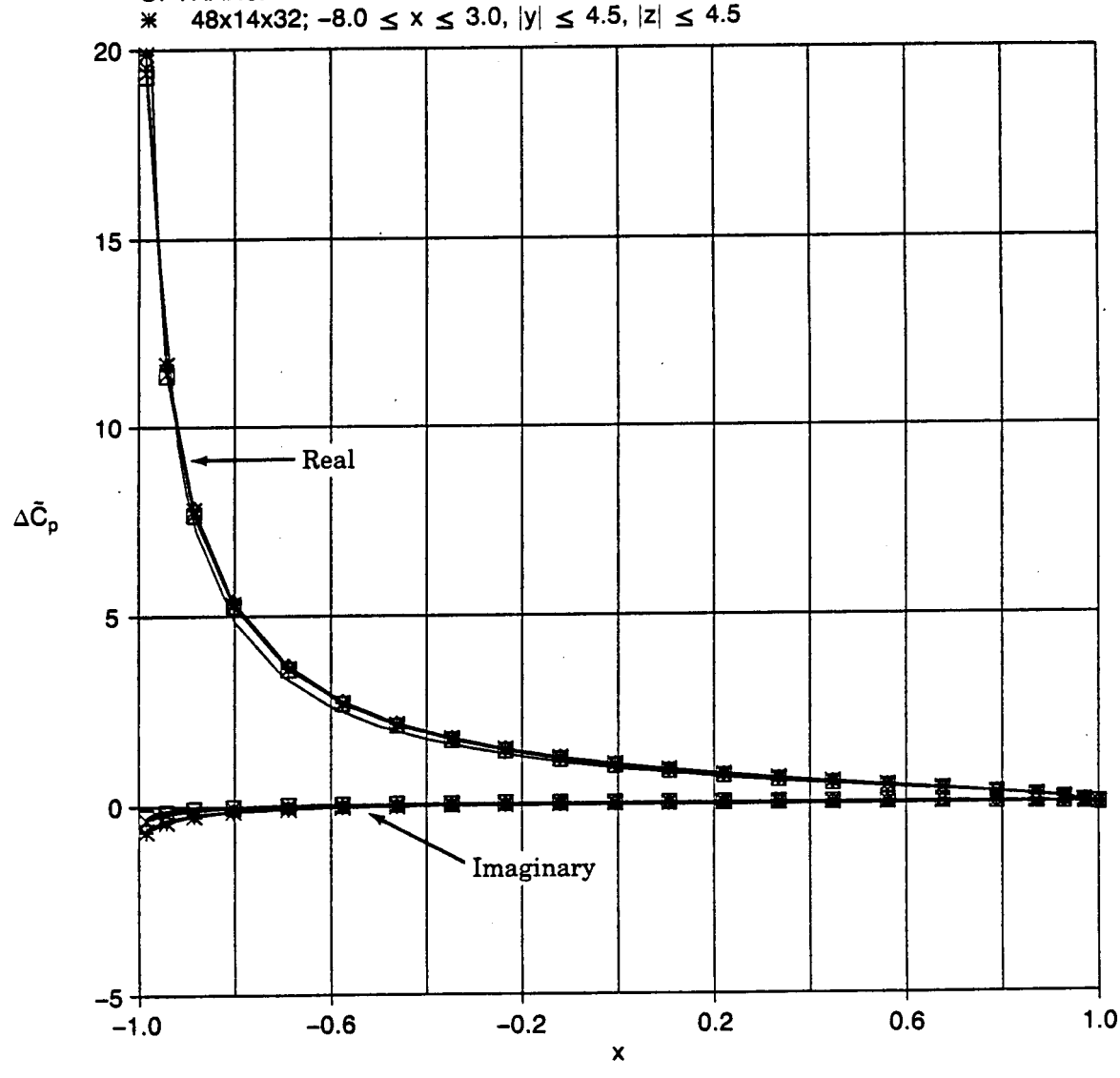

Figure 13b. Comparison of Pressure Distributions From OPTRAN3 for Four Outboard Boundary Locations and From RHO4 for a Rectangular Wing; M = 0.8, k = 0.01, η = 0.885

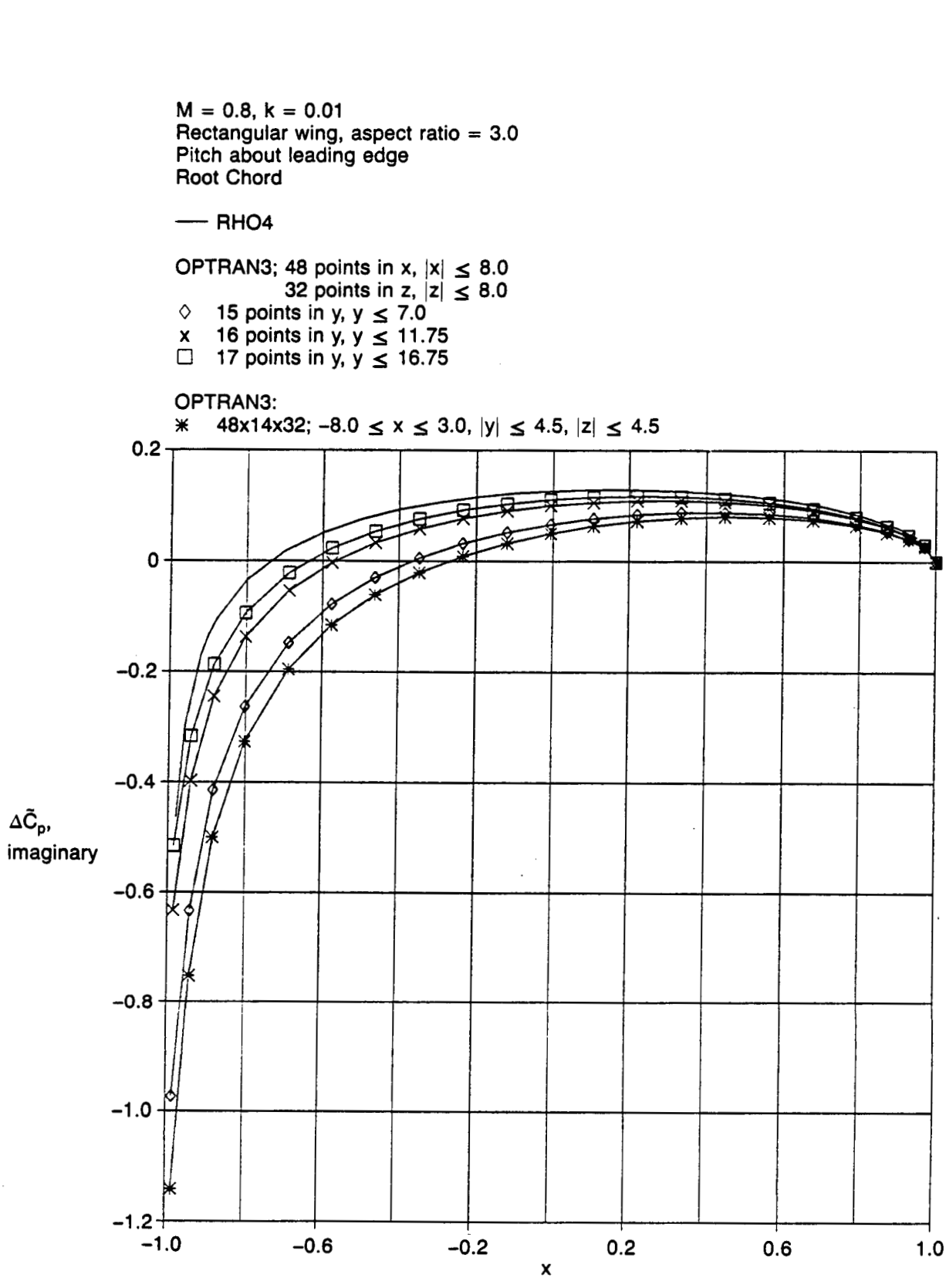

Figure 14a. Comparison of Pressure Distributions From OPTRAN3 for Four Outboard Boundary Locations and From RHO4 for a Rectangular Wing; M = 0.8, k = 0.01, Imaginary Part, Enlarged Scale, Root Chord

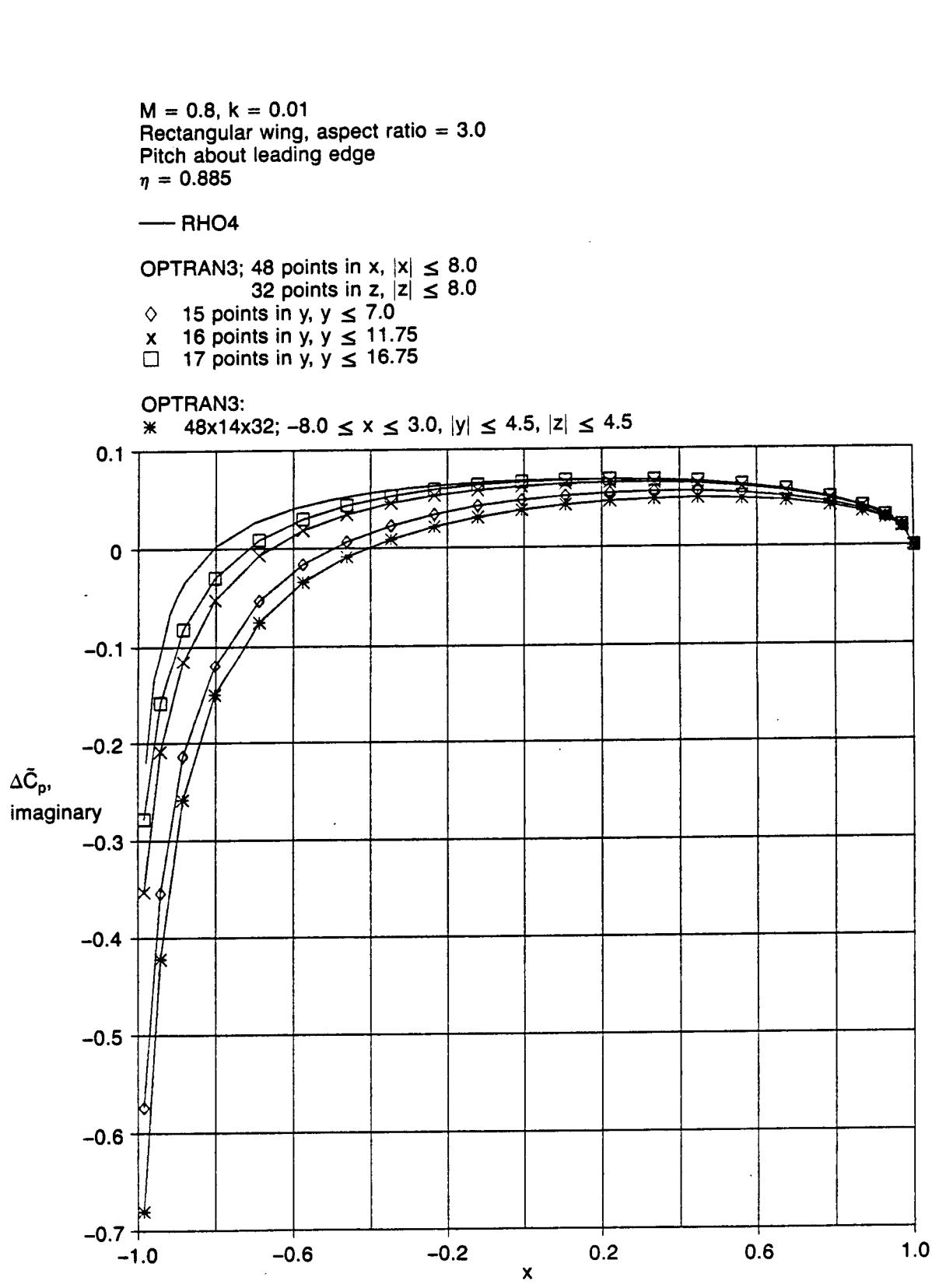

Figure 14b. Comparison of Pressure Distributions From OPTRAN3 for Four Outboard Boundary Locations and From RH04 for a Rectangular Wing; M = 0.8, k = 0.01, Imaginary Part, Enlarged Scale, $\tilde{\eta}$ = 0.885

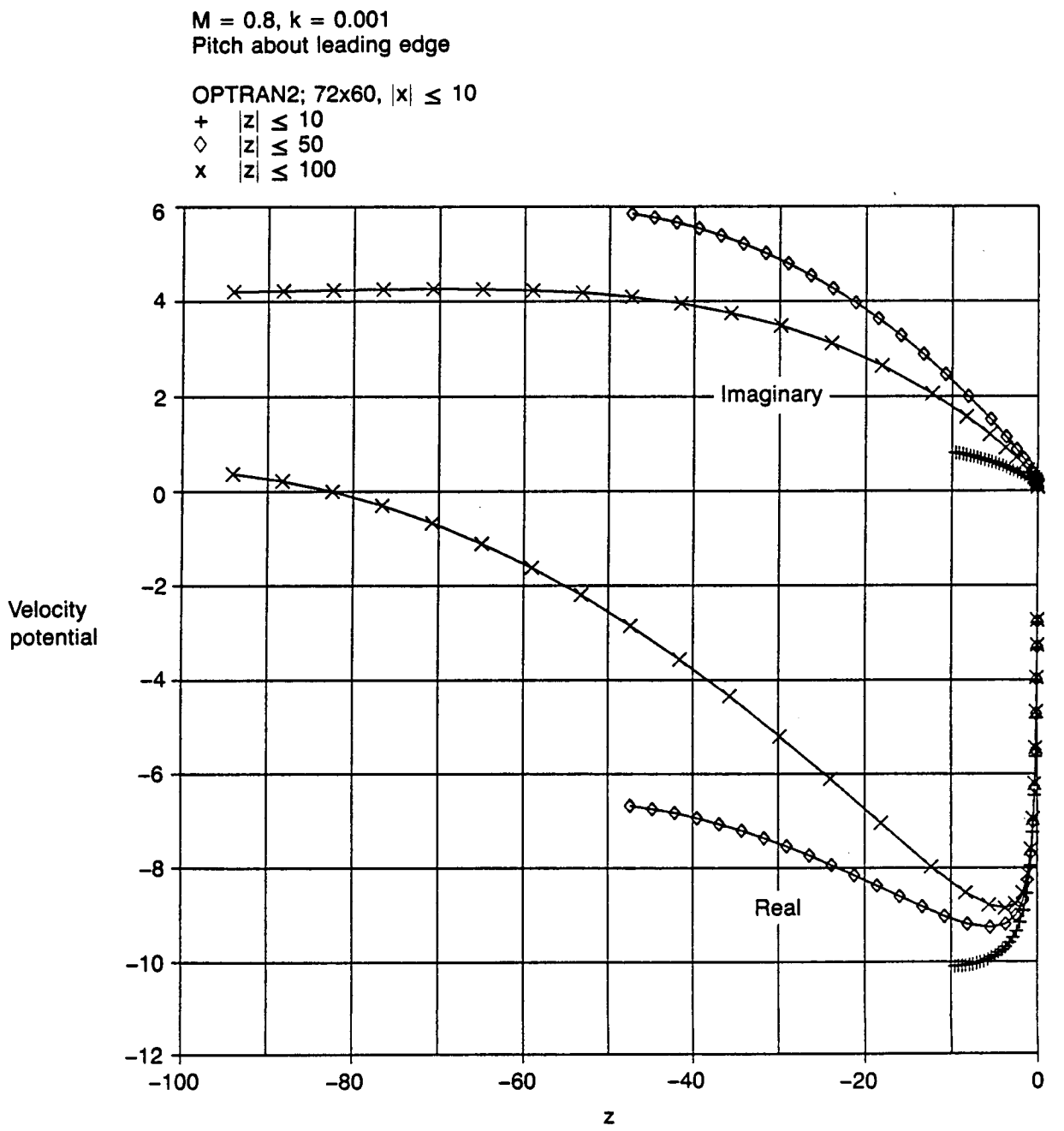

Figure 15a. Comparison of Velocity Potential Along a Column of Points From OPTRAN3 for Three Upper/Lower Boundary Locations for a Typical Section; M = 0.8, k = 0.001

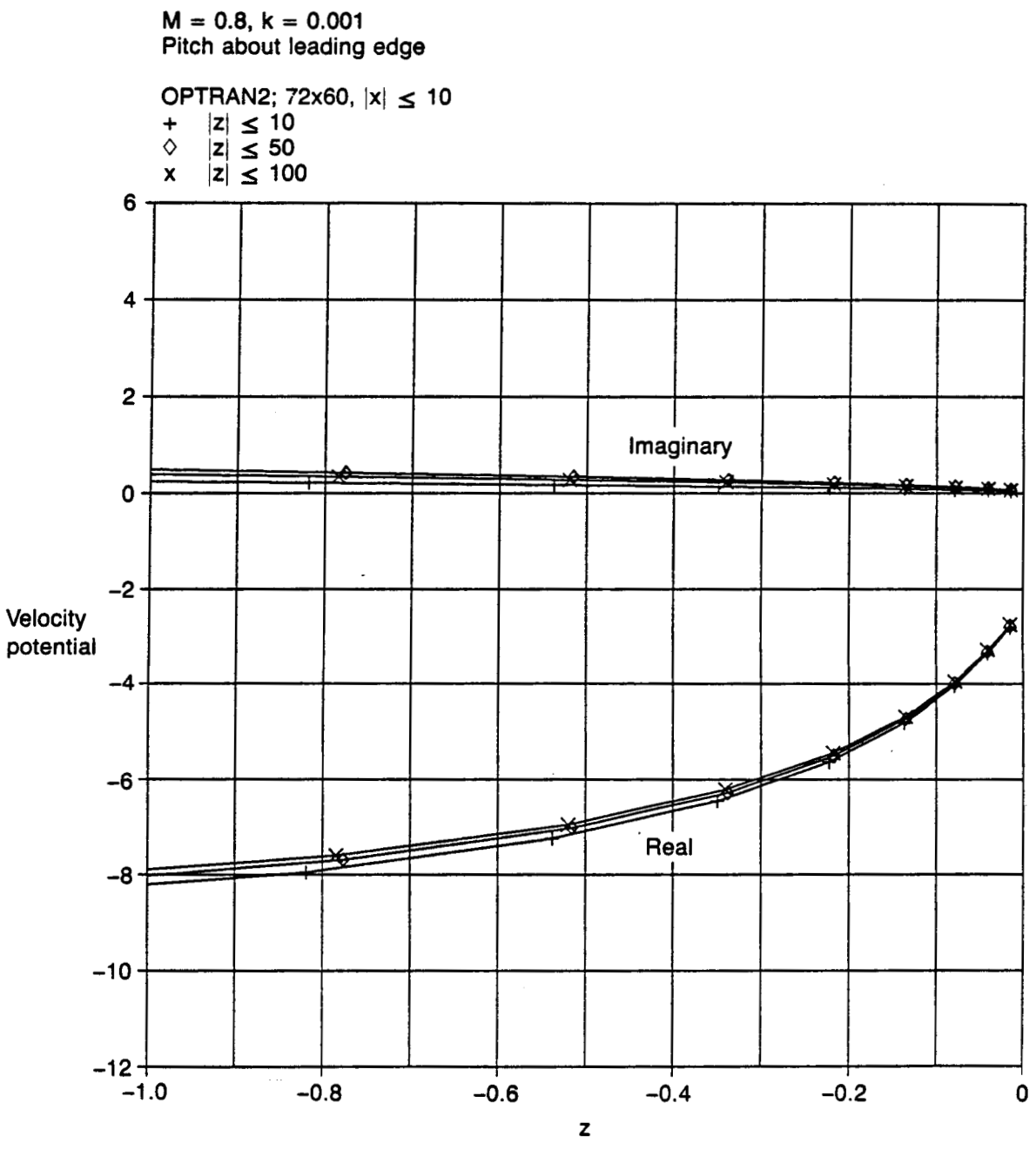

Figure 15b. Comparison of Velocity Potential Along a Column of Points From OPTRAN3 for Three Upper/Lower Boundary Locations for a Typical Section; M = 0.8, k = 0.001, Enlarged Scale

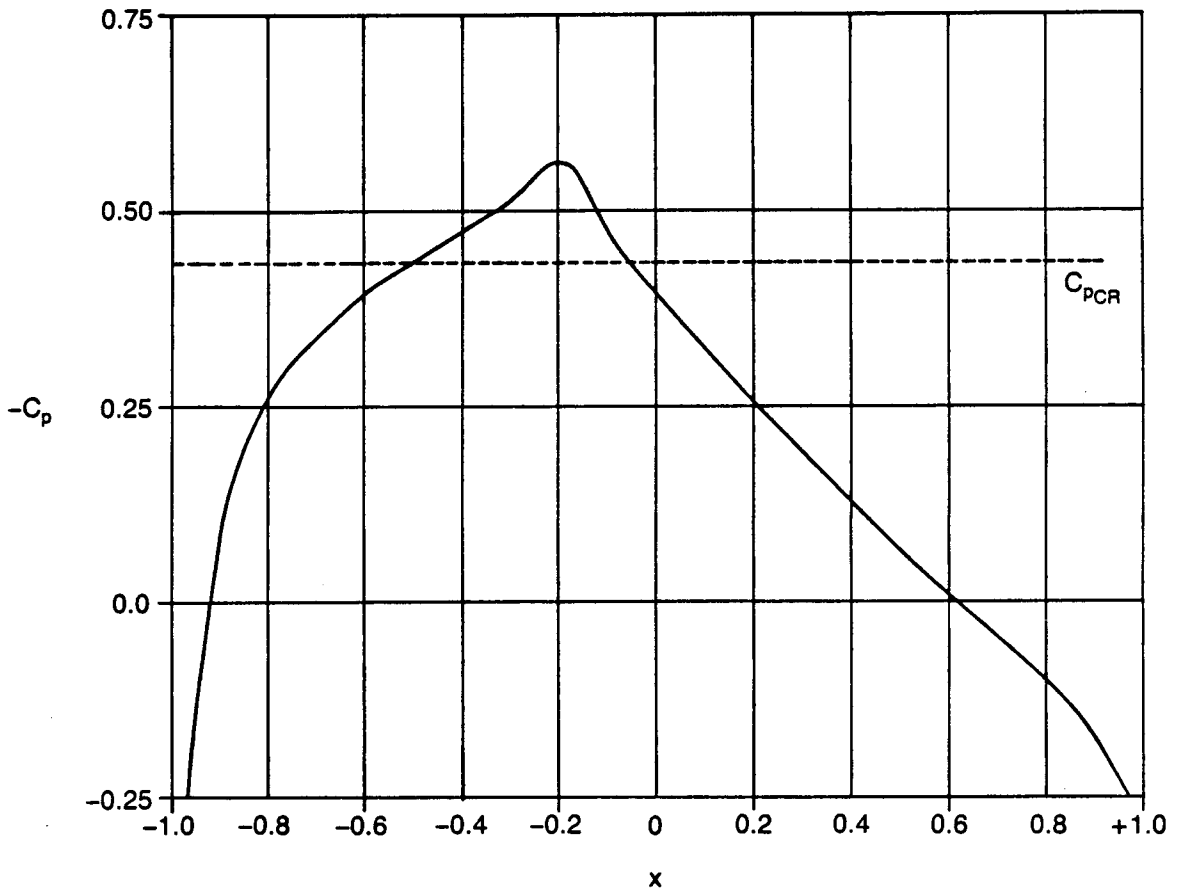

Figure 16. Steady Pressure Distribution Over the Root Chord of a Rectangular Wing With a NACA 64A010 Airfoil Section; Aspect Ratio = 3.0, M = 0.8

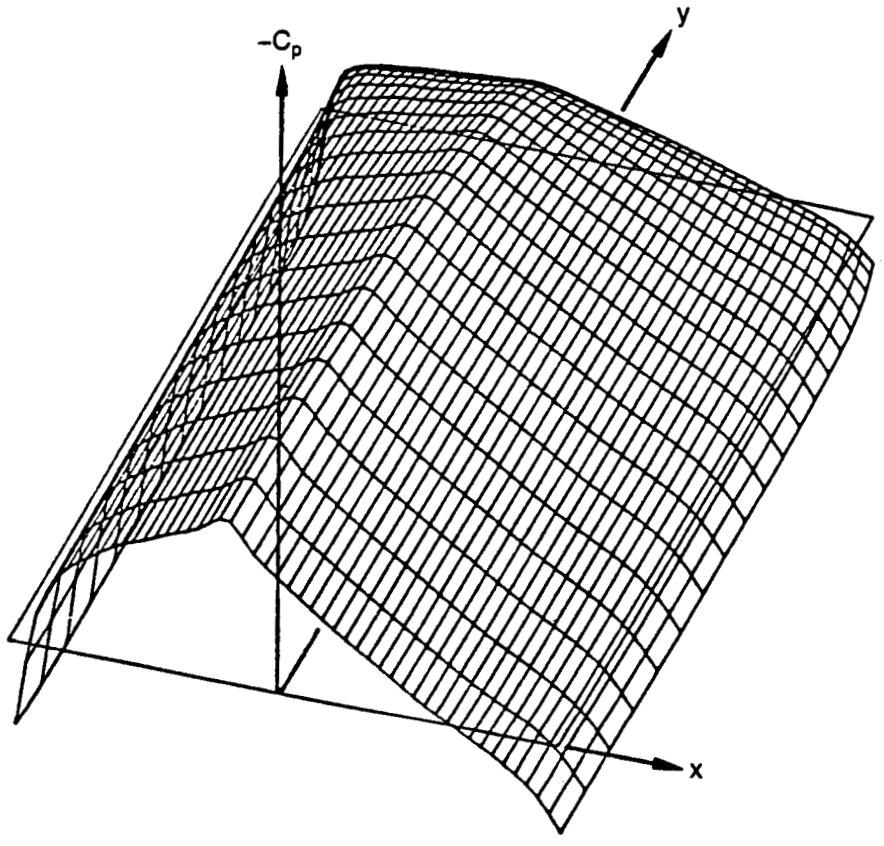

Figure 17. Steady Pressure Distribution Over the Upper Surface of a Rectangular Wing With a NACA 64A010 Airfoil Section; Aspect Ratio = 3.0, M = 0.8

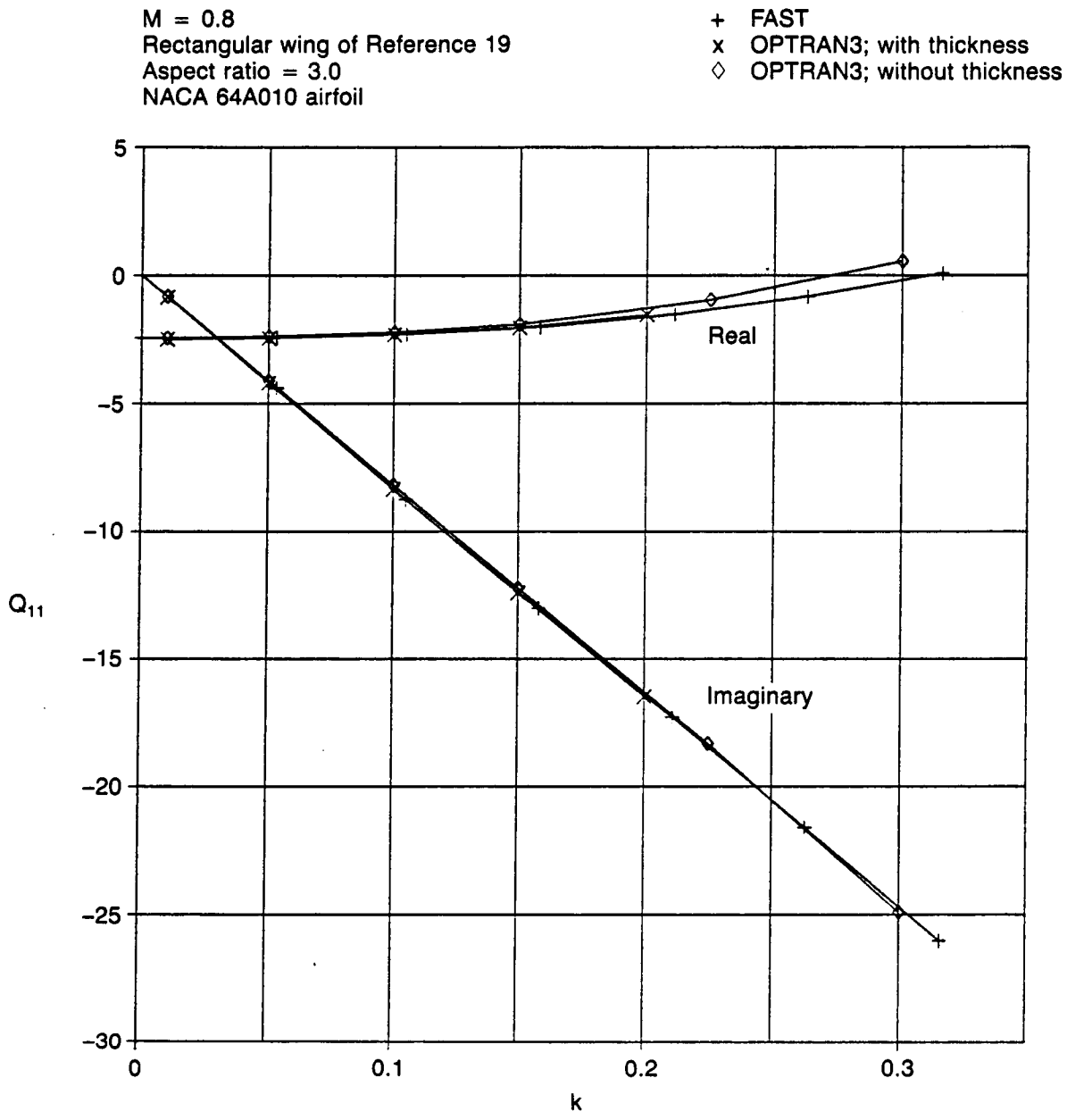

Figure 18a. The Q_{11} Generalized Force Versus Reduced Frequency for a Rectangular Wing; M = 0.8, Aspect Ratio = 3.0

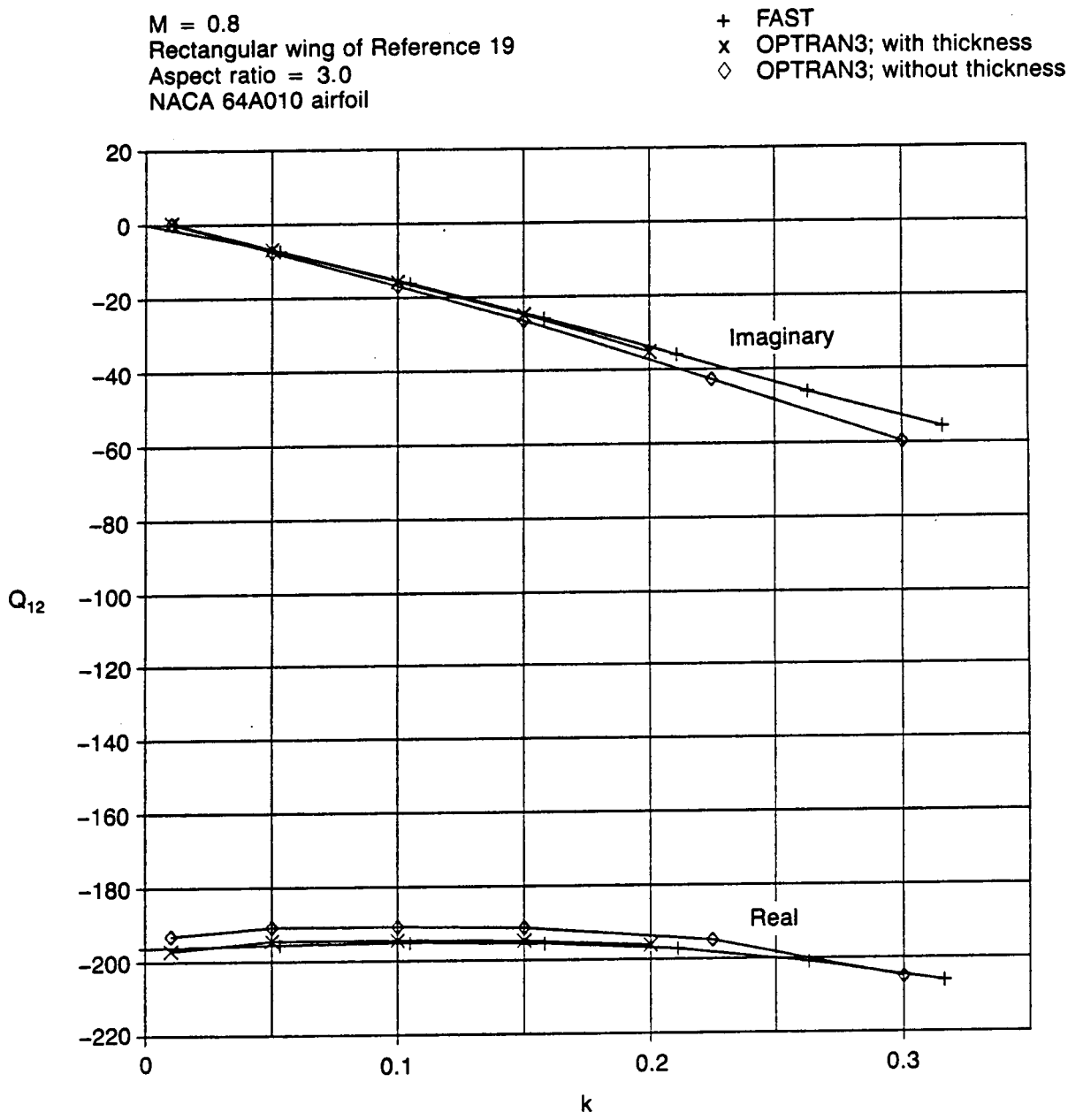

Figure 18b. The Q_{12} Generalized Force Versus Reduced Frequency for a Rectangular Wing; M = 0.8, Aspect Ratio = 3.0

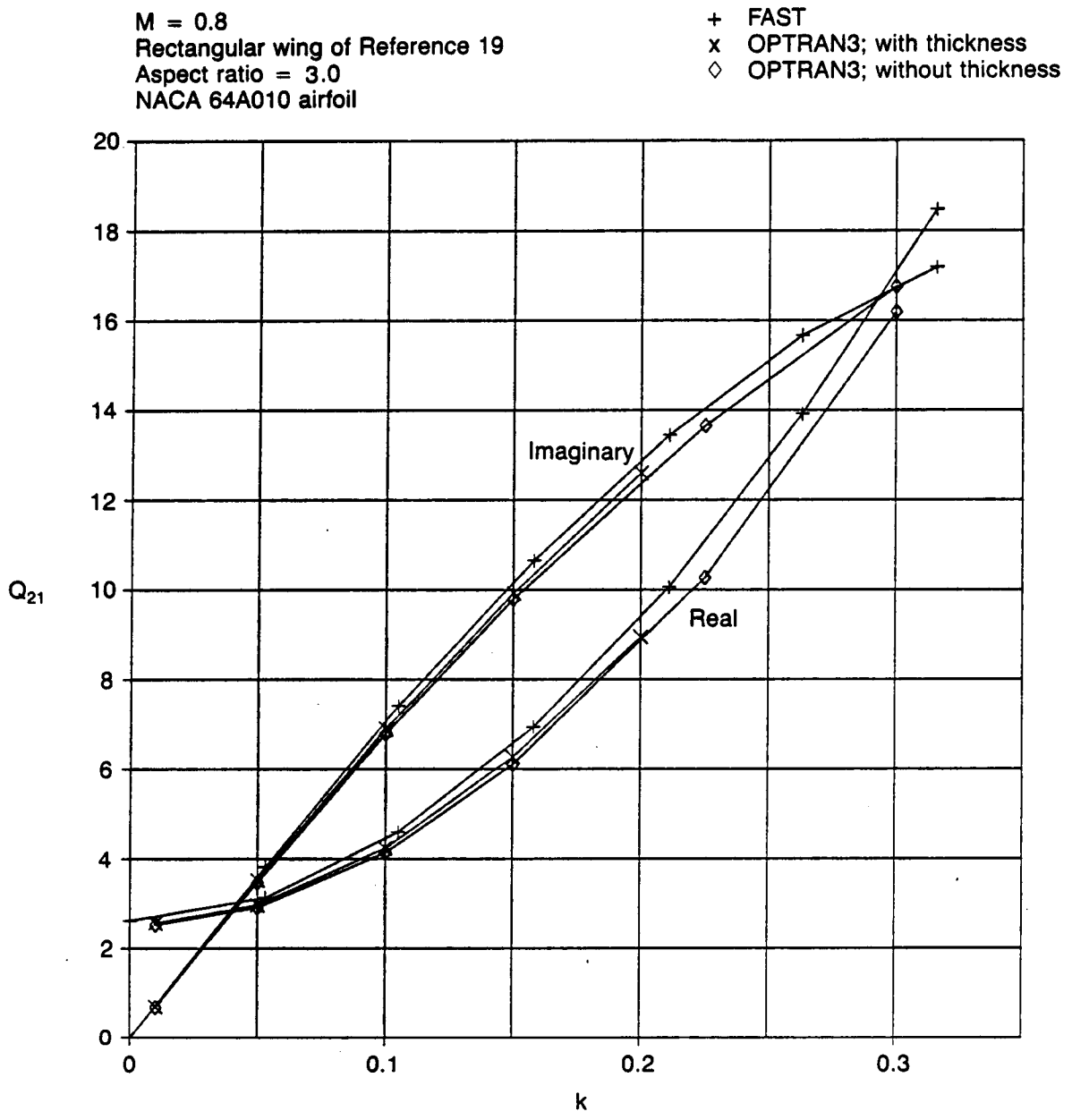

Figure 18c. The Q_{21} Generalized Force Versus Reduced Frequency for a Rectangular Wing; M = 0.8, Aspect Ratio = 3.0

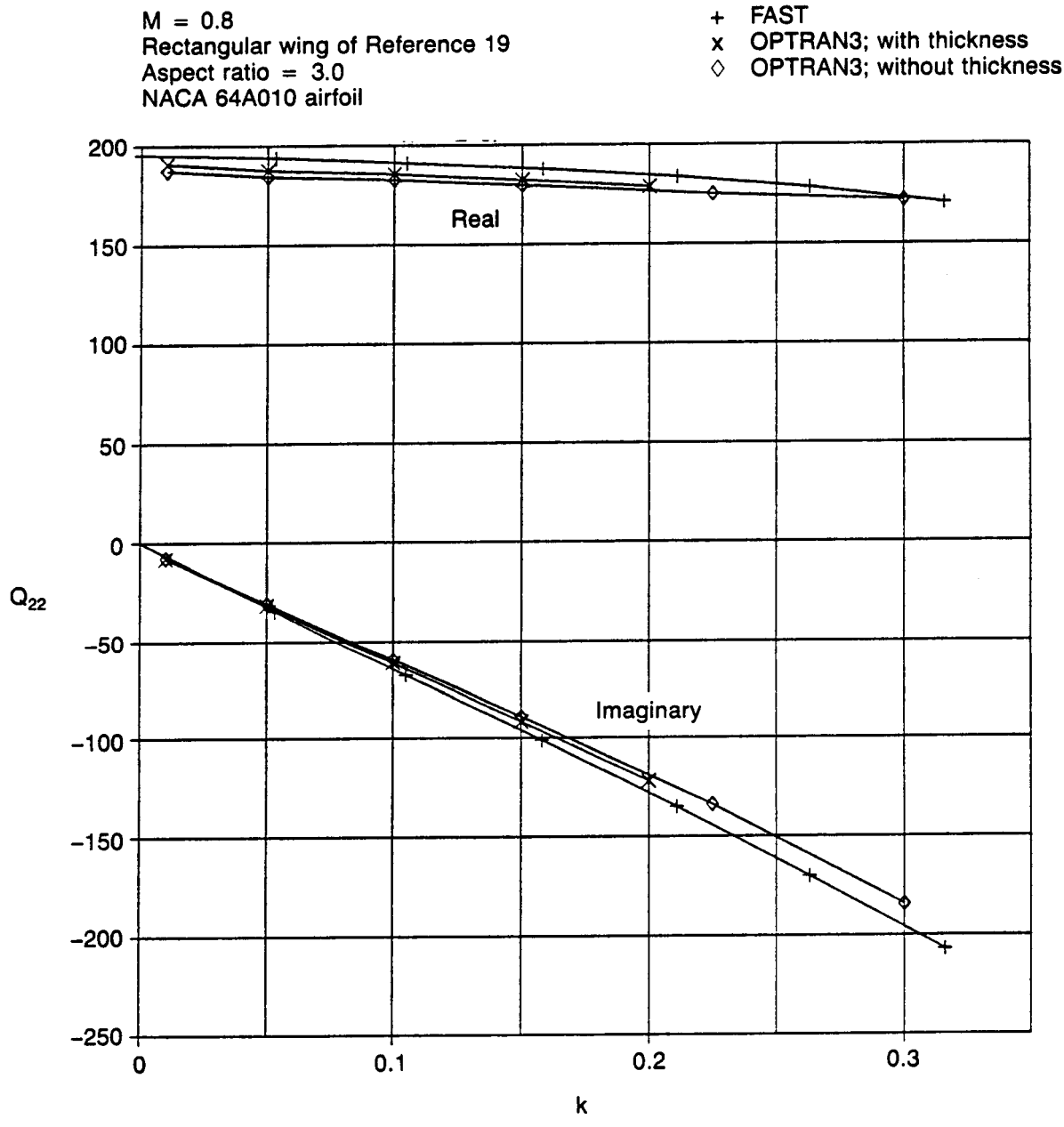

Figure 18d. The Q_{22} Generalized Force Versus Reduced Frequency for a Rectangular Wing; M = 0.8, Aspect Ratio = 3.0

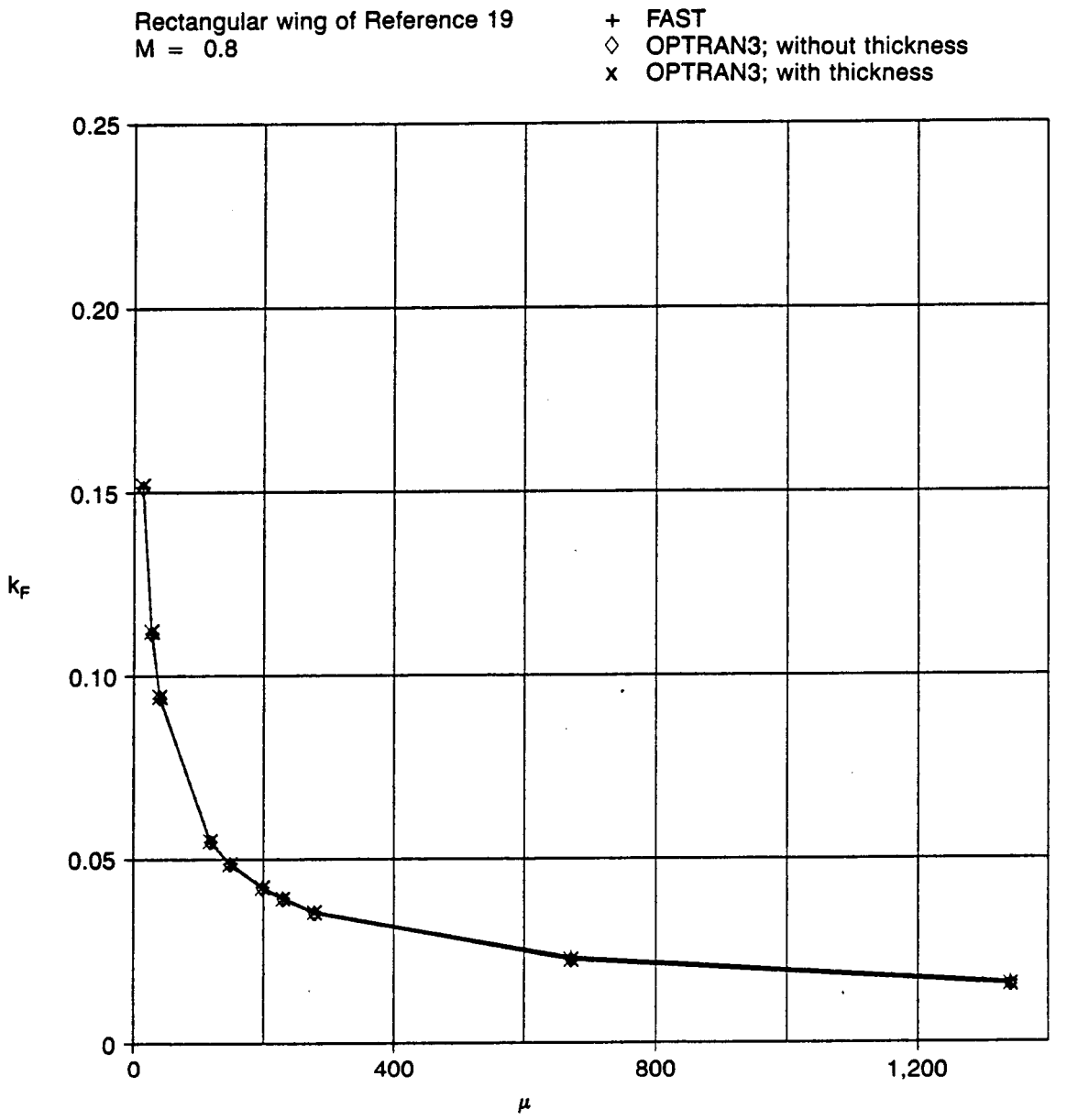

Figure 19. Comparisons Between Flutter Calculations From OPTRAN3 and FAST; Reduced Frequency Versus Mass Ratio

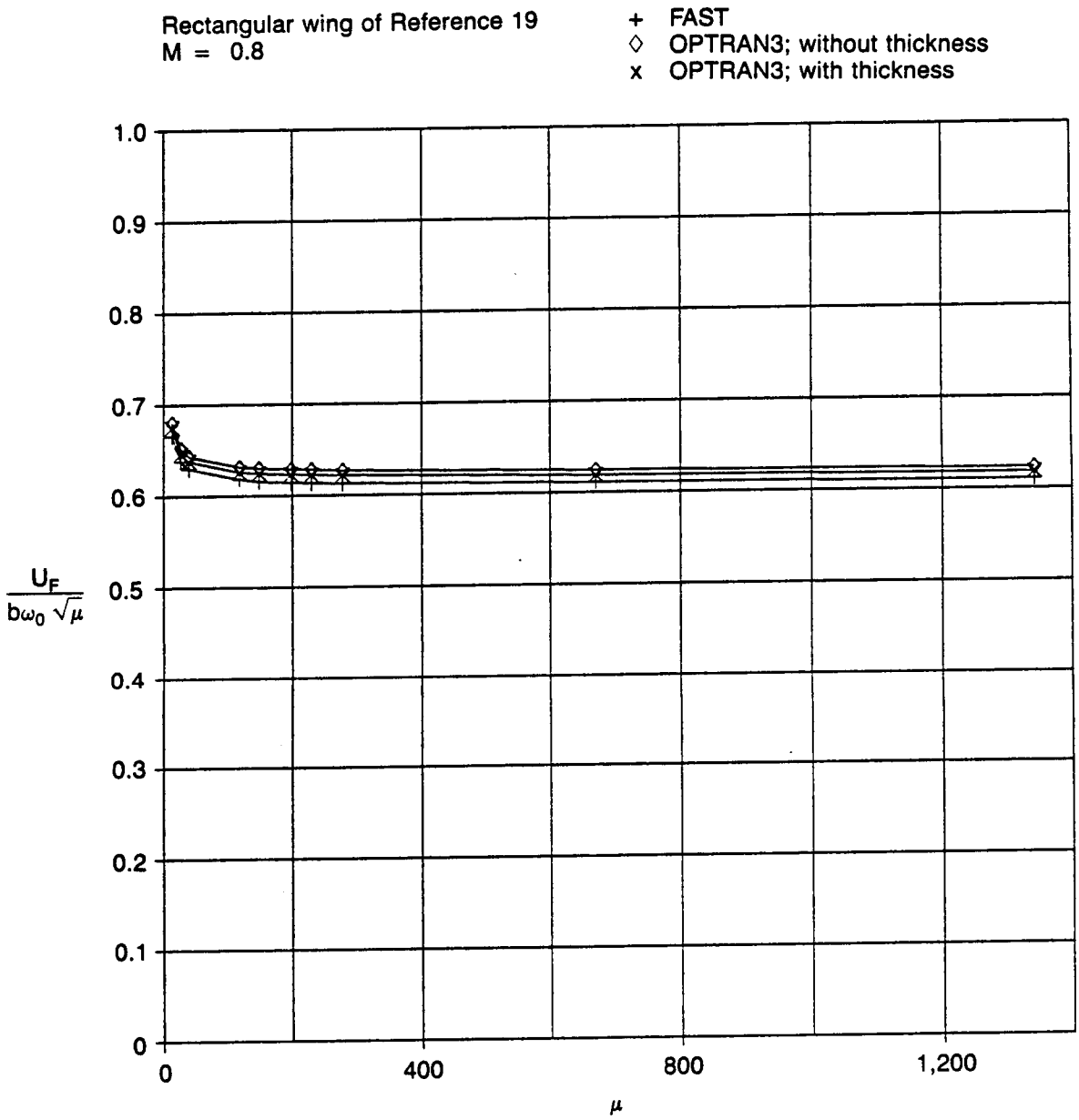

Figure 20. Comparisons Between Flutter Calculations From OPTRAN3 and FAST; Flutter Speed Index Versus Mass Ratio

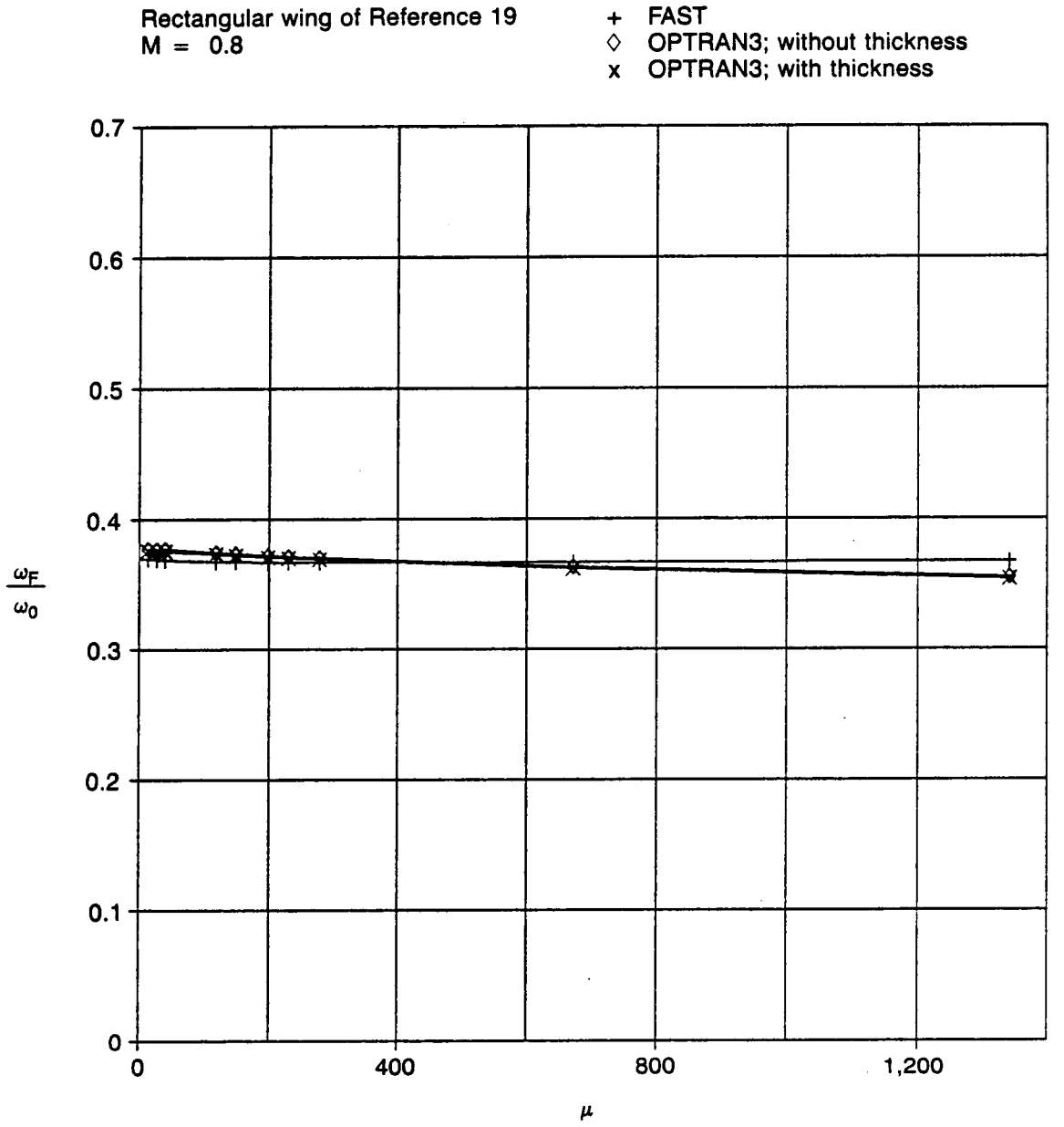

Figure 21. Comparisons Between Flutter Calculations From OPTRAN3 and FAST; Flutter Frequency Ratio Versus Mass Ratio

APPENDIX

A COORDINATE TRANSFORMATION SYSTEM FOR SWEPT AND TAPERED WINGS

A.1 THE BASIC TRANSFORMATION EQUATIONS

In setting up mesh patterns for swept and/or tapered wings, it is desirable to set up grid patterns with the points aligned in some sense with the leading and trailing edges of the planform. The formulation that follows provides such a mapping system starting with a rectangular region in the physical $x-y$ plane. The planform leading and training edges are extended to the outer mesh boundary (fig. 22), and transformations between (x,y) of the physical plane and (ξ,η) of the transformation plane are defined for the regions upstream of the leading edge, between the leading and trailing edges, and downstream of the trailing edge. The transformations provide for continuous second derivatives everywhere. Also, the sharp apex at the root of a swept wing is rounded to avoid singularities at the root plane.

Let $x = X_{LE}(y)$ represent the leading edge of the wing, including its extension to the outer mesh boundary. The semichord $S(y)$ is also extended to the outer mesh boundary. Both $X_{LE}(y)$ and $S(y)$ have continuous second derivatives. For the wing region, $-1 < \xi < 1$, we use the transformation

$$\xi = \left[x - X_{LE}(y)\right]/S(y) - 1 \tag{A-1}$$

$$\eta = y \tag{A-2}$$

Solving equation (A-1) for x yields

$$x = X_{LE}(y) + S(y)\cdot(\xi + 1) \tag{A-3}$$

differentiating with respect to x yields

$$1 = S(y)\cdot\xi_x$$

and

$$\xi_x = 1/S(y) \tag{A-4}$$

Differentiating equation (A-3) with respect to y leads to

$$0 = X'_{LE} + S'(y)\cdot(\xi + 1) + \xi_y/\xi_x$$

and

$$\xi_y/\xi_x = -X_{LE} - S'(y)\cdot(\xi+1) \tag{A-5}$$

For the mapping upstream of the wing, $\xi < -1$, we consider a form that has continuous second derivatives everywhere. Analogous to equation (A-3), we write

$$x = X_{LE}(y) + S(y)\cdot(\xi+1) + \left(\frac{\xi+1}{\xi_1+1}\right)^3 f(y) \tag{A-6}$$

We choose $f(y)$ so that at $\xi=\xi_1$, $x = x_1$. Thus

$$x_1 = X_{LE} + S(y)\cdot(\xi_1+1) + f(y)$$

and we obtain

$$x = X_{LE}(y) + S(y)\cdot(\xi+1) + \left(\frac{\xi+1}{\xi_1+1}\right)^3 \left[x_1 - X_{LE}(y) - S(y)\cdot(\xi_1+1)\right] \tag{A-7}$$

We now find ξ_x and ξ_y. Differentiating equation (A-7) with respect to x yields

$$1 = \left\{S(y) + \frac{3(\xi+1)^2}{(\xi_1+1)^3}\left[x_1 - X_{LE}(y) - S(y)\cdot(\xi_1+1)\right]\right\}\xi_x$$

and

$$\xi_x = 1\Big/\left\{S(y) + \frac{3(\xi+1)^2}{(\xi_1+1)^3}\left[x_1 - X_{LE}(y) - S(y)\cdot(\xi+1)\right]\right\} \tag{A-8}$$

Differentiating equation (A-7) with respect to y yields

$$0 = X'_{LE} + S'(y)\cdot(\xi+1) - \left(\frac{\xi+1}{\xi_1+1}\right)^3 \left[X'_{LE} + S'(y)\cdot(\xi_1+1)\right] + \xi_y/\xi_x$$

and

$$\xi_y/\xi_x = -X'_{LE} - S'(y)\cdot(\xi+1) + \left(\frac{\xi+1}{\xi_1+1}\right)^3 \left[X'_{LE} + S'(y)\cdot(\xi_1+1)\right] \tag{A-9}$$

Downstream of the wing region where $\xi > 1$, we define a mapping of the form

$$x = X_{LE} + S(y)\cdot(\xi+1) + \left(\frac{\xi-1}{\xi_{max}-1}\right)^3 g(y)$$

and determine $g(y)$ so that at $\xi = \xi_{max}$ we obtain $x = x_{max}$. Then

$$g(y) = x_{max} - X_{LE}(y) - S(y)\cdot(\xi_{max}+1)$$

and

$$x = X_{LE}(y) + S(y)\cdot(\xi+1) + \left(\frac{\xi-1}{\xi_{max}-1}\right)^3 \left[x_{max} - X_{LE}(y) - S(y)\cdot(\xi_{max}+1)\right] \tag{A-10}$$

Differentiating with respect to x yields

$$1 = S(y) \cdot \xi_x + \frac{3(\xi-1)^2}{(\xi_{max}-1)^3}\left[x_{max} - X_{LE}(y) - S(y)\cdot\left(\xi_{max}+1\right)\right]\xi_x$$

$$\text{and} \quad \xi_x = 1/\left\{S(y) + \frac{3(\xi-1)^2}{(\xi_{max}-1)^3}\left[x_{max} - X_{LE}(y) - S(y)\cdot\left(\xi_{max}+1\right)\right]\right\} \tag{A-11}$$

Differentiating with respect to y leads to

$$0 = X'_{LE} + S'(y)\cdot(\xi+1) - \left(\frac{\xi-1}{\xi_{max}-1}\right)^3\left[X'_{LE} + S'(y)\cdot\left(\xi_{max}+1\right)\right] + \xi_y/\xi_x$$

$$\text{and} \quad \xi_y/\xi_x = -X'_{LE} - S'(y)\cdot(\xi+1) + \left(\frac{\xi-1}{\xi_{max}-1}\right)^3\left[X'_{LE}(y) - S'(y)\cdot\left(\xi_{max}+1\right)\right] \tag{A-12}$$

In the finite difference operators, we need

$$F = 1/\xi_x \quad , \quad G = \xi_y/\xi_x$$

and

$$G_2 = G^2/F$$

which are defined by equations (A-4) to (A-12) above. The metrics are calculated from these expressions in the program.

A.2 EXTENSIONS OF THE LEADING AND TRAILING EDGES OF THE WING WITH SECOND-DERIVATIVE CONTINUITY

To eliminate the singularity of the leading edge at the line of symmetry, $y = 0$, we turn the leading edge so that it has zero slope at the plane of symmetry. Thus we express the leading edge in the form

$$X_{LE} = X_{LE}(2) + ay^2 + by^3 \quad \text{for} \quad y(2) \le y \le y(N) \quad (\text{or } 0 \le y \le y_N) \tag{A-13}$$

where $y(2) = 0$ is the plane of symmetry and $y = y(N) \equiv y_N$ is the value of y at which the slope of the new curved edge matches the slope of the straight leading edge (see fig. 22). Thus we require $X''_{LE}(y_N) = 0$, since we consider wings with straight edges. Thus

$$X''_{LE} = 2a + 6by_N = 0$$

and

$$b = -a/(3y_N) \tag{A-14}$$

Then

$$X_{LE}(y) = X_{LE}(2) + a\left[y^2 - y^3/(3y_N)\right] \tag{A-15}$$

At $y = y_N$, we have $X'_{LE} = y_N \tan \theta_{LE} = c_1$. Differentiating equation A-15 then yields

$$X'_{LE}(y_N) = a\left[2y_N - 3y_N^2/(3y_N)\right] = ay_N$$

Hence

$$a = c_1/y_N$$

The equation for the leading edge for the section near the plane of symmetry then becomes

$$X_{LE} = X_{LE}(2) + c_1\left[y^2/y_N - y^3/(3y_N^2)\right] \qquad \text{for } 0 \le y \le y_N \tag{A-16}$$

At $y = y_N$, we have from equation (B-49) of Reference 8

$$X_{LE}(y_N) = -1 + c_1 y_N$$

Thus equation (A-16) at $y = y_N$ becomes

$$X_{LE} = X_{LE}(2) + 2c_1 y_N/3$$

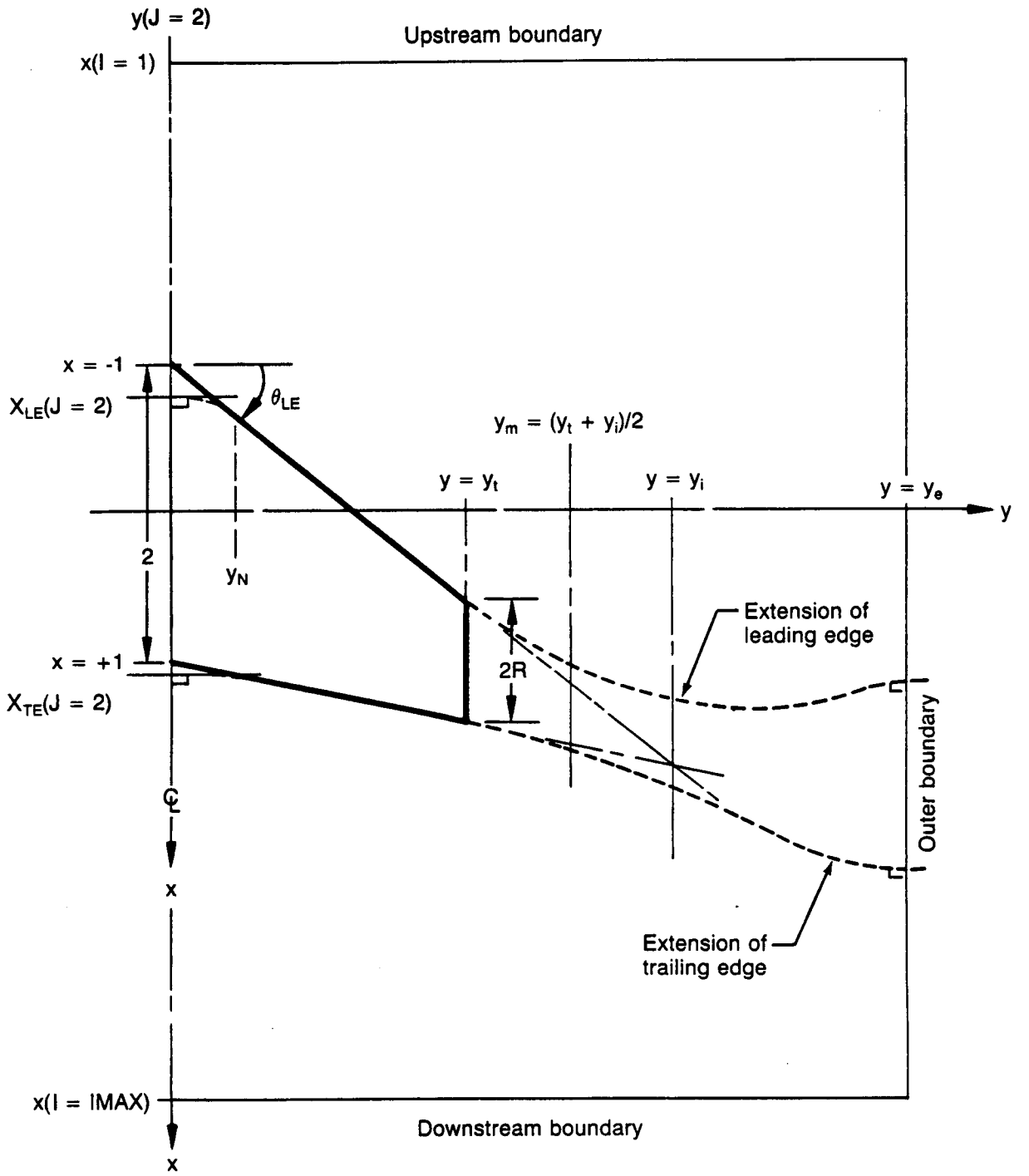

Figure 22. Parameters for Extending the Leading and Trailing Edges of a Swept and Tapered Wing

Hence $a = c_1/y_N$ and

$$X_{LE}(y_N) = X_{LE}(2) + 2c_1y_N/3 = -1 + c_1y_N$$

Finally, we obtain for equations (A-16)

$$X_{LE}(y) = -1 + c_1\left[y^2/y_N - y^3/(3y_N^2) + y_N/3\right] \quad \text{for } 0 \le y \le y_N \tag{A-17}$$

Similarly, for the trailing edge we write

$$X_{TE}(y) = 1 + (c_1 + 2c_2)\cdot\left[y^2/y_N - y^2/(3y_N) + y_N/3\right] \tag{A-18}$$

from which we obtain

$$S(y) = \left[X_{TE}(y) - X_{LE}(y)\right] / 2 = 1 + c_2\left[y^2/y_N - y^3/(3y_N) + y_N/3\right] \tag{A-19}$$

For $y_t > y > y_N$, i.e., the straight portions of the leading and trailing edges, we have from equations (B-49) and (B-50) of Reference 8

$$X_{LE}(y) = -1 + c_1y \tag{A-20}$$

$$X_{TE}(y) + 1 + (c_1 + 2c_2)y \tag{A-21}$$

Extending the leading and trailing edges beyond the tip, we find that the two edges intersect at $y = y_i$

or

$$-1 + c_1y_i = 1 + (c_1 + 2c_2)y_i$$

or

$$y_i = -1/c_2 \tag{A-22}$$

Differentiating equations (A-17) and (A-14) with respect to y yields

$$X'_{LE}(y) = c_1(2t - t^2), \qquad t = y/y_N \tag{A-23}$$

$$S'(y) = c_2(2t - t^2) \tag{A-24}$$

For $y_N < y < y_t$, we have

$$X_{LE}(y) = -1 + c_1 y \tag{A-25}$$

$$X_{TE}(y) = 1 + (c_1 + 2c_2)y \tag{A-26}$$

$$S(y) = 1 + c_2 y \tag{A-27}$$

$$X'_{LE}(y) = c_1 \tag{A-28}$$

$$S'(y) = c_2 \tag{A-29}$$

We extend the wing leading and trailing edges beyond the tip, y_t, with a cubic in y. Choose the point $y = y_m$ to lie halfway between wing tip and the intersection of the linearly extended leading and trailing edges, or

$$y_m = (y_t + y_i)/2 = (y_t - 1/c_2)/2 \tag{A-30}$$

Thus, for $y_t < y < y_m$, we write for the equation of the leading edge

$$X_{LE}(y) = -1 + c_1 y + b(y - y_t)^3 \tag{A-31}$$

The mean slope is chosen for both leading and trailing edges at $y = y_m$. Thus

$$\left[(c_1 + 2c_2) + c_1\right]/2 = c_1 + c_2 \tag{A-32}$$

Hence at $y = y_m$

$$X'_{LE}(y_m) = c_1 + 3b(y_m - y_t)^2 = c_1 + c_2$$

or

$$b = c_2 / \left[3(y_m - y_t)^2\right] \tag{A-33}$$

Similarly, for the extension of the trailing edge we write

$$X_{TE}(y) = 1 + (c_1 + 2c_2)\, y + b_1 (y - y_t)^3 \tag{A-34}$$

$$X'_{TE}(y) = (c_1 + 2c_2) + 3b_1(y_m - y_t)^2 = c_1 + c_2$$

Thus, at $y = y_m$, b_1 becomes

$$b_1 = -c_2 / \left[3(y_m - y_t)^2\right] = -b \tag{A-35}$$

After substituting b and b_1, the leading- and trailing-edge extensions then become for $y_t < y < y_m$

$$X_{LE}(y) = -1 + c_1 y + c_2 (y - y_t)^3 / [3(y_m - y_t)^2] \tag{A-36}$$

$$X_{TE}(y) = 1 + (c_1 + 2c_2) y - c_2 (y - y_t)^3 / [3(y_m - y_t)^2] \tag{A-37}$$

For the semichord $S(y)$ we obtain

$$S(y) = 1 + c_2 \{ y - (y - y_t)^3 / [3(y_m - y_t)^2] \} \tag{A-38}$$

Differentiating equations (A-36) and (A-38) with respect to y yields

$$X'_{LE}(y) = c_1 + c_2 (y - y_t)^2 / (y_m - y_t)^2 \tag{A-39}$$

$$S'(y) = c_2 [1 - (y - y_t)^2 / (y_m - y_t)^2] = c_1 + c_2 - X'_{TE}(y) \tag{A-40}$$

To simplify the outer mesh boundary conditions, we extend the leading and trailing edges for $y = y_m$ to y_e, the outside boundary, by a third-degree polynomial, so that slopes $X'_{LE} = X'_{TE} = S' = 0$ at y_e. Thus we write

$$\begin{aligned} X_{LE}(y) = X_{LEM} &+ a [(y - y_e)^2 - (y_m - y_e)^2] \\ &+ b [(y - y_e)^3 - [y_m - y_e)^3] \end{aligned} \tag{A-41}$$

where X_{LEM} is the x leading edge coordinate at $y = y_m$, the point halfway between y_t and the point of intersections of the leading and trailing edges. From equation (A-36) we have

$$\begin{aligned} X_{LE}(y) = -1 + c_1 y_m + c_2 (y_m - y_t)/3 &+ a [(y - y_e)^2 - (y_m - y_e)^2] \\ &+ b [(y - y_e)^3 - (y_m - y_e)^3] \end{aligned} \tag{A-42}$$

At $y_1 = y_m$, we must have $X'_{LE} = c_1 + c_2$, or the average of the leading- and trailing-edge slopes at the wing tips. Thus

$$X'_{LE}(y_m) = a[2(y_m - y_e) + b[3(y_m - y_e)^2] = c_1 + c_2 \tag{A-43}$$

To match the second derivative at $y = y_m$, we have from equations (A-39)

$$X''_{TE}(y_m) = 2c_2 / (y_m - y_t)$$

Thus from equation (A-42) we obtain

$$2a + 6b(y_m - y_e) = 2c_2 / (y_m - y_t)$$

or

$$a + 3b(y_m - y_e) = c_2 / (y_m - y_t) \tag{A-44}$$

Eliminating b between equations (A-43) and (A-44) yields for a

$$a = (c_1 + c_2)/(y_m - y_e) - c_2/(y_m - y_t) \tag{A-45}$$

From equation (A-44) we have

$$3b(y_m - y_e) = c_2/(y_m - y_t) - a$$

or

$$b = \left[c_2/(y_m - y_t) - a\right]/\left|3(y_m - y_e)\right| \tag{A-46}$$

Similiarly, for the trailing edge we write

$$\begin{aligned} X_{TE}(y) &= 1 + (c_1 + 2c_2)y_m - c_2(y_m - y_t)/3 \\ &\quad + a_1\left[(y - y_e)^2 - (y_m - y_e)^2\right] \\ &\quad + b_1\left[(y - y_e)^3 - (y_m - y_e)^3\right] \end{aligned} \tag{A-47}$$

At $y = y_m$, $X'_{TE} = c_1 + c_2$ and equation (A-47) yields

$$2a_1 + 3b_1(y_m - y_e) = (c_1 + c_2)/(y_m - y_e) \tag{A-48}$$

At $y = y_m$, we have from equation (A-37)

$$X''_{TE}(y) = -2c_2/(y_m - y_t)$$

Thus

$$\begin{aligned} X''_{TE}(y) &= 2a_1 + 6b_1(y_m - y_e) = -2c_2/(y_m - y_t) \\ a_1 + 3b_1(y_m - y_e) &= -c_2/(y_m - y_t) \end{aligned} \tag{A-49}$$

Solving equations (A-44) and (A-45) for a_1 and b_1 yields

$$a_1 = (c_1 + c_2)/(y_m - y_t) + c_2/(y_m - y_t) \tag{A-50}$$

and

$$b_1 = -\left[c_2/(y_m - y_t) + a_1\right]/\left|3(y_m - y_e)\right| \tag{A-51}$$

Let

$$\begin{aligned} X_{TEM} &= 1 + (c_1 + 2c_2)y_m - c_2(y_m - y_t)/3 \\ &\quad - a_1(y_m - y_e)^2 - b_1(y_m - y_e)^3 \end{aligned} \tag{A-52}$$

Then

$$X_{TE}(y) = X_{TEM} + a_1(y - y_e)^2 + b_1(y - y_e)^3 \tag{A-53}$$

Let

$$X_{LEM} = -1 + c_1 y_m + c_2(y_m - y_t)/3 - a(y_m - y_e)^2 - b(y_m - y_e)^3 \tag{A-54}$$

then

$$X_{LE}(y) = X_{LEM} + a(y - y_e)^2 + b(y - y_e)^3 \tag{A-55}$$

Let

$$S_{LEM} = (X_{TEM} - X_{LEM})/2 \tag{A-56}$$

then

$$\begin{aligned} S(y) &= S_{LEM} + (a_1 - a)(y - y_e)^2/2 + (b_1 - b)(y - y_e)^3/2 \\ X'_{LE}(y) &= 2a(y - y_e) + 3b(y - y_e)^2 \\ S'(y) &= (a_1 - a)(y - y_e) + 3(b_1 - b)(y - y_e)^2/2 \end{aligned} \tag{A-57}$$

For convenience, we summarize the results and include the first derivatives of the leading edge and semichord that we will need in the calculation of the coefficients of the difference equations.

For $0 < y < y_N$

$$X_{LE}(y) = -1 + c_1 y_N(t^2 - t^3/3 + 1/3) \quad , \quad t = y/y_N \tag{A-58}$$

$$S(y) = 1 + c_2 y_N(t^2 - t^3/3 + 1/3) \tag{A-59}$$

$$X'_{LE}(y) = c_1(2t - t^2) \tag{A-60}$$

$$S'(y) = c_2(2t - t^2) \tag{A-61}$$

For $y_N < y < y_t$

$$X_{LE}(y) = -1 + c_1 y \tag{A-62a}$$

$$X_{TE}(y) = S(y) + (c_1 + c_2)y \tag{A-62b}$$

$$S(y) = 1 + c_2 y \tag{A-63}$$

$$X'_{LE}(y) = c_1 \tag{A-64}$$

$$S'(y) = c_2 \tag{A-65}$$

For $y_t < y < y_m$

$$X_{LE}(y) = -1 + c_1 y + c_2 (y - y_t)^2 / \left| 3(y_m - y_t)^2 \right| \tag{A-66}$$

$$S(y) = 1 + c_2 (y - y_t)^3 / \left| 3(y_m - y_t)^2 \right| \tag{A-67}$$

$$X'_{LE}(y) = c_1 + c_2 (y - y_t)^2 / (y_m - y_t)^2 \tag{A-68}$$

$$S'(y) = c_1 + c_2 - X'_{LE} \tag{A-69}$$

For $y_m < y < y_e$, where $y_e = y(\text{JMAX})$

$$X_{LEM} = -1 + c_1 y_m + c_2 (y_m - y_t)/3 - a(y_m - y_e)^2 - b(y_m - y_e)^3 \tag{A-70}$$

$$X_{LE}(y) = X_{LEM} + a(y - y_e)^2 + b(y - y_e)^3 \tag{A-71}$$

$$a = (c_1 + c_2)/(y_m - y_e) - c_2/(y_m - y_t) \tag{A-72}$$

$$b = \left[c_2/(y_m - y_t) - a \right] / \left[3(y_m - y_e) \right] \tag{A-73}$$

$$X_{TEM} = 1 + (c_1 + 2c_2) y_m - c_2 (y_m - y_t)/3 - a_1 (y_m - y_e)^2 - b_1 (y_m - y_e)^3 \tag{A-74}$$

$$X_{TE}(y) = X_{TEM} + a_1 (y - y_e)^2 + b_1 (y - y_e)^3 \tag{A-75}$$

$$a_1 = (c_1 + c_2)/(y_m - y_e) + c_2/(y_m - y_t) \tag{A-76}$$

$$b_1 = -\left[c_2/(y_m - y_t) + a_1\right]/\left[3(y_m - y_e)\right] \tag{A-77}$$

$$S_{LEM} = (X_{TEM} - X_{LEM})/2 \tag{A-78}$$

$$S(y) = S_{LEM} + (a_1 - a)(y - y_e)^2/2 + (b_1 - b)(y - y_e)^3/2 \tag{A-79}$$

$$X'_{LE}(y) = 2a(y - y_e) + 3b(y - y_e)^2 \tag{A-80}$$

$$S'(y) = (a_1 - a)(y - y_e) + 3(b_1 - b)(y - y_e)^2/2 \tag{A-81}$$

A.3 TRANSFORMATION OF THE DIFFERENTIAL EQUATION FOR A SWEPT AND TAPERED WING IN TRANSONIC FLOW

A.3.1 Basic Formulation

The governing equation for the unsteady potential for harmonic motion of a wing in transonic flow is given by

$$(u\varphi_{1x})_x + \varphi_{1yy} + \varphi_{1zz} - 2i\omega\varphi_{1x}/\epsilon + \omega^2\varphi_1/\epsilon = 0 \tag{A-82}$$

where $u = \mathrm{K} - (\gamma+1)\varphi_{ox}$. The quantities φ_o and φ_1 are the steady and unsteady perturbation potentials, respectively. The variables x, y, z are the Cartesian coordinates. We define a coordinate transformation that aligns the leading and trailing edges with coordinate lines. For points on the wing, we let

$$\xi = \left[x - \mathrm{X_{LE}}(y)\right]/\mathrm{S}(y) - 1$$
$$\eta = y \tag{A-83}$$
$$\zeta = z$$

where $\mathrm{X_{LE}}(y)$ is the x coordinate of the leading edge as a function of the spanwise variable y and $\mathrm{S}(y)$ is the semichord. We consider a more general transformation

$$\xi = \xi(x,y)$$
$$\eta = y \tag{A-84}$$
$$\zeta = z$$

then

$$\varphi_{1x} = \varphi_{1\xi}\xi_x \qquad \varphi_{1y} = \varphi_{1\eta} + \varphi_{1\xi}\xi_y \tag{A-85}$$

The differential equation becomes

$$\xi_x(u\varphi_{1\xi}\xi_x)_\xi + \left(\varphi_{1\eta} + \varphi_{1\xi}\xi_y\right)_\eta + \xi_y(\varphi_{1\eta} + \varphi_{1\xi}\xi_y)_\xi \tag{A-86}$$
$$+ \varphi_{1\zeta\zeta} - 2i\omega\varphi_{1\xi}\xi_x/\epsilon + \omega^2\varphi_1/\epsilon = 0$$

To express the equation in conservation form, we consider

$$\frac{\partial}{\partial\xi}\left[\frac{\xi_y}{\xi_x}\left(\varphi_{1\eta}+\varphi_{1\xi}\xi_y\right)\right] = \frac{\partial}{\partial\xi}\left(\frac{\xi_y}{\xi_x}\right)\left(\varphi_{1\eta}+\varphi_{1\xi}\xi_y\right) + \frac{\xi_y}{\xi_x}\frac{\partial}{\partial\xi}\left(\varphi_{1\eta}+\varphi_{1\xi}\xi_y\right) \tag{A-87}$$

$$\frac{\partial}{\partial\eta}\left[\frac{1}{\xi_x}\left(\varphi_{1\eta}+\varphi_{1\xi}\xi_y\right)\right] = \frac{\partial}{\partial\eta}\left(\frac{1}{\xi_x}\right)\left(\varphi_{1\eta}+\varphi_{1\xi}\xi_y\right)\frac{1}{\xi_x}\frac{\partial}{\partial\eta}\left(\varphi_{1\eta}+\varphi_{1\xi}\xi_y\right)$$

Since $x = \chi(\xi,y)$ differentiation with respect to x and y yields

$$1 = = \chi_\xi\xi_x \qquad \text{or} \qquad \xi_x = 1/\chi_\xi \tag{A-88a}$$

$$0 = \chi_\xi\xi_y+\chi_\eta \qquad \text{or} \qquad \xi_y = -\chi_\eta/\chi_\xi \tag{A-88b}$$

Hence

$$\frac{\partial}{\partial\xi}\left(\frac{\xi_y}{\xi_x}\right) = \frac{\partial}{\partial\xi}\left(-\chi_\eta\right) = -\chi_{\xi\eta} \tag{A-89}$$

$$\frac{\partial}{\partial\eta}\left(\frac{1}{\xi_x}\right) = \frac{\partial}{\partial\eta}\left(\chi_\xi\right) = \chi_{\xi\eta}$$

When the two equations (A-88) and (A-89) are combined in equation (A-86), the first terms on the right-hand side of equation (A-87) cancel and equation (A-86) becomes

$$\left(u\xi_x\varphi_{1\xi}\right)_\xi + \left[\frac{\xi_y}{\xi_x}\left(\varphi_{1\eta}+\varphi_{1\xi}\xi_y\right)\right]_\xi + \left[\frac{1}{\xi_x}\left(\varphi_{1\eta}+\varphi_{1\xi}\xi_y\right)\right]_\eta$$
$$+\varphi_{1\zeta\zeta}/\xi_x - 2i\omega\varphi_{1\xi}/\epsilon + \omega^2\varphi_1/\left(\epsilon\xi_x\right) = 0 \tag{A-90}$$

$$\text{Let } \mathrm{F} = 1/\xi_x \quad \theta = \xi_y/\xi_x \quad \theta_2 = \xi_y^2/\xi_x \quad \bar{u} = u\xi_x$$

Then the differential equation takes the form

$$\left[\left(\bar{u}+\mathrm{G}_2\right)\varphi_{1\xi}\right]_\xi + \left(\mathrm{F}\varphi_{1\eta}\right)_\eta + \left(\mathrm{F}\varphi_{1\zeta}\right)_\zeta \tag{A-91}$$
$$+\left(\mathrm{G}\varphi_{1\eta}\right)_\xi + \left(\mathrm{G}\varphi_{1\xi}\right)_\eta - 2i\omega\varphi_{1\xi}/\epsilon + \omega^2\mathrm{F}\varphi_1/\epsilon = 0$$

A.3.2 The Derivation of the Difference Equations

We now express the differential equation in difference form, following the notation of Reference 7 for the coefficients. For the first term, we have for elliptic points

$$\frac{1}{2}\left(\bar{u}\varphi_{1\xi}\right)_{\xi} = c_i\bar{u}_{i+1/2jk}\left(\varphi_{i+1jk}-\varphi_{ijk}\right) - d_i\bar{u}_{i-1/2jk}\left(\varphi_{ijk}-\varphi_{i-1jk}\right) \tag{A-92}$$

and for hyperbolic points

$$\frac{1}{2}\left(\bar{u}\varphi_{1\xi}\right)_{\xi} = c_{i-1}\bar{u}_{i-1/2jk}\left(\varphi_{ijk}-\varphi_{i-1jk}\right) - d_{i-1}u_{i-3/2jk}\left(\varphi_{i-1jk}-\varphi_{i-2jk}\right) \tag{A-93a}$$

where

$$c_i = 1/\left[\left(x_{i+1}-x_{i-1}\right)\left(x_{i+1}-x_i\right)\right]$$

and (A-93b)

$$d_i = 1/\left[\left(x_{i+1}-x_{i-1}\right)\left(x_i-x_{i-1}\right)\right]$$

Following the procedure in the ADI method, we combine the two procedures and obtain

$$\begin{aligned}&\mathrm{D2}_k\left[c_i\bar{u}_{i+1/2jk}\left(\varphi_{i+1jk}-\varphi_{ijk}\right)-d_i\bar{u}_{i-1/2jk}\left(\varphi_{ijk}-\varphi_{i-1jk}\right)\right]\\ &+\mathrm{D1X}_k\left[c_{i-1}\bar{u}_{i-1/2jk}\left(\varphi_{ijk}-\varphi_{i-1jk}\right)-d_{i-1}\bar{u}_{i-3/2jk}\left(\varphi_{i-1jk}-\varphi_{i-2jk}\right)\right]\end{aligned} \tag{A-94a}$$

The variables D2 and D1X are zero or one for elliptic or hyperbolic points to select the appropriate operator. For a shock passing between points (i,j,k) and $(i+1,j,k)$;

$$\begin{aligned}\mathrm{D1X}_k &= \left(x_i-x_{i-2}\right)/\left[\left(x_i-x_{i-2}\right)+\left(x_{i+1}-x_{i-1}\right)\right]\\ \mathrm{D2}_k &= \left(x_{i+1}-x_{i-1}\right)/\left[\left(x_i-x_{i-2}\right)+\left(x_{i+1}-x_{i-1}\right)\right]\end{aligned} \tag{A-94b}$$

(see ref. 7).

For the second term, we write

$$\frac{1}{2}\left[\mathrm{G}_2\varphi_{1\xi}\right]_{\xi} = c_i\mathrm{G}_{2i+1/2jk}\left(\varphi_{i+1jk}-\varphi_{ijk}\right) - d_i\mathrm{G}_{2i-1/2jk}\left(\varphi_{ijk}-\varphi_{i-1jk}\right) \tag{A-95}$$

For the remaining terms, we have

$$\frac{1}{2}\left[F\varphi_\eta\right]_\eta = a_{y_j} F_{ij-1/2k}\left(\varphi_{ij-1k}-\varphi_{ijk}\right) - b_{y_j} F_{ij+1/2k}\left(\varphi_{ijk}-\varphi_{ij+1k}\right) \tag{A-96}$$

$$\frac{1}{2}\left(F\varphi_\zeta\right)_\zeta = F_{ij}\left[a_{z_k}\left(\varphi_{ijk-1}-\varphi_{ijk}\right) - b_{z_k}\left(\varphi_{ijk}-\varphi_{ijk+1}\right)\right] \tag{A-97}$$

$$\frac{\partial}{\partial\xi}\left(G\varphi_{1\eta}\right) = c_{1i}G_{i+1j}\left[c_{1y_j}\varphi_{i+1j+1k} + \left(d_{1y_j}-c_{1y_j}\right)\varphi_{i+1jk} - d_{1y_j}\varphi_{i+1j-1k}\right] \tag{A-98}$$

$$+ \left(d_{1i}-c_{1i}\right)G_{ij}\left[c_{1y_j}\varphi_{ij+1k} + \left(d_{1y_j}-c_{1y_j}\right)\varphi_{ijk} - d_{1y_j}\varphi_{i-1j-1k}\right]$$

$$- d_{1i}G_{i-1j}\left[c_{1y_j}\varphi_{i-1j+1k} + \left(d_{1y_j}-c_{1y_j}\right)\varphi_{i-ijk} - d_{1y}\varphi_{i-1jk}\right]$$

$$\frac{\partial}{\partial\eta}\left[G\varphi_{1\xi}\right] = c_{1y_j}G_{ij+1}\left[c_{1i}\varphi_{i+1j+1k} + \left(d_{1i}-c_{1i}\right)\varphi_{ij+1k} - d_{1y_j}\pi_{i-1jk}\right] \tag{A-99}$$

$$+\left(d_{1y_j}-c_{1y_j}\right)G_{ij}\left[c_{1i}\varphi_{i+1jk} + \left(d_{1i}-c_{1i}\right)\varphi_{ijk} - d_{1i}\varphi_{i-1jk}\right]$$

$$- d_{1y_j}G_{ij-1}\left[c_{1i}\varphi_{i+1j-1k} + \left(d_{1i}-c_{1i}\right)\varphi_{ij-1k} - d_{1i}\varphi_{i-1j-1k}\right]$$

For the first derivative with respect to ξ, we have for elliptic points

$$-i\omega\varphi_{1\xi}/\epsilon = -\left(i\omega/\epsilon\right)\left[c_{1i}\left(\varphi_{i+1jk}-\varphi_{ijk}\right) + d_{1i}\left(\varphi_{ijk}-\varphi_{i-1jk}\right)\right] \tag{A-100}$$

and for hyperbolic points

$$-i\omega\varphi_{1\xi}/\epsilon = -\left(i\omega/\epsilon\right)\left[c_{2i}\left(\varphi_{ijk}-\varphi_{i-1jk}\right) - d_{1i-1}\left(\varphi_{i-1jk}-\varphi_{i-2jk}\right)\right] \tag{A-101}$$

At the shock point, we use the operator defined in Reference 7. Thus

$$-i\omega\varphi_{1\xi}/\epsilon = -\left(i\omega/\epsilon\right)\left[\frac{\varphi_{i+1jk}+\varphi_{ijk}-\varphi_{i-1jk}-\varphi_{i-2jk}}{\xi_{i+1}+\xi_i-\xi_{i-1}-\xi_{i-2}}\right] \tag{A-102}$$

We combine these three operators in the form

$$-i\omega\varphi_{1\xi}/\epsilon = \left(i\omega/\epsilon\right)\left[c_{hk1}\varphi_{i+1jk}+c_{hk2}\varphi_{ijk}+c_{hk3}\varphi_{i-1jk}+c_{hk4}\varphi_{i-2jk}\right] \tag{A-103}$$

where the coefficients are listed in the table below

	c_{hk1}	c_{hk2}	c_{hk3}	c_{hk4}
Elliptic	$-c_{1_i}$	$c_{1_i}-d_{1_i}$	d_{1_i}	0
Shock point	$-1/\Delta\xi$	$-1/\Delta\xi$	$+1/\Delta\xi$	$+1/\Delta\xi$
Hyperbolic	0	$-c_{2i}$	$c_{2i}+d_{1i-1}$	$-d_{1i-1}$

where

$$\Delta\xi = \xi_{i+1} + \xi_i - \xi_{i-1} - \xi_{i-2}$$

Finally, combining equations (A-94) through (A-103), we obtain the following difference equation

$$\begin{aligned}
&\mathrm{D1X}_k \left[c_{i-1}\bar{u}_{i-1/2jk}\left(\varphi_{ijk}-\varphi_{i-1jk}\right) - d_{i-1}\bar{u}_{i-3/2}\left(\varphi_{i-1jk}-\varphi_{i-2jk}\right)\right] \\
&+\mathrm{D2}_k \left[c_i\bar{u}_{i+1/2jk}\left(\varphi_{i+1jk}-\varphi_{ijk}\right) - d_i\bar{u}_{i-1/2jk}\left(\varphi_{ijk}-\varphi_{i-1jk}\right)\right] \\
&+c_i\mathrm{G}_{2i+1/2j}\left(\varphi_{i+1jk}-\varphi_{ijk}\right) - d_i\mathrm{G}_{2i-1/2j}\left(\varphi_{ijk}-\varphi_{i-1jk}\right) \\
&+a_{y_j}\mathrm{F}_{ij-1/2}\left(\varphi_{ij-1k}-\varphi_{ijk}\right) - b_{y_j}\mathrm{F}_{ij+1/2}\left(\varphi_{ijk}-\varphi_{ij+1k}\right) \\
&+\mathrm{F}_{ij}\left[a_{z_k}\left(\varphi_{ijk-1}-\varphi_{ijk}\right) - b_{z_k}\left(\varphi_{ijk}-\varphi_{ijk+1}\right)\right] \qquad \text{(A-104)} \\
&+\Big\{c_{1i}\mathrm{G}_{i+1j}\left[c_{1y_j}\varphi_{i+1j+1k} + \left(d_{1y_j}-c_{1y_j}\right)\varphi_{i+1jk} - d_{iy_j}\varphi_{i+1j-1k}\right] \\
&+\left(d_{1i}-c_{1i}\right)\mathrm{G}_{ij}\left[c_{1y_j}\varphi_{ij+1k} + \left(d_{1y_j}-c_{1y_j}\right)\varphi_{ijk} - d_{1y_j}\varphi_{ij-1k}\right] \\
&-d_{1i}\mathrm{G}_{i-1j}\left[c_{1y_j}\varphi_{i-1j+1k} + \left(d_{1y_j}-c_{1y_j}\right)\varphi_{i-1jk} - d_{1y_j}\varphi_{i-1j-1k}\right]\Big\}/2 \\
&+\Big\{c_{1y_j}\mathrm{G}_{ij+1}\left[c_{1i}\varphi_{i+1j+1k} + \left(d_{1i}-c_{1i}\right)\varphi_{ij+1k} - d_{1i}\varphi_{i-1j+1k}\right) \\
&+\left(d_{1y_j}-c_{1y_j}\right)\mathrm{G}_{ij}\left[c_{1i}\varphi_{i+1jk} + \left(d_{1i}-c_{1i}\right)\varphi_{ijk} - d_{1i}\varphi_{i-1jk}\right] \\
&-d_{1y_j}\mathrm{G}_{ij-1}\left[c_{1i}\varphi_{i+1j-1k} + \left(d_{1i}-c_{1i}\right)\varphi_{ij-1k} - d_{1i}\varphi_{i-1j-1k}\right]\Big\}/2 \\
&+\left(i\omega/\epsilon\right)\left[c_{hk1}\varphi_{i+1jk} + c_{hk2}\varphi_{ijk} + c_{hk3}\varphi_{i-1jk} + c_{hk4}\varphi_{i-2jk}\right] \\
&+\omega^2\mathrm{F}_{ij}\varphi_{ijk}/(2\epsilon) \quad = 0
\end{aligned}$$

In figure 1, we illustrate the labeling of the coefficients of equation (A-104). With this labeling, the difference equation takes the form

$$\begin{aligned}&\mathrm{SUB}(k)*\varphi_{ijk-1} + \mathrm{DIAG}(k)*\varphi_{ijk} + \mathrm{SUPER}(k)*\varphi_{ijk+1} + \mathrm{CFOR2}(k)\varphi_{i-2jk}\\&+\mathrm{CFOR}(k)*\varphi_{i-1jk} + \mathrm{CAFT}(k)*\varphi_{i+1jk} + \mathrm{CFORIN}(k)*\varphi_{i-1j-1k}\\&+\mathrm{CIN}(k)*\varphi_{ij-1k} + \mathrm{CAFTIN}(k)*\varphi_{i+1j-1k} + \mathrm{CFORO}(k)*\varphi_{i-1j+1k}\\&+\mathrm{COUT}(k)*\varphi_{ij+1k} + \mathrm{CAFTO}(k)*\varphi_{i+1jk} = \mathrm{RHS}(k)\end{aligned} \tag{A-105}$$

Combining all like terms in equation (A-103), we obtain for the coefficients

$$\begin{aligned}
\varphi_{i-1j-1k}: \quad & d_{1i}d_{1y_j}\left(\mathrm{G}_{i-1j}+\mathrm{G}_{ij-1}\right)/2 = \mathrm{CFORIN}(k)\\
\varphi_{ij-1k}: \quad & a_{y_j}\mathrm{F}_{ij-1/2} - d_{1y_j}\left(d_{1i}-c_{1i}\right)\left(\mathrm{G}_{ij}-\mathrm{G}_{ij-1}\right)/2 = \mathrm{CIN}(k)\\
\varphi_{i+1j-1k}: \quad & -c_{1i}d_{1y_j}\left(\mathrm{G}_{i+1j} + \mathrm{G}_{ij-1}\right)/2 = \mathrm{CAFTIN(k)}\\
\varphi_{i-1jk}: \quad & \mathrm{D2}_k d_i\bar{u}_{i-1/2jk} - \mathrm{D1X}_k\left(c_{i-1}\bar{u}_{i-1/2jk}+d_{i-1}\bar{u}_{i-3/2jk}\right) + i\omega c_{hk3}/\epsilon\\
& + d_i\mathrm{G}_{2i-1/2j} - d_{1i}\left(d_{1y_j} - c_{1y_j}\right)\left(\mathrm{G}_{i-1j}+\mathrm{G}_{ij}\right)/2 = \mathrm{CFOR}(k)\\
\varphi_{ijk}: \quad & -\mathrm{D2}_k\left(c_i\bar{u}_{i+1/2jk} + d_i\bar{u}_{i-1/2jk}\right) + \mathrm{D1X}_k c_{i-1}\bar{u}_{i-1/2jk} + (i\omega/\epsilon)\, c_{hk2}\\
& - a_{y_j}\mathrm{F}_{ij-1/2} - b_{y_j}\mathrm{F}_{ij+1/2} - \mathrm{F}_{ij}\left(a_{z_k}+b_{z_k}\right)\\
& - c_i\mathrm{G}_{2i+1/2j} - d_i\mathrm{G}_{2i-1/2j} + \left(d_{1i}-c_{1i}\right)\left(d_{1y_j}-c_{1y_j}\right)\mathrm{G}_{ij}\\
& + \omega^2\mathrm{F}_{ij}/(2\epsilon) = \mathrm{DIAG}(k)\\
\varphi_{i+1jk}: \quad & \mathrm{D}_{2k}c_i\bar{u}_{i+1/2jk} + c_i\mathrm{G}_{2i+1/2j} + i(\omega/\epsilon)\, c_{hk1}\\
& + c_{1i}\left(d_{1y_j}-c_{1y_j}\right)\left(\mathrm{G}_{i+1j} + \mathrm{G}_{ij}\right)/2 = \mathrm{CAFT}(k)\\
\varphi_{i-1j+1k}: \quad & -d_{1i}c_{1y_j}\left(\mathrm{G}_{ij+1}+\mathrm{G}_{i-1j}\right)/2 = \mathrm{CFORO}(k)\\
\varphi_{ij+1k}: \quad & b_{y_j}\mathrm{F}_{ij+1/2} + c_{1y_j}\left(d_{1i}-c_{1i}\right)\left(\mathrm{G}_{ij}+\mathrm{G}_{ij+1}\right)/2 = \mathrm{COUT}(k)\\
\varphi_{i-2jk}: \quad & \mathrm{D1X}_k d_{i-1}\bar{u}_{i-3/2jk} + i\omega c_{hk4}/\epsilon = \mathrm{CFOR2}(k)\\
\varphi_{i+1j+1k}: \quad & c_{1y_j}c_{1i}\left(\mathrm{G}_{i+1j} + \mathrm{G}_{ij+1}\right)/2 = \mathrm{CAFTO}(k)
\end{aligned} \tag{A-106}$$

A.3.3 Boundary Conditions on the Mesh Boundary

On the left mesh boundary, we apply the outgoing wave boundary conditions used in References 3 to 8. Thus, on $x=(x_1 + x_2)/2$, we have

$$\varphi_{1\xi}\xi_x - i\omega\mathrm{M}\varphi_1/(1-\mathrm{M}) = 0 \tag{A-107}$$

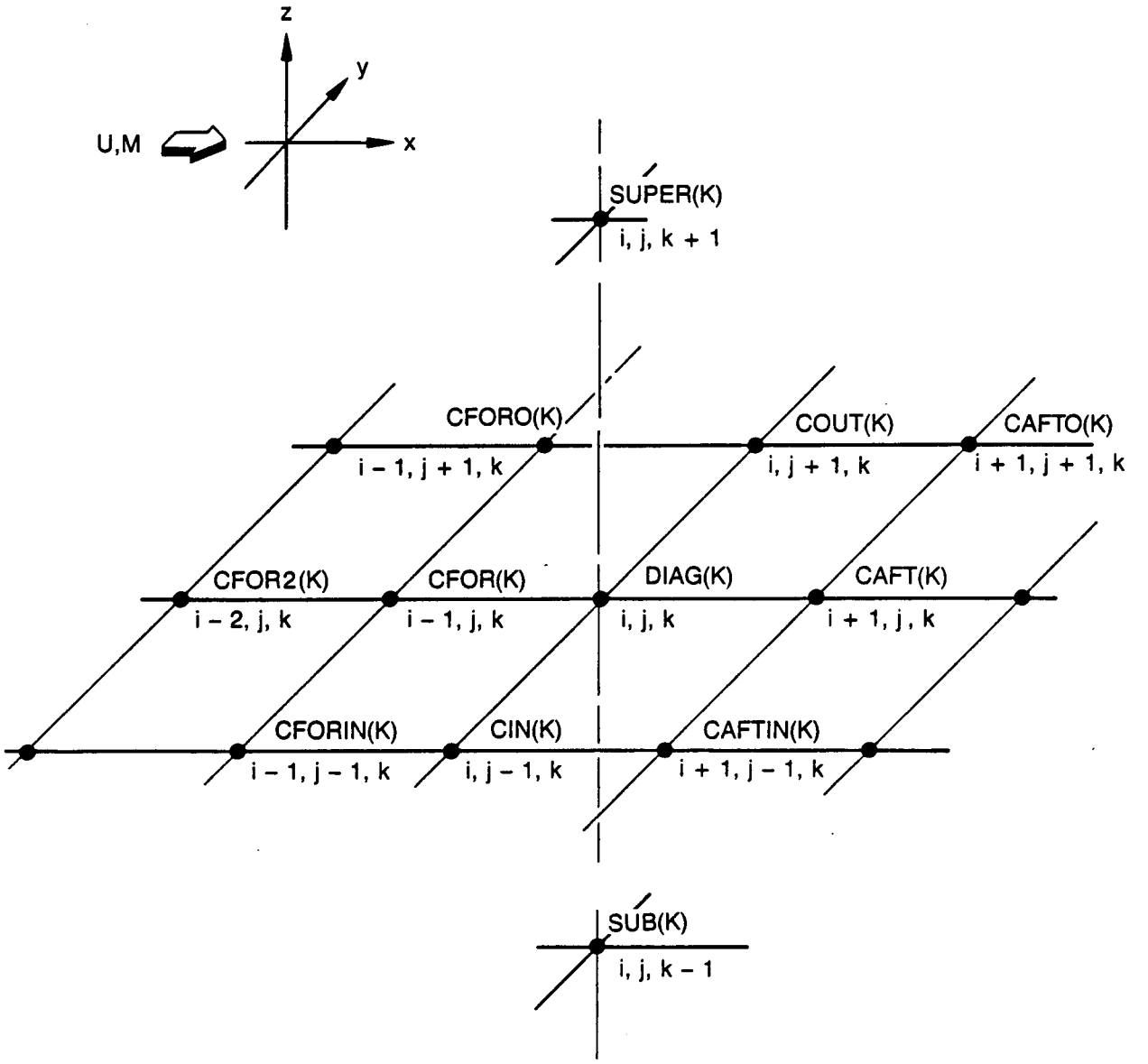

Figure 23. Definition of the Coefficients for the Finite Difference Operator

Since $\xi_x = 1/F$, we obtain for the difference form of equation (A-107)

$$\frac{\varphi_{2jk} - \varphi_{1jk}}{\xi_2 - \xi_1} - \frac{i\omega M F_{3/2i}}{1-M} \cdot \frac{\varphi_{2jk} + \varphi_{1jk}}{2} = 0$$

or

$$\left[1 - \frac{i\omega M \cdot \Delta\xi_1 \cdot F_{3/2i}}{2(1-M)}\right]\varphi_{2jk} - \left[1 + \frac{i\omega M \cdot \Delta\xi_1 \cdot F_{3/2i}}{2(1-M)}\right]\varphi_{1jk} = 0 \qquad \text{(A-108)}$$

where $\Delta\xi_1 = \xi_2 - \xi_1$ We write

$$\varphi_{1jk} = \bar{c}_{K1j}\varphi_{2jk} \qquad \text{(A-109)}$$

where

$$\bar{c}_{K1j} = \frac{1 - c_{K1i}}{1 + c_{K1j}} \qquad \text{(A-110)}$$

and

$$c_{K1j} = \frac{i\omega M \cdot \Delta\xi_1}{2(1-M)} F_{3/2j} \qquad \text{(A-111)}$$

Similarly, on the downstream boundary we have

$$\varphi_{1\xi}\xi_x + \frac{i\omega M}{1+M} \cdot \varphi = 0 \qquad \text{(A-112)}$$

In difference form, this becomes for $i = i_{max} - 1$

$$\frac{\varphi_{i+1ik} - \varphi_{iik}}{\xi_{i+1} - \xi_i} + \frac{i\omega M F_{i+1/2i}}{1+M} \cdot \frac{\varphi_{i+1ik} + \varphi_{iik}}{2} = 0$$

or

$$\varphi_{i+1jk}\left[1 + \frac{i\omega M \cdot \Delta\xi_m \cdot F_{i+1/2i}}{2(1+M)}\right] - \varphi_{ijk}\left[1 - \frac{i\omega M \cdot \Delta\xi_m \cdot F_{i+1/2i}}{2(1+M)}\right] = 0$$

Introducing similar notation leads to

$$\varphi_{i_{max}jk} = c_{K2j}\varphi_{i_{max}-1jk}$$

where

$$\bar{c}_{K2j} = \left(1 - c_{K2j}\right)/\left(1 + c_{K2j}\right) \tag{A-113}$$

$$c_{K2j} = i\omega M \cdot \Delta\xi_m \cdot F_{i_{max}-1/2jk}/\left[2(1+M)\right]$$

On the line of symmetry, $y = \eta = 0$, we apply the symmetry condition

$$\varphi_{1y} = \varphi_{1\eta} = 0$$

In difference form, this becomes

$$\varphi_{i1k} = \varphi_{i3k} \tag{A-114}$$

where $j = 2$ is the plane of symmetry and leading and trailing edges are turned normal to the plane $y = y(2) = 0$.

At the outboard spanwise mesh boundary, $y = (y_{j_{max}} + y_{j_{max}-1})/2$, we apply the outgoing wave-type boundary conditions in the form

$$\varphi_{1y} + \frac{i\omega M\sqrt{K}}{1-M^2}\varphi_1 = 0$$

or

$$\varphi_{1\eta} + \xi_y\varphi_{1\xi} + \frac{i\omega M\sqrt{K}}{1-M^2}\varphi_1 = 0$$

We select a mapping so that $\xi_y = 0$. Hence, for $j = j_{max} - 1$, we have for the difference equation

$$\frac{\varphi_{ij+1k} - \varphi_{ijk}}{\eta_{j+1} - \eta_j} + \frac{i\omega M\sqrt{K}}{1-M^2}\left[\frac{\varphi_{ij+1k} + \varphi_{ijk}}{2}\right] = 0$$

This may be written as

$$\varphi_{ij+1k} = \bar{c}_{K3}\,\varphi_{ijk} \tag{A-115}$$

where

$$\bar{c}_{K3} = \left(1 - c_{K3}\right)/\left(1 + c_{K3}\right)$$

$$c_{K3} = i\omega\, M\sqrt{K} \cdot \Delta\eta_m/\left[2\left(1-M^2\right)\right] \tag{A-116}$$

$$\Delta\eta_m = \eta_{j_{max}} - \eta_{j_{max}-1}$$

On the lower boundary where $z = (z_1 + z_2)/2$, we have

$$\varphi_z - \frac{i\omega M\sqrt{K}}{1-M^2}\varphi = 0$$

which leads to

$$\varphi_{ij1} = \bar{c}_{K4}\,\varphi_{ij2} \tag{A-117}$$

where

$$\bar{c}_{K4} = (1-c_{K4})/(1+c_{K4})$$

$$c_{K4} = i\omega M\cdot\Delta z_i\cdot\sqrt{K}\ /\ \left[2(1-M^2)\right] \tag{A-118}$$

$$\Delta z_1 = z_2 - z_1$$

Similarly, on the upper boundary where $z = (z_{k_{max}-1} + z_{k_{max}})/2$, we have

$$\varphi_z + \frac{i\omega M\sqrt{K}}{1-M^2}\varphi = 0$$

or

$$\varphi_{ijk_{max}} = \bar{c}_{K2j}\varphi_{ijk_{max}-1} \tag{A-119}$$

where

$$\bar{c}_{K5} = (1-c_{K5})/(c_{K5})$$

$$c_{K5} = i\omega M\cdot\Delta z_m\cdot\sqrt{K}/\left[2(1-M^2)\right] \tag{A-120}$$

$$\Delta z_m = z_{k_{max}} - z_{k_{max}-1}$$

We now apply the boundary conditions on the mesh boundaries to the difference equations. On the left boundary $x = (x_1 + x_2)/2$, the term

$$\text{CFORIN}(k)\cdot\varphi_{1j-1k}$$

is replaced by

$$\text{CFORIN}(k)\cdot\varphi_{2j-1k}$$

then these two coefficients are modified by

$$\mathrm{CIN}(k) = \mathrm{CIN}(k) + \bar{c}_{K1_{j-1}} \cdot \mathrm{CFORIN}(k) \tag{A-121}$$

$$\mathrm{CFORIN}(k) = 0$$

Similarly, CFOR $(k) \cdot \varphi_{ijk}$ is replaced by CFOR $(k) \cdot \bar{c}_{\mathrm{K1}_j} \varphi_{2jk}$

and the coefficients are modified by

$$\mathrm{DIAG}(k) = \mathrm{DIAG}(k) + c_{\mathrm{K1}_j} * \mathrm{CFOR}(k)$$

$$\mathrm{CFOR}(k) = 0 \tag{A-122}$$

On the plane of symmetry we have, for $j = 2$,

$$\varphi_{i1k} = \varphi_{i3k} \tag{A-123}$$

and the coefficients are modified by

$$\mathrm{COUT}(k) = \mathrm{COUT}(k) + \mathrm{CIN}(k)$$

$$\mathrm{CIN(k)} = 0 \tag{A-124}$$

On the boundary outboard of the wing, we have for $j = j_{\max} - 1$

$$\varphi_{ij+1k} = \bar{c}_{\mathrm{K3}}\, \varphi_{ijk} \tag{A-125}$$

and the coefficients are modified by

$$\mathrm{DIAG}(k) = \mathrm{DIAG}(k) + \bar{c}_{\mathrm{K3}} * \mathrm{COUT}(k)$$

$$\mathrm{COUT}(k) = 0 \tag{A-126}$$

Similarly, on the right, downstream boundary, we substitute

$$\varphi_{i_{\max}jk} = \bar{c}_{\mathrm{K2}j} \varphi_{i_{\max}-1jk} \tag{A-127}$$

and modify the coefficients by

$$\mathrm{DIAG}(k) = \mathrm{DIAG}(k) + \bar{c}_{\mathrm{K2}j} * \mathrm{CAFT}(k)$$

$$\mathrm{CAFT}(k) = 0$$

$$\mathrm{CIN}(k) = \mathrm{CIN}(k) + \bar{c}_{\mathrm{K2}j} * \mathrm{CAFTIN}(k), \qquad j \neq 2$$

(A-128)

$$\text{CAFTIN}(k) = 0$$

$$\text{COUT}(k) = \text{COUT}(k) + \bar{c}_{\text{K2}j} * \text{CAFTO}(k), \qquad j \neq j_{\max} - 1$$

$$\text{CAFTO}(k) = 0$$

On the lower boundary for $z = (z_1 + z_2)/2$ and $k = 2$, we have similar conditions, namely,

$$\varphi_{ij1} = \bar{c}_{\text{K4}}\, \varphi_{ij2}$$

and the coefficients are modified by

$$\text{DIAG}(2) = \text{DIAG}(2) + \bar{c}_{\text{K4}} * \text{SUB}(2) \tag{A-129}$$

$$\text{SUB}(2) = 0$$

Similarly, for the upper boundary we obtain

$$\varphi_{ijk_{\max}} = \bar{c}_{\text{K5}}\, \varphi_{ijk_{\max}-1} \tag{A-130}$$

and

$$\text{DIAG}(k_{\max}-1) = \text{DIAG}(k_{\max}-1) + \bar{c}_{\text{K5}} * \text{SUPER}(j_{\max}-1) \tag{A-131}$$

$$\text{SUPER}(k_{\max}-1) = 0$$

A.3.4 Wake Boundary Conditions

The condition that the pressure be continuous across the wake is given by

$$\Delta\varphi_x + i\omega\Delta\varphi = 0 \tag{A-132}$$

where $\Delta\varphi$ is the jump in unsteady potential across the wake. This may be integrated to yield

$$\Delta\varphi_i = \Delta\varphi_{i_{1}+1} \exp\left(-i\omega\left(x_i - x_{i_{1}+1}\right)\right) \tag{A-133}$$

We express the argument

$$\text{ARG} = -\omega\,(x_i - x_{i_{1}+1}) \tag{A-134}$$

in terms of the variable ξ. Thus, for the downstream region for $\xi > 1$, we have from equation (A-7) in the section on the coordinate transformation

$$x = X_{LE}(j) + S(j)\cdot(\xi+1) + \left(\frac{\xi-1}{\xi_{max}-1}\right)^3 \left[\xi_{max} - X_{LE}(j) - S(j)\cdot\left(\xi_{max}+1\right)\right] \quad \text{(A-135a)}$$

where we have chosen $X_{max} = \xi_{max}$. For the trailing-edge point $i_1 + 1$ from equation (A-10), we obtain

$$x_{i_1+1} = X_{LE}(j) + S(j)\cdot\left(\xi_{i_1+1} + 1\right) + \left(\frac{\xi_{i_1+1}-1}{\xi_{max}-1}\right)^3 \left[\xi_{max} - X_{LE}(j) - S(j)\cdot\left(\xi_{max}+1\right)\right] \quad \text{(A-135b)}$$

and for the general point x

$$x_i = X_{LE}(j) + S(j)\cdot\left(\xi_i + 1\right) + \left(\frac{\xi_i-1}{\xi_{max}-1}\right)^3 \left[\xi_{max} - X_{LE}(j) - S(j)\cdot\left(\xi_{max}+1\right)\right] \quad \text{(A-136)}$$

Thus the argument in equation (A-134) finally takes the form

$$ARG = \omega\left\{S(j)\cdot\left(\xi_{i_1+1} - \xi_i\right) + \left[\xi_{max} - X_{LE}(j) - S(j)\cdot\left(\xi_{max}+1\right)\right]\left[\left(\frac{\xi_{i_1+1}-1}{\xi_{max}-1}\right)^3 - \left(\frac{\xi_i-1}{\xi_{max}-1}\right)^3\right]\right\} \quad \text{(A-137)}$$

To satisfy the Kutta conditions at $\xi = \xi_{i_1}$, we set the pressure jump at the trailing edge equal to zero, i.e., from equation (A-132),

$$\Delta\varphi_{1x} + i\omega\cdot\Delta\varphi_1 = 0$$

which in the transformed grid variables becomes

$$\Delta\varphi_{1\xi} + i\omega F\cdot\Delta\varphi_1 = 0 \quad \text{(A-138)}$$

At $\xi = \xi_{i_1}$ or $x = x_{i_1}$, this becomes in difference form

$$c_{1i_1}\cdot\left(\Delta\varphi_{i_1+1,j} - \Delta\varphi_{i_1 j}\right) + d_{1i_1}\cdot\left(\Delta\varphi_{i_1 j} - \Delta\varphi_{i_1-1,j}\right) + i\omega F_{i_1 j}\cdot\Delta\varphi_{i_1 j} = 0$$

We solve this expression for the value of $\Delta\varphi_{i_1+1}$ at the first point in the wake and obtain

$$\Delta\varphi_{i_1+1,j} = \Delta\varphi_{i_1 j} - \left(d_{1i_1}/c_{1i_1}\right)\left(\Delta\varphi_{i_1 j} - \Delta\varphi_{i_1-1,j}\right) - i\omega\left(F_{i_1 j}/c_{1i_1}\right)\cdot\Delta\varphi_{i_1 j}$$

or

$$\Delta\varphi_{i_1+1j} = \left(1 - d_{1i_1}/c_{1i_1} - i\omega F_{i_1j}/c_{1i_1}\right)\Delta\varphi_{i_1j} + \left(d_{1i_1}/c_{1i_1}\right)\Delta\varphi_{i_1-1j}$$

This may be written more conveniently as

$$\Delta\varphi_{i_1+1j} = c_{Kc1}\cdot\Delta\varphi_{i_1j} + c_{Kc2}\cdot\Delta\varphi_{i_1-1j} \tag{A-139}$$

where

$$c_{Kc1} = 1 - d_{1i_1}/c_{1i_1} - i\omega\cdot F_{i_1j}/c_{1i_1}$$

$$c_{Kc2} = d_{1i_1}/c_{1i_1} \tag{A-140}$$

$$\Delta\varphi_{ij} = \varphi_{ijk_m+1} - \varphi_{ijk_m} - c_{S1}\left(\varphi_{ijk_m+2} - \varphi_{ijk_m+1}\right)$$

$$- c_{S2}\left(-\varphi_{ijk_m} - \varphi_{ijk_m-1}\right) - \left(d_{S1}F_{ij}^{U} + d_{S2}F_{ij}^{L}\right)$$

In general, the jump in potential across the airfoil is seen from Reference 1 to be given by

$$\Delta\varphi_{ij} = \varphi_{ijk_m+1} - \varphi_{ijk_m} - c_{S1}\left(\varphi_{ijk_m+2} - \varphi_{ijk_m+1}\right)$$

$$- c_{S2}\left(\varphi_{ijk_m} - \varphi_{ijk_m-1}\right) - \left(d_{S1}F_{ij}^{U} + d_{S2}F_{ij}^{L}\right) \tag{A-141}$$

where

$$c_{S1} = 1/\left[4S_1(S_1+1)\right] \qquad c_{S2} = 1/\left[4S_2(S_2+1)\right]$$

$$d_{S1} = h(2S_1+1)/\left[4(S_1+1)\right] \qquad d_{S2} = h(2S_2+1)/\left[4(S_2+1)\right]$$

$$h = z_{k_m+1} - z_{k_m}$$

$$S_1 = \left(z_{k_m+2} - z_{k_m+1}\right) \qquad S_2 = \left(z_{k_m} - z_{k_m-1}\right)$$

Combining like terms leads to

$$\Delta\varphi_{ij} = \left(1+c_{S1}\right)\cdot\varphi_{ijk_m+1} - \left(1+c_{S2}\right)\cdot\varphi_{ijk_m} + c_{S1}\varphi_{ijk_m+2} + c_{S2}\varphi_{ijk_m-1} - \left(d_{S1}F^{U}_{ij} + d_{S2}F^{L}_{ij}\right) \quad \text{(A-142)}$$

Then, to satisfy the Kutta condition, we have

$$\begin{aligned}\Delta\varphi_{i_1+1j} = {} & c_{Kc1}\left[\left(1+c_{S1}\right)\varphi_{i_1jk_m+1} - \left(1+c_{S2}\right)\varphi_{i_1jk_m} - c_{S1}\varphi_{i_1jk_m+2} + c_{S2}\varphi_{i_1jk_m-1}\right] \\ & + c_{Kc2}\left[\left(1+c_{S1}\right)\varphi_{i_1-1jk_m-1} - \left(1+c_{S2}\right)\varphi_{i_1-1jk_m} - c_{S1}\varphi_{i_1-1jk_m+2} + c_{S2}\varphi_{i_1-1jk_m+2}\right] \\ & - c_{Kc1}\cdot\left(d_{S1}F^{U}_{i_1j} + d_{S2}F^{L}_{i_1j}\right) - c_{Kc2}\cdot\left(d_{S1}F^{U}_{i_1-1j} + d_{S2}F^{L}_{i_1-1j}\right)\end{aligned} \quad \text{(A-143)}$$

For convenience, we define new variables

$$\begin{aligned}A_{11} &= c_{Kc2}c_{S2} \\ A_{12} &= -c_{Kc2}\left(1 + c_{S2}\right) \\ A_{13} &= c_{Kc2}\left(1 + c_{S1}\right) \\ A_{14} &= -c_{Kc2}c_{S1} \\ A_{21} &= c_{Kc1}c_{S2} \\ A_{22} &= -c_{Kc1}\left(1 + c_{S2}\right) \\ A_{23} &= c_{Kc1}\left(1 + c_{S1}\right) \\ A_{24} &= -c_{Kc1}c_{S1}\end{aligned} \quad \text{(A-144)}$$

Thus we have for

$$\begin{aligned}\Delta\varphi_{i_1+1j} = {} & A_{11}\varphi_{i_1-1jk_m-1} + A_{12}\varphi_{i_1-1jk_m} + A_{13}\varphi_{i_1-1jk_m+1} + A_{14}\varphi_{i_1-1jk_m+2} + A_{21}\varphi_{i_1jk_m-1} + A_{22}\varphi_{i_1jk_m} \\ & + A_{23}\varphi_{i_1jk_m+1} + A_{24}\varphi_{i_1jk_m+2} - c_{Kc1}\left(d_{S1}F^{U}_{i_1j} + d_{S2}F^{L}_{i_1j}\right) \\ & - c_{Kc2}\left(d_{S1}F^{U}_{i_1-1j} + d_{S2}F^{L}_{i_1-1j}\right)\end{aligned} \quad \text{(A-145)}$$

For the value of k below the wing surface $k = k_m$, we add for the ith column for $i > i_1 + 1$,

$$-b_{z_{k_m}} F_{ij} \Delta\varphi_{i_1+1,j} \exp\left(i\omega(x_i - x_{i_1+1})\right) \tag{A-146}$$

and define

$$\begin{aligned}
W_{K11} &= -b_{z_{k_m}} A_{11} F_{ij} \\
W_{K12} &= -b_{z_{k_m}} A_{12} F_{ij} \\
W_{K13} &= -b_{z_{k_m}} A_{13} F_{ij} \\
W_{K14} &= -b_{z_{k_m}} A_{14} F_{ij} \\
W_{K21} &= -b_{z_{k_m}} A_{21} F_{ij} \\
W_{K22} &= -b_{z_{k_m}} A_{22} F_{ij} \\
W_{K23} &= -b_{z_{k_m}} A_{23} F_{ij} \\
W_{K24} &= -b_{z_{k_m}} A_{24} F_{ij}
\end{aligned} \tag{A-147}$$

$$\text{RHSL} = b_{z_{k_m}} \left[c_{Kc1} \left(d_{S1} F^{U}_{i_1 j} + d_{S2} F^{L}_{i_1 j} \right) + c_{Kc2} \left(d_{S1} F_{i_1 - 1_j} + d_{S2} F^{L}_{i_1 - 1 j} \right) \right]$$

Similarly for $k = k_m + 1$ we add for $i > i_1 + 1$ and j less than the tip value

$$a_{z_{k_m+1}} F_{k_m+1} \cdot \Delta\varphi_{i_1+1,j} \exp\left(-i\omega(x_i - x_{i_1+1})\right) \tag{A-148}$$

and define the variables

$$\begin{aligned}
W_{K31} &= a_{z_{k_m+1}} A_{11} F_{ij} \\
W_{K32} &= a_{z_{k_m+1}} A_{12} F_{ij} \\
W_{K33} &= a_{z_{k_m+1}} A_{13} F_{ij} \\
W_{K34} &= a_{z_{k_m+1}} A_{14} F_{ij} \\
W_{K41} &= a_{z_{k_m+1}} A_{21} F_{ij} \\
W_{K42} &= a_{z_{k_m+1}} A_{22} F_{ij} \\
W_{K43} &= a_{z_{k_m+1}} A_{23} F_{ij} \\
W_{K44} &= a_{z_{k_m+1}} A_{24} F_{ij} \\
\text{RHSU} &= -a_{z_{k_m+1}} \cdot \text{RHSL} / b_{z_{k_m}}
\end{aligned} \tag{A-149}$$

Finally, we set $E_\omega = -\exp\left(-i\omega(x_i - x_{i-1})\right)$ and for $k = k_m$, $i > i_1 + 1$

$$\text{RHS(KM)} = \text{RHSL} \cdot E_\omega \tag{A-150}$$

$$\text{WAK11} = W_{K11} \cdot E_\omega$$

$$\text{WAK12} = W_{K12} \cdot E_\omega$$

$$\text{WAK13} = W_{K13} \cdot E_\omega$$

$$\text{WAK14} = W_{K14} \cdot E_\omega$$

$$\text{WAK21} = W_{K21} \cdot E_\omega$$

$$\text{WAK22} = W_{K22} \cdot E_\omega$$

$$\text{WAK23} = W_{K23} \cdot E_\omega$$

$$\text{WAK24} = W_{K24} \cdot E_\omega$$

Similarly, for $k = k_m + 1$ and $i > i_1 + 1$,

$$\text{RHS(KMP)} = \text{RHSU} \cdot E_\omega$$

$$\text{WAK31} = W_{K31} \cdot E_\omega$$

$$\text{WAK32} = W_{K32} \cdot E_\omega$$

$$\text{WAK33} = W_{K33} \cdot E_\omega$$

$$\text{WAK34} = W_{K34} \cdot E_\omega$$

$$\text{WAK41} = W_{K41} \cdot E_\omega$$

$$\text{WAK42} = W_{K42} \cdot E_\omega \tag{A-151}$$

$$\text{WAK43} = W_{K43} \cdot E_\omega$$

$$\text{WAK44} = W_{K44} \cdot E_\omega$$

For $k = k_m$, the coefficients of φ associated with the wake are

$$\begin{aligned} -b_{z_{k_m}} \cdot \Delta\varphi_{ij} = {} & \text{WAK11} \cdot \varphi_{i_1-1jk_m-1} + \text{WAK12} \cdot \varphi_{i_1-1jk_m} \\ & \text{WAK13} \cdot \varphi_{i_1-1jk_m+1} + \text{WAK14} \cdot \varphi_{i_1-1jk_m+2} \\ & \text{WAK21} \cdot \varphi_{i_1jk_m-1} + \text{WAK22} \cdot \varphi_{i_1jk_m} \\ & \text{WAK23} \cdot \varphi_{i_1jk_m+1} + \text{WAK24} \cdot \varphi_{i_1jk_m+2} \end{aligned} \tag{A-152}$$

Similarly for $k = k_m + 1$, $i > i_1 + 1$

$$\begin{aligned} a_{z_{k_m+1}} \cdot \Delta\varphi_{ij} = {} & \text{WAK31} \cdot \varphi_{i_1-1jk_m-1} + \text{WAK32} \cdot \varphi_{i_1-1jk_m} \\ & + \text{WAK33} \cdot \varphi_{i_1-1jk_m+1} + \text{WAK34} \cdot \varphi_{i_1-1jk_m+2} \\ & + \text{WAK41} \cdot \varphi_{i_1jk_m-1} + \text{WAK42} \cdot \varphi_{i_1jk_m} \\ & + \text{WAK43} \cdot \varphi_{i_1jk_m+1} + \text{WAK44} \cdot \varphi_{i_1jk_m+2} \end{aligned} \tag{A-153}$$

A. 4 THE COEFFICIENT MATRIX AND SOLUTION PROCEDURE

The resulting set of finite difference equations may be written in the matrix form as $Ax = B$. The coefficient matrix, A, for a rectangular planform is a sparse asymmetric matrix with coefficients arranged along the principal diagonal, four bands of unit width above the diagonal, and five bands of unit width below the diagonal. The number of nonzero elements in any row is nine for a rectangular planform. The actual bandwidth of the system is large, being NS*(JMAX-2)*KXB+2*KXB, where NS is 2 for subsonic and 3 for mixed flow, and KXB is KMAX-2 for a full asymmetric flow and KMAX/2-1 for symmetric flow. For swept wings, two more bands are added both above and below the diagonal, the number of nonzero elements in a row is 13, and the system bandwidth is increased by 2*KXB. There are additional terms due to the wake that lie outside the banded system described above, and these are the same for both rectangular and swept planforms. The right-hand-side matrix, B, includes the wing boundary conditions.

The general solution procedure developed for this report stores the coefficients in blocks using out-of-core storage. The basic banded set of coefficients is stored in A. The additional coefficients in A due to the wake are stored as part of B. The resulting system is solved using LU decomposition, and a Sherman-Morrison update procedure is then used to include the additional wake terms and thus obtain the complete solution (see ref. 24).